Spring 2011

Assessment of methanotroph presence and activity in dilute vinyl chloride contaminated groundwater

Meredith Lynn Dobson
University of Iowa

ASSESSMENT OF METHANOTROPH PRESENCE AND ACTIVITY IN DILUTE VINYL CHLORIDE CONTAMINATED GROUNDWATER

by

Meredith L. Dobson

A thesis submitted in partial fulfillment
of the requirements for the Master of
Science degree in Civil and Environmental Engineering
in the Graduate College of
The University of Iowa

May 2012

Thesis Supervisor: Associate Professor Timothy E. Mattes

Graduate College
The University of Iowa
Iowa City, Iowa

CERTIFICATE OF APPROVAL

_____

MASTER'S THESIS

_____

This is to certify that the Master's thesis of

Meredith L. Dobson

has been approved by the Examining Committee
for the thesis requirement for the Master of Science
degree in Civil and Environmental Engineering at the May 2012 graduation.

Thesis Committee: _____
Timothy E. Mattes, Thesis Supervisor

_____
Jerald L. Schnoor

_____
Craig L. Just

To my family, for providing an endless supply of encouragement, optimism, humor and support

ACKNOWLEDGMENTS

It is only through the labor of support, patience, and generosity of the people in my life that I am able to conclude this part of my journey in reflection and with gratitude.

Foremost, I extend a sincere thank you to my advisor, Tim Mattes, for his patience during my graduate career and his dedication to helping me learn not only in the lab, but in the classroom as well. I also extend thanks to the other members of my defense committee, Jerry Schnoor and Craig Just.

To my friends in the Environmental Engineering department at Iowa, thank you for your camaraderie. Your company and companionship was a highlight of my graduate school career. I give special thanks to Yang Oh Jin for his endless support in the lab. The successful completion of my master's research was only accomplished by standing on Yang's previous laboratory triumphs. Thanks to Josh Livermore for his patience while educating me on phylogenic trees and for his help constructing the phylogenetic tree used in this thesis. Thanks to Andres Martinez for his patience and boundless help formatting this document. And, last but not least, thanks to Anne Alexander for her help acquainting me with the Mattes lab and for her instruction on culturing methanotrophs.

Finally, I give special thanks to my family, particularly my parents George and Cathy and my husband, Sean. Their love, encouragement, optimism, humor, and perspective serve as the foundation for all my past achievements and future endeavors. Thanks to my parents for everything they have done to make this day possible and for fostering my love for the environment at a young age, for without that, I never would have been inspired to take this route. To my husband, Sean, thank you for being my rock during the rollercoaster ride you and I have come to know as graduate school. When I started this master's program and began to climb the steep graduate school mountain, there were moments when I would dare to look down the precipice only to have my confidence shaken; however, your encouragement, optimism and perspective were

always there as my safety net, ensuring beyond any doubt that I would reach the summit. I look forward to the road ahead of us, full of new adventures to be had and new summits to be conquered.

ABSTRACT

The extensive use of tetrachloroethylene (PCE) and trichloroethylene (TCE) as cleaning solvents has resulted in widespread contamination of groundwater systems with vinyl chloride (VC). VC, a known human carcinogen, is primarily formed in groundwater via incomplete anaerobic reductive dechlorination of PCE and TCE. Aerobic, methane-degrading bacteria (methanotrophs), which are capable of VC cometabolism while growing on methane, could be important in natural attenuation of VC plumes that escape anaerobic treatment. Real-time PCR (qPCR) represents an innovative approach for detecting and quantifying the presence and activity of these VC-degrading microbes. Immediate applications of this technique include use in a laboratory setting to help elucidate the potential bacterial-substrate interactions occurring in the subsurface environments at these contaminated sites; interactions that could ultimately affect the role of methanotrophs in VC degradation. This technique could also provide lines of evidence for natural attenuation of VC, thus support existing anaerobic bioremediation technologies that generate VC as a metabolic intermediate.

In this work, we evaluated several PCR primer sets from the literature for use in methanotroph qPCR assays of groundwater samples. PCR primers targeting two functional genes involved in VC cometabolism, *pmoA* (sub-unit of particulate methane monooxygenase (pMMO)) and *mmoX* (sub-unit of soluble MMO (sMMO)), as well as 16S rRNA gene primers that targeted Bacteria, and Type I and Type II methanotrophs were tested. These assays were made quantitative by constructing standard curves with DNA from *Methylococcus capsulatus* (Type I) and *Methylocystis* sp. strain Rockwell (Type II). Primer sets were evaluated by comparing gene abundance estimated against known amounts of Type I and Type II methanotroph DNA. After primer validation, an effort to substantiate this methanotroph qPCR method was made by attempting to investigate methanotroph populations in groundwater samples from VC-contaminated

sites. Some samples studied were also subjected to 16S rRNA gene pyrosequencing, allowing for relative abundance comparisons with qPCR analyses.

Following our primer assessment experiments, effective primer sets were used to estimate the presence of methanotrophs at environmental sites in Soldotna, Alaska; Naval Air Station Oceana, Virginia Beach, Virginia; and Carver, Massachusetts. Results showed that methanotrophs were present in nearly all wells sampled from all environmental sites. Estimations of methanotroph relative abundance in environmental samples were determined by comparing the Type I and Type II primer estimates to those of the 16S universal primers. Methanotrophs in these groundwater samples ranged from 0.2% to 6.6% of the total bacterial population. Pyrosequencing analysis of the same samples showed methanotroph relative abundances that ranged from 1.7% to 54%. In groundwater samples where both DNA and RNA was extracted, the quantities of functional gene transcripts per gene copy was compared, revealing that the transcripts/gene ratio for both *pmoA* and *mmoX* was less than one, implying relatively low methanotroph activity. Analysis of *mmoX* environmental sample dissociation curves revealed a double peak, indicating possible non-specific PCR products.

Our data suggests that most of the qPCR primer sets used in the environmental samples adequately detect methanotrophs, though the mmoX primers need to be further validated. These primer sets will be useful for supporting VC bioremediation strategies by providing a rapid, convincing, and cost effective alternative the enrichment culture technique currently employed. Comparison of qPCR and pyrosequencing analysis revealed biases in either one, or both techniques. Finally, our preliminary transcripts/gene data suggests that the methanotrophs at the Carver site are not actively expressing pMMO and sMMO genes above basal levels.

TABLE OF CONTENTS

LIST OF TABLES

LIST OF FIGURES

.

CHAPTER 1

INTRODUCTION

Vinyl chloride (VC), a known human carcinogen [1] and common groundwater contaminant [2], is often generated in groundwater by incomplete reductive dechlorination of the widely used chlorinated solvents tetrachloroethylene (PCE) and trichloroethylene (TCE), also common groundwater contaminants [2]. PCE and TCE, as well as their daughter products dichloroethylene (DCE) and VC, are key contaminants of concern. Anaerobic reductive dechlorination is a promising biotechnology for remediation of PCE- and TCE-contaminated groundwater, but the potential for production of a mobile VC plume by this process represents a threat to public health if the VC plume migrates, or could migrate, into drinking water source zones. At some sites, VC will escape the anaerobic zone and enter aerobic groundwater, forming dilute plumes. Aerobic groundwater zones are typically low in organic carbon content, which limits the use of natural attenuation strategies that rely on the generation of reducing conditions in the aquifer. However, VC is often observed to readily degrade in aerobic groundwater [3, 4]. It seems likely that microorganisms are responsible for the observed aerobic attenuation of VC. The formation of methane and ethene under anaerobic conditions that may comigrate into aerobic zones along with VC can potentially contribute to cometabolic VC oxidation by methanotrophic bacteria [5]. Methanotrophs are characterized by their ability to use methane as their sole carbon and energy source [6]. Active remedial strategies involving cometabolism of VC by methane-degrading bacteria are currently being developed. One potential strategy involves injection of methane and oxygen into a dilute VC plume to stimulate growth of the methanotrophs and subsequent cometabolic oxidation of VC. However, to effectively implement these remedial strategies it is important to know if methanotrophs are present in the aquifer. The presence or absence of methanotrophs is currently measured with enrichment culture

techniques that involve taking a groundwater sample and mixing it with a nutrient containing media. The sample is then amended with methane and oxygen and monitored for methane degradation with an accompanied increase in turbidity indicating microbial growth. This analysis works well, but typically requires 15-30 days to complete. A variety of molecular biology tools (e.g. real-time PCR) for quantifying the abundance of methanotrophs, which can degrade VC cometabolically, in environmental samples have been developed [7, 8]. As a result, there is now the opportunity to apply this knowledge to site cleanup. The aim of this study was to develop quantitative molecular biology techniques for assessing the presence and activity of VC-degrading methanotrophs that would be rapid, convincing, and more cost effective than current practices. Previous reports of real-time PCR assays for methanotrophs [7, 8] will be the starting point for this study. The proposed techniques, when coupled with rate studies, will improve the ability to evaluate, demonstrate and measure natural and enhanced attenuation of dilute VC plumes. The resulting improved VC bioremediation approach would thereby improve decision making, save time, and ultimately, reduce the life cycle costs for remediation of dilute VC plumes.

Specific Objectives:

- Develop and validate real-time PCR techniques that can quantify both the *presence and activity* of methanotrophs in environmental samples
- Perform literature review to find methanotroph qPCR primers
- Construct standard curves using literature primers and DNA from pure cultures
- Optimize standard curves characteristics
- Validate primer sets by using them to quantify known amounts of methanotroph genomic DNA
- Validate qPCR technique at sites where VC remedial efforts are ongoing

CHAPTER 2

BACKGROUND AND LITERATURE REVIEW

Vinyl Chloride Presence and Degradation in Groundwater Systems

Sources of VC, ethene, and methane

Vinyl chloride (VC) is a known human carcinogen [1] that has been demonstrated to cause cancer in humans and experimental animals [9, 10]. VC is a common groundwater contaminant [2] and poses a cancer risk to exposed populations through either ingestion of contaminated drinking water or inhalation during showering [11, 12]. Due to its toxicity and carcinogenicity, the US EPA has set the maximum contaminant level for VC in drinking water at 2 ppb [13]. VC's presence in the environment can be attributed to both natural and anthropogenic sources [14]. Although 95% of VC production occurs during the rendering of polyvinyl chloride (PVC), its widespread presence in groundwater is predominately attributed to the extensive use of chlorinated ethenes [15]. Tetrachloroethylene (PCE), the main constituent of dry cleaning fluid, and trichloroethylene (TCE), a widely used industrial metal degreaser, also common groundwater pollutants [2], are among the parent compounds responsible for VC contamination [16]. Once spilled into the environment, PCE and TCE leach into aquifers where they subsequently induce anaerobic conditions. Once the aquifers turn anaerobic, the indigenous microbial populations readily dehalogenate PCE and TCE to produce VC [16-18]. In contrast to PCE and TCE, VC exhibits a diminished capacity for reductive dechlorination due to its already relatively reduced state [18]. Consequently, VC tends to accumulate in anaerobic aquifers [19-21] and, in some cases, has been detected at concentrations of more than 12 mg/liter in groundwater contaminated with PCE and TCE [22]. However, in most cases VC plumes are found at concentrations below 1 mg/L and are difficult to remediate at these dilute concentrations. In addition to VC, ethene and

methane are also likely to be present at these contaminated sites [23]. Ethene, a plant hormone commonly found in the environment [24] and a product of reductive dechlorination (Figure 1), and methane, a compound produced under methanogenic conditions in anaerobic environments [25], are important molecules involved in the biotransformation of VC to carbon dioxide (CO_2) [26-28]. Once in the environment, there are several options for both reductive and oxidative biodegradation of VC.

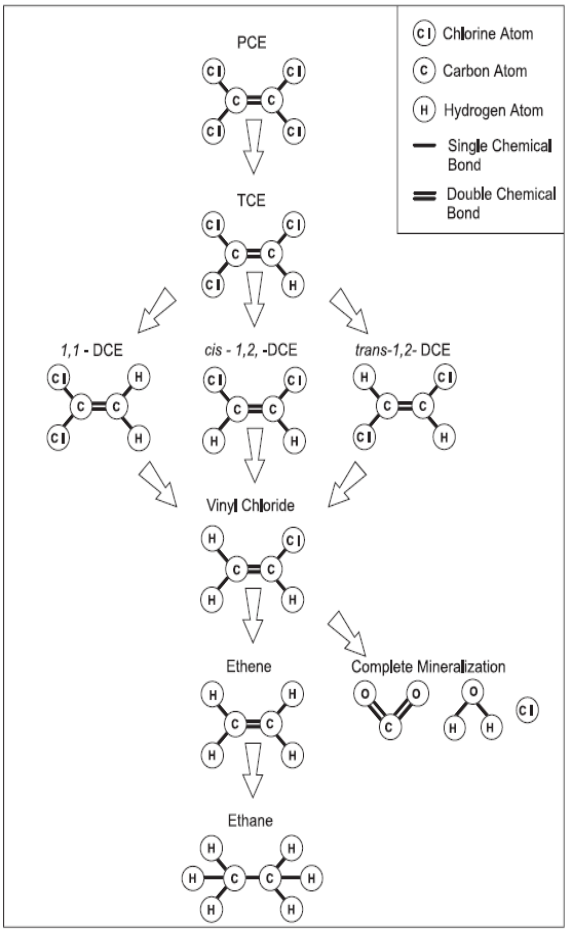

Figure 1: Sequential reduction of PCE by anaerobic reductive dechlorination [23].

Reductive Dechlorination of PCE, TCE, and VC

Reductive dechlorination is a microbially mediated process in which bacteria use chlorinated compounds as the terminal electron acceptor in their electron transport chain and sequentially remove chlorine atoms from the core carbon molecule (Figure 1) [29]. Certain environmental conditions must prevail in order for a contaminated site to support this process. First, the site must contain microorganisms capable of degrading chlorinated ethenes. For PCE and TCE, many bacteria in the genera *Dehalobacter*, *Desulfomonile*, *Desulfitobacterium*, and *Dehalococcoides* have been identified that are able to perform reductive dechlorination (Table 1); however, *Dehalococcoides* is currently the only genera able to dechlorinate past cDCE [30-35].

Table 1: Characteristics of major genera of bacteria capable of reductive dechlorination [29].

	Electron Donor	**Electron Acceptor**	**Product of PCE Reduction**
Dehalobacter	H_2	PCE, TCE	DCE
Desulfomonile	H_2, formate, pyruvate, lactate, benzoate	PCE	DCE
Desulfitobacterium	H_2, formate, pyruvate, lactate	Chlorophenols, PCE	TCE
Dehalococcoides	H_2, lactate	PCE, TCE	Ethene

The oxidation-reduction (redox) capacity of an aquifer is also an important consideration. The redox capacity of a contaminated site is important because it determines microbial energetics and, consequently, the likelihood of reductive dechlorination occurring. The most common method of assessing groundwater redox conditions is by monitoring native terminal electron acceptors (TEAs). The traditional

TEAs are oxygen, nitrate, manganese, iron, sulfate, and methane [36]. Because oxygen is the most energetically favorable, theoretically it should be the first TEA consumed followed by nitrate, manganese, iron, sulfate, and methane, respectively. However, although there is usually a dominant TEA being used in any one location in an aquifer, there is always overlap due to the presence of microenvironments that can support the use of multiple TEAs [37]. As these TEAs are consumed sequentially, the aquifer becomes a more reduced environment (Figure 2). In order for the reductive dechlorination of PCE and TCE to occur, the redox conditions must be at least sulfate reducing [36]. Table 2 and Table 3 demonstrate conditions under which reductive dechlorination would be both favorable and unfavorable.

(oxidative/aerobic) $O_2 > NO_3 > Mn > Fe^{3+} > SO_4^{2-} > CH_4$ (reductive/anaerobic)

Figure 2: Common terminal electron acceptors found in groundwater. TEAs are arranged in order from most oxidative to most reductive.

In order for reductive dechlorination to occur, a contaminated site must also have an ample source of primary growth substrate (i.e. carbon source, electron donor). This is an important condition for the following reasons: (1) the presence and consumption of an abundant carbon source can drive an aquifer anaerobic and, consequently, provide the redox conditions that support reductive dechlorination; (2) Because the microbial redox reactions must balance, the total mass of chlorinated ethenes degraded by the microbial population is determined by the amount of carbon available for oxidation. When a carbon source becomes exhausted, reductive dechlorination will cease and highly chlorinated compounds will not be dechlorinated. Although the subsurface of some contaminated sites contain naturally occurring organic carbon that is used as the electron donor and carbon source of these microbes, anthropogenic organic carbon sources (i.e.

vegetable oil and acetate for remedial purposes) are much more common. The ideal electron donor for these contaminated sites is hydrogen (H_2). Since there are no carbon atoms associated with the H_2 molecule, when H_2 is used as an electron donor an organic carbon source, such as acetate, is also needed [29]. Hydrogen concentrations of 1 nM can support reductive dechlorination [36]. Table 2 and Table 3 list geochemical conditions in which reductive dechlorination of TCE is both favorable and unfavorable.

Table 2: Example groundwater conditions that would be strongly indicative of anaerobic biodegradation (reductive dechlorination) of chlorinated organics [23].

Analyte	**Concentration in Most Contaminated Zones**
Dissolved Oxygen	0.1 mg/L
Nitrate	0.3 mg/L
Iron (II)	10 mg/L
Sulfate	2 mg/L
Methane	5 mg/L
Oxidation-Reduction Potential	-190 mV
Chloride	3 times background
PCE (released)	1,000 µg/L
TCE (none released)	1200 µg/L
cDCE (none released)	500 µg/L
VC (none released)	20 µg/L

Table 3: Example groundwater conditions that would be unfavorable for anaerobic biodegradation (reductive dechlorination) of chlorinated organics [23].

Analyte	Concentration in Most Contaminated Zones
Dissolved Oxygen	3 mg/L
Nitrate	0.3 mg/L
Iron (II)	Not Detected
Sulfate	10 mg/L
Methane	Not Detected
Oxidation-Reduction Potential	+100 mV
Chloride	background
PCE (released)	1,000 µg/L
TCE (none released)	1200 µg/L
cDCE (none released)	Not Detected
VC (none released)	Not Detected

The final condition necessary for reductive dechlorination is the absence of competing electron acceptors. Because chlorinated ethenes act as electron acceptors during reductive dechlorination, the native geochemical compounds, such as oxygen, nitrate and iron, become competitors in the electron transfer processes that generate energy for microorganisms. For this reason, reductive dechlorination will not occur in the presence of oxygen, nitrate or ferric iron [36].

Oxidative Degradation

Anaerobic Oxidation

Oxidative degradation of chlorinated hydrocarbons can occur in both anaerobic and aerobic environments. The tendency of chlorinated ethenes to undergo oxidation increases as the number of chlorine substituents associated with each molecule decreases [18]. As a result, oxidation of vinyl chloride can occur under anaerobic conditions, if a sufficiently strong oxidant is available to drive microbial degradation [30]. In this situation, it becomes energetically favorable for some microorganisms to use VC as the electron donor to oxidize various possible TEAs. Rapid anaerobic biodegradation of VC contaminants has been observed under Fe(III)-reducing conditions [30], humic acid-reducing [38], Mn(IV)-reducing [39], SO_4^{2-}-reducing [38], and methanogenic conditions [32, 38, 39]. In all these cases, experimental results showed evidence of VC and DCE oxidation to CO_2. Microorganisms capable of anaerobic VC and cDCE oxidation seem to occur at many sites, and are active under a variety of terminal-electron-accepting conditions; however, there is no known microorganism able to oxidize VC or cDCE anaerobically for growth [40].

Aerobic Oxidation

Aerobic oxidation, typically a microbially mediated process, is a chemical reaction in which one substance is combined with oxygen in a reaction catalyzed by oxygenase enzymes. Many of these oxygenase enzymes have a broad substrate range and are capable of fortuitously oxidizing chloroethenes. The oxidation of chloroethenes yields an unstable chlorinated epoxide intermediate that will spontaneously degrade to one of several chloroacetic acids, such as dichloroacetic acid [40, 41]. These chloroacetic acids are soluble in water and will slowly degrade to CO_2, chloride, and water.

Microorganisms capable of oxidizing VC as a carbon and energy source are said to be metabolic oxidizers of VC. One class of microorganisms capable of such oxidation

are known as the etheneotrophs. Etheneotrophic bacteria consume ethene as their preferred carbon and energy source, yet are capable of growth on VC after extended incubations with the substrate as the sole carbon and energy source [42, 43]. Conversely, methanotrophic bacteria, which are bacteria that consume methane as their sole carbon and energy source, are capable of only cometabolic VC oxidation. Cometabolic oxidation of VC by methanotrophs is a process by which the oxidation of VC is fortuitous and only occurs in the presence of the growth substrate, methane. Sustained oxidation of VC at dissolved oxygen (DO) concentrations of less than 0.02 mg/L has been reported [37].

Where an environmental pollutant does not support microbial growth, aerobic cometabolism offers a biological method for the removal of the pollutant from the contaminated environment. This approach to bioremediation is particularly appropriate for chlorinated solvents and related compounds when other methods (such as reductive dechlorination) are less likely to result in the complete mineralization of the target compound.

Methanotrophs

Methanotrophs are distinguished from other microorganisms by their ability to utilize methane (CH_4) as their sole carbon and energy source [6]. With the exception of the genus *Methylocella* [44], aerobic methanotrophic bacteria are unable to grow on substrates containing carbon-carbon bonds. These microorganisms, which play a key role in the global carbon cycle by controlling anthropogenic and natural emissions [45, 46] of CH_4, and which have been widely used for bioremediation of chlorinated solvents [47-49], occur ubiquitously [46, 50, 51] and are capable of growth in many diverse environments. Methanotrophs have been isolated from such environments as the air, the tissues of higher organisms, soils, wetlands, freshwater and marine sediments and water columns, sewage sludge, groundwater, rice paddies, and peat bogs [46, 50-52]. Although

moderate pH (5–8) and temperature ranges (20–35 °C) are advantageous growth parameters for most known methanotrophs [46], extremophiles have also been discovered. Psychrophilic (growth < 15 °C) [53, 54], thermophilic (growth > 40 °C) [55, 56], alkaliphilic (growth at pH> 9.0) [57], and acidophilic (growth at pH < 5) [51, 58] methanotrophs have been successfully isolated from the environment.

Particulate and Soluble Methane Monooxygenase

Despite their diversity, the general pathway by which CH_4 is oxidized to CO_2 is remarkably similar between the diverse genera of methanotrophs, particularly in the initial oxidation of CH_4 to methanol via monooxygenase enzymes. For this conversion, two forms of methane monooxygenase have been found: a particulate, membrane-bound form (pMMO) and a soluble, cytoplasmic form (sMMO). Particulate MMO, located in the cytoplasmic membrane, has been reported in all methanotrophs except for the genus *Methylocella* [59], while sMMO, located in the cytoplasm, is found only in some methanotrophs [60]. It has been discovered that, for methanotrophs possessing both forms of MMO, copper (Cu) plays a key role in the gene regulation and enzymatic activity of pMMO and sMMO [61, 62]. For instance, a Cu-to-biomass ratio greater than 5.64 mmolCu g^{-1} protein has been shown to inhibit sMMO activity [63].

The sMMO is a well characterized, three component enzyme consisting of a hydroxylase, a reductase, and a regulatory protein (Figure 3). The catalytic center of this enzyme, which contains a unique di-iron site, has a broad substrate range including TCE, DCE, and VC [52]. The well-studied biochemistry of sMMO has revealed that the hydroxylase component of this enzyme is composed of three subunits. The α, β, and γ-subunits, approximately 54 kDa, 42 kDa, and 22 kDa, respectively, constitute one monomer of the enzyme. The hydroxylase is then formed when two monomers combine yielding a dimer protein with the structure $(\alpha\beta\gamma)_2$ [52, 64] (Figure 3). The sMMO operon, which occurs in a single copy in the genome of M. *capsulatus* (Bath) [65],

contains six genes that code for the hydroxylase α, β, and γ-subunit (*mmoX*, *mmoY*, *mmoZ*), the reductase enzyme (*mmoC*), and the regulatory protein (*mmoB*) [66]. The purpose of the sixth gene in the operon, *orfY* (*mmoD*), is unknown but it is thought to play a role in assembly of the unique di-iron center of the sMMO enzyme [67].

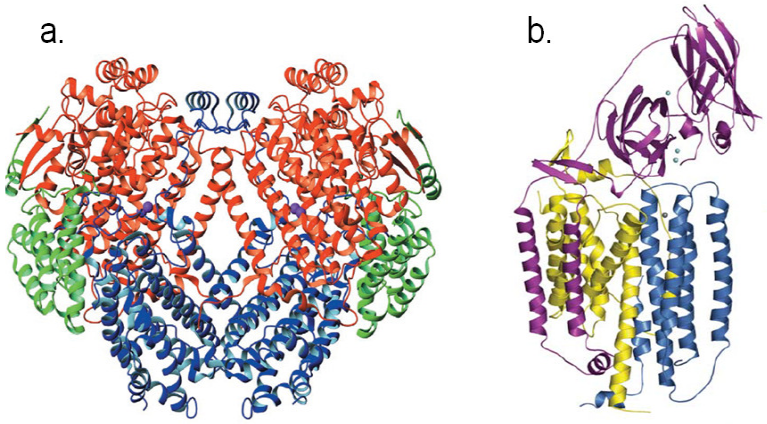

Figure 3: (a) The crystal structure of sMMO's hydroxylase component. The α-subunit is shown in red, the β-subunit in blue, and the γ-subunit in green. Iron atoms are shown as purple spheres [64]. (b) The crystal structure of the pMMO subunits. PmoB is shown in magenta, pmoA is shown in yellow, and pmoC is shown in blue. Three copper ions are shown (cyan), and one zinc ion is shown (grey) [68].

In contrast to sMMO, little is known about the molecular properties of pMMO; however, it is understood that this enzyme consists of three, integral-membrane, polypeptide subunits (αβγ) and has a catalytic center containing copper. The α, β, and γ-subunits, approximately 45 kDa, 26 kDa, and 23 kDa, respectively, constitute one monomer of the enzyme (Figure 3). The pMMO is then formed when three monomers combine yielding a trimer protein with the structure $(\alpha\beta\gamma)_3$ [68] (Figure 3). The pMMO operon, which occurs in duplicate copies in *Methylococcus capsulatus* Bath, *Methylocystis s*p. strain M, and *Methylosinus trichosporium* OB3b [6], contains three

genes that code for the α, β, and γ-subunit (*pmoB*, *pmoA*, *pmoC*) [69]. Degradation kinetics rates for TCE, DCE, and VC by either sMMO or pMMO-expressing methanotrophs is shown in Table 4.

Type I and Type II Methanotrophs

Despite their diversity, methanotrophic bacteria share several characteristics that allow them to be classified as either a Type I or a Type II methanotrophs (Figure 4). Type I methanotrophs, which fall under the Gamma subdivision of *Proteobacteria*, typically have intracytoplasmic membranes throughout the cell that occur as bundles of vesicular disks, utilize the ribulose monophosphate (RuMP) pathway (Figure 5) for carbon assimilation, and have signature phospholipid fatty acids that are 4 and 16 carbons in length. Type II strains, which fall under the Alpha subdivision of the *Proteobacteria*, typically have intracytoplasmic membranes that are aligned along the periphery of the cell, utilize the serine pathway for carbon assimilation (Figure 6), and have signature phospholipid fatty acids 18 carbons in length [6]. Based on 16S rRNA gene sequence analyses, Type I methanotroph genera include *Methylobacter*, *Methylococcus*, *Methylomicrobium*, *Methylomonas*, *Methylocaldum*, *Methylohalobius*, *Methtyhlothermus*, *Methylosarcina*, *Methylosoma*, and *Methylosphaera* [46, 55, 70-75]. Type II methanotroph genera include *Methylocystis*, *Methylosinus*, *Methylocella*, and *Methylocapsa* [46, 58, 76-78]. Although the majority of known methanotrophs fall within the *Proteobacteria* phylum, some have been isolated and characterized that group within the *Verrucomicrobia* phylum [56, 79, 80]. A summary of methanotrophs and their characteristics can be found in Table 5, Table 6, and Table 7.

Table 4: Kinetics of halogenated hydrocarbon degradation by methanotrophs known to be expressing either sMMO or pMMO [6].

Compound	sMMO-expressing cells			pMMO-expressing cells		
	Ks (μM)	Vmax (nmol min^{-1} mg protein $^{-1}$)	k1 (mL min^{-1} mg $protein^{-1}$	Ks (μM)	Vmax (nmol min^{-1} mg protein $^{-1}$)	k1 (mL min^{-1} mg $protein^{-1}$
Methane	92	726	7.9	19	450	25
Vinyl Chloride	160	2100	13	26	42	1.6
trans-Dichloroethylene	148	662	4.5	42	61	1.5
cis-Dichloroethylene	30	364	12.1	0.8	0.12	0.15
1,1-Dichloroethylene	5	12	2.4	2.5	0.23	0.092
Trichloroethylene	145	580	4	7.9	4.1	0.52

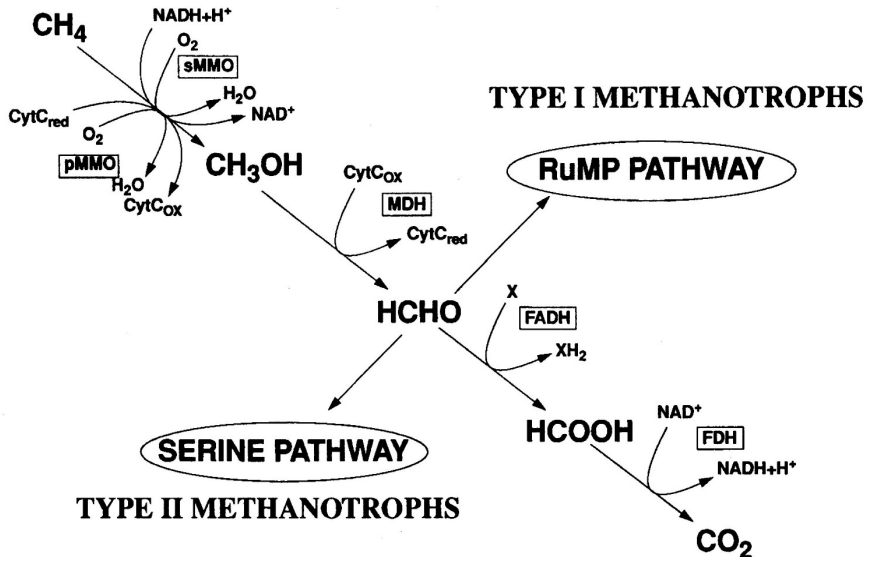

Figure 4: Pathways for oxidation of methane and assimilation of formaldehyde. This figure shows substrate metabolism by methanotrophs to demonstrate both their common and distinguishing metabolic features. Formaldehyde plays a central metabolic role as an intermediate in catabolism and anabolism. Abbreviations: CytC, cytochrome c; FADH, formaldehyde dehydrogenase; FDH, formate dehydrogenase [46].

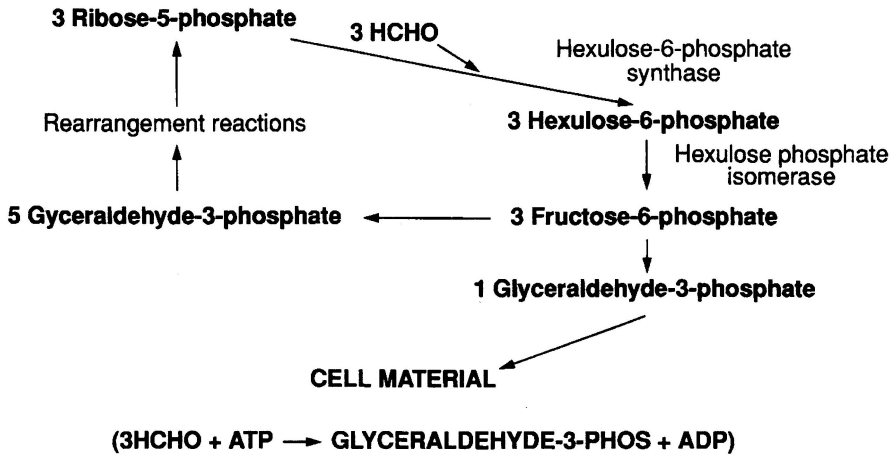

Figure 5: RuMP pathway for formaldehyde fixation. The unique enzymes of this pathway, hexulose-6-phosphate synthase and hexulose-phosphate isomerase, are indicated [46].

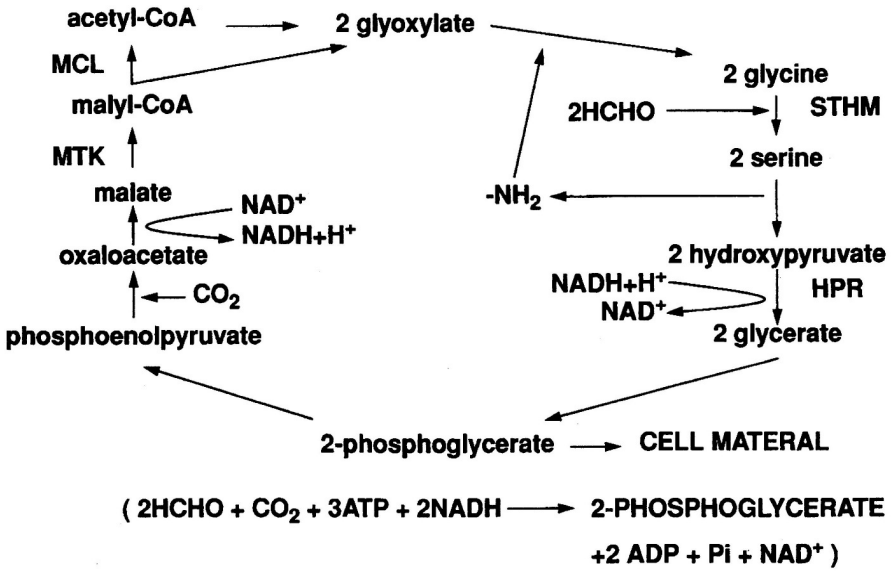

Figure 6: Serine pathway for formaldehyde fixation. The enzymes of this pathway, serine hydroxymethyl transferase, hydroxypyruvate reductase, malate thiokinase, malyl coenzyme A lyase, are indicated [46].

Phylogenetic relationships between methanotrophs are commonly examined using *16S* rRNA and *pmoA* sequence data. Figure 7 and Figure 8 show general phylogenetic trees for methanotrophs based on 16S and *pmoA* sequences, respectively. The 16S and *pmoA* sequences are the target genes of this research and, thus, these trees will be important in predicting primer bias and quantification accuracy of the quantitative polymerase chain reaction method.

Methanotrophic Bioremediation of VC

The ability of methanotrophs to cometabolize VC is well established [81] and attributed to the nonspecific nature of both pMMO and sMMO. Comparatively, sMMO is much more non-specific with respect to potential substrates than pMMO [6]. Although CH_4 is the preferred substrate of both enzymes, sMMO and pMMO will bind and oxidize chlorinated hydrocarbons [6, 82]. Oxidation of VC by MMOs results in the formation of chlorooxirane, an epoxide intermediate (Figure 9). Chlorooxirane is a very unstable

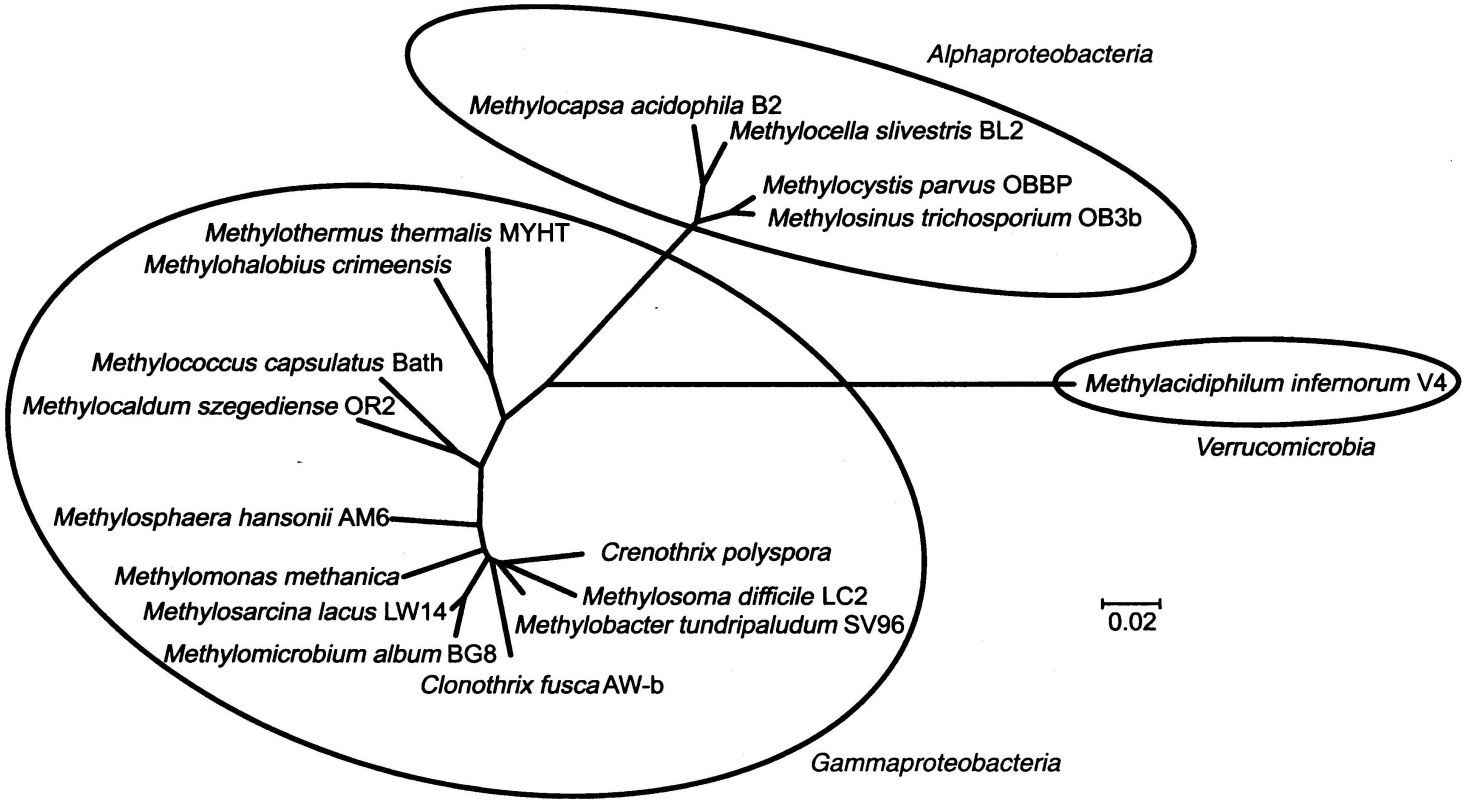

Figure 7: Phylogenetic relationships between known methanotrophs based on 16S rRNA gene sequences using MEGA4. The tree was constructed using the neighbor-joining method with 1304 positions of 16S rRNA gene. The bootstrap consensus tree was inferred from 500 replicates. Evolutionary distances were computed using the maximum composite likelihood method. The scale bar indicates 0.02 base substitutions per site [6].

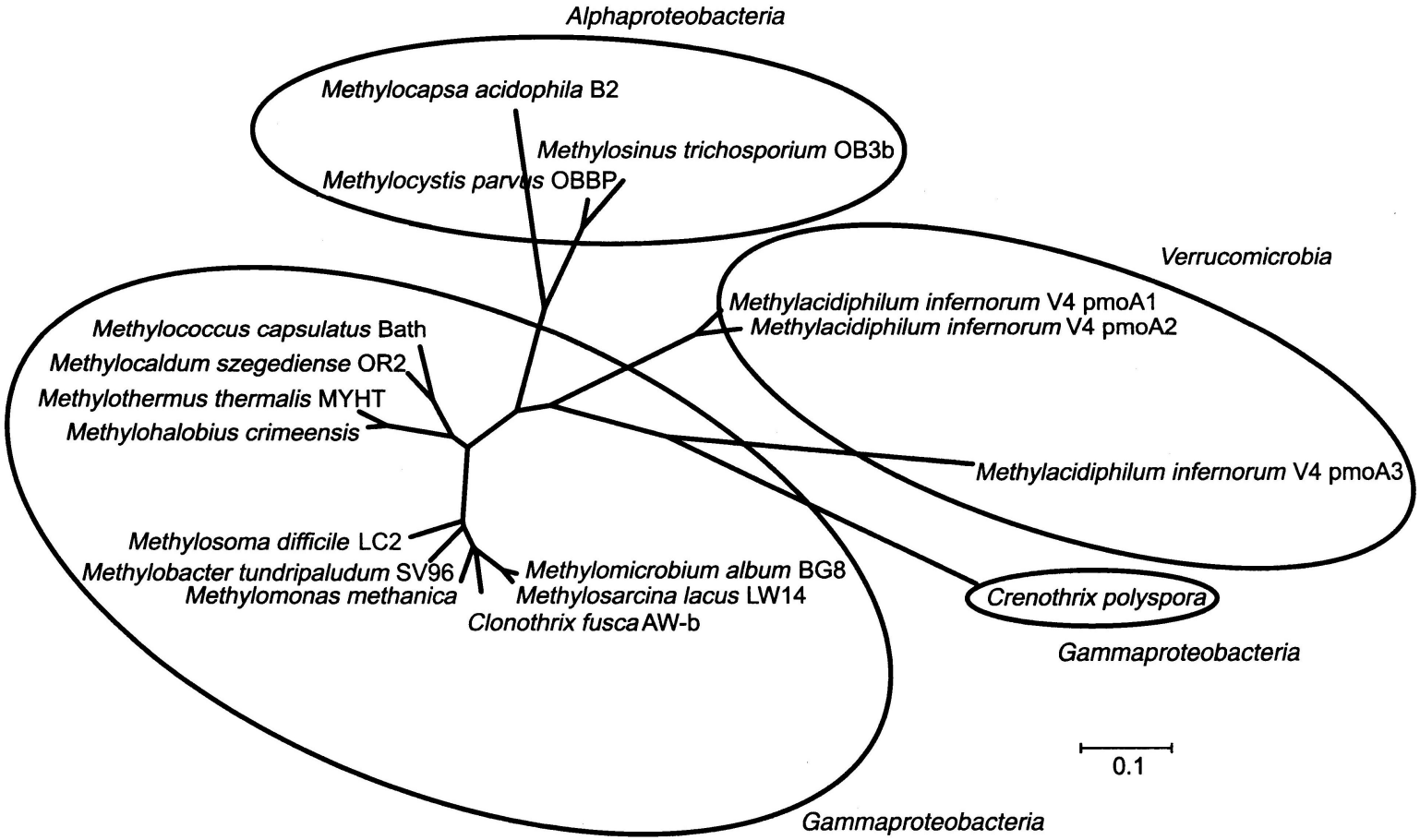

Figure 8: Phylogenetic relationships between known methanotrophs based on deduced *PmoA* sequences using MEGA4. The tree was constructed using the neighbor-joining method with 101 amino-acid positions. The bootstrap consensus tree was inferred from 500 replicates. Evolutionary distances were computed using the PAM Dayhoff matrix. The scale bar indicates 0.1 amino-acid substitutions per site [6].

Table 5: Methane monooxygenase characteristics of methanotrophic genera within Gammaproteobacteria [6].

Characteristic	***Methylobacter***	***Methylococcus***	***Methylomicrobium***	***Methylomona***	***Methylocaldum***
pMMO	+	+	+	+	+
sMMO	-	+	-	-	-
Characteristic	***Methylohalobius***	***Methtyhlothermus***	***Methylosarcina***	***Methylosoma*,**	***Methylosphaera***
pMMO	+	+	+	+	+
sMMO	-	-	-	-	-

Table 6: Methane monooxygenase characteristics of methanotrophic genera within Alphaproteobacteria [6].

Characteristic	***Methylocystis***	***Methylosinus***	***Methylocapsa***	***Methylocella***
pMMO	+	+	+	-
sMMO	Varies between species	+	-	+

Table 7: General characteristics of known families of methanotrophs [6].

Characteristic				
Phylum	*Gammaproteobacteria*	*Alphaproteobacteria*	*Alphaproteobacteria*	*Verrucomicrobia*
Family	*Methylococcaceae*	*Methylocystaceae*	*Beijerinckaceae*	*Methylacidiphilaceae*
Genera	*Methylobacter*, *Methylococcus*, *Methylomicrobium*, *Methylomonas*, *Methylocaldum*, *Methylohalobius*, *Methtyhlothermus*, *Methylosarcina*, *Methylosoma*, *Methylosphaera, Crenothrix, Clonothrix*	*Methylocystis*, *Methylosinus*	*Methylocella*, *Methylocapsa*	*Methylacidiphilum*
RuMP pathway	+	-	-	-
Serine pathway	-	+	+	+
pMMO	+	+	Varies between species	+
sMMO	Varies between species	Varies between species	Varies between species	-

compound with a half-life of less than two minutes in aqueous solutions [83]. Due to its instability, after formation the epoxide is quickly transformed via spontaneous reactions or microbially mediated processes [84]. Methanotrophic degradation of VC will only occur in the presence of O_2 due to the fact that they are obligate aerobes [52]. Oxygen must also be present because it is the reactant molecule inserted into VC. Furthermore, since the process is cometabolic, and since nearly all known methanotrophs are non-facultative [44], methane must also be present in groundwater systems for VC oxidation to occur. Consequently, methanotrophic oxidation of VC is thought to occur at the anaerobic/aerobic interfaces of contaminated aquifers where VC, CH_4 and O_2 are all present [28, 85].

It is known that oxidation of chlorinated hydrocarbons will negatively affect methanotrophic growth for several reasons. First, these pollutants compete with CH_4 for the MMO binding site and, because the pollutant oxidation reaction is fortuitous, inhibit the microbes' ability to ascertain energy. Furthermore, the oxidation of VC consumes vital reducing equivalents needed for microbial growth, and the formation of toxic epoxide by-products adversely affects microbial health [83]. Experimental results have shown that methanotrophs expressing sMMO are capable of degrading pollutants at much faster rates than cells expressing other MMOs [86], yet cells expressing pMMO are able to survive more readily in the presence of chlorinated ethenes, and can actually degrade more of these compounds at high concentrations [87, 88]. The pMMO results are likely due to the greater specificity of pMMO for CH_4 and the subsequent slower rates of pollutant transformation to more toxic products. Thus, these findings suggest that pMMO may play a greater role in *in situ* environmental remediation of VC.

Possible Methanotroph/Ethenotroph Interactions

Etheneotrophs are aerobic, ethene-degrading bacteria that are capable of both fortuitous and growth-linked VC oxidation [89]. Methane and ethene are often present at

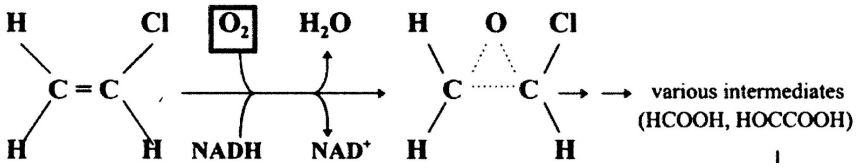

Figure 9: Transformation of vinyl chloride to chlorooxirane [90]

many VC contaminated sites as they are also produced during anaerobic reductive dechlorination of chloroethenes. Their ubiquity suggests that methanotrophs [5] and etheneotrophs [42, 84] could play major roles in oxidative VC degradation in groundwater. Although it is likely that the substrates of these two microorganisms interact, the extent and effects each substrate has on these microbes is not well understood. Microcosm studies using contaminated sediments have shown that in the presence of ethene and VC, methane consumption is inhibited [28]. These results would imply amensalism between the two microorganisms; yet, ethenotrophs possess the necessary enzymatic pathways for degradation of the toxic epoxide intermediate that result from methanotroph oxidation of VC [84]. This knowledge would suggest a synergistic relationship. Furthermore, it has been shown that the chlorooxirane epoxide intermediate stimulates etheneotrophic growth and VC degradation [91]; yet another implication of commensalism. In order to elucidate the dynamics between each bacterial population and the effects of their substrates on one another, a microcosm study measuring changes in substrate concentrations as well as changes in the genomic and transcriptional DNA and RNA levels of key enzymatic pathways is needed.

Quantitative Real-Time Polymerase Chain Reaction

End Point PCR Technology

Polymerase chain reaction (PCR) is a scientific technique in molecular biology used to amplify small amounts of DNA across several orders of magnitude, generating

thousands to millions of copies of a particular DNA sequence. The main components of a PCR reaction are Taq polymerase enzymes, primers targeting a specific DNA sequence, single nucleotide base pairs, and template DNA. Using this mixture, a DNA sequence can be duplicated by cycling the reaction through several temperatures. Typically, the temperature cycle consists of a 95 °C, a 60 °C, and a 70 °C step. During the 95 °C process, double stranded DNA is denatured yielding two single strands of DNA. During the 60 °C step, both primer and enzyme anneal to the single stranded DNA sequence of interest. During the 70 °C process, elongation of the primer is executed by the polymerase enzyme, yielding, at the end of the process, an exact duplicate of the targeted DNA sequence. Theoretically, after each cycle the amount of targeted DNA in each reaction should double. Under these theoretical circumstances, the PCR efficiency of the reaction is said to be 100% [92].

Using the PCR technique, extremely small amounts of DNA (and RNA converted into cDNA by reverse-transcription) can be amplified; however, this amplification technique presents obstacles for accurately quantifying the initial amount of DNA or cDNA in a sample. For example, assuming a 100% amplification efficiency, a PCR of only 20 cycles amplifies the initial amount of DNA or cDNA over a million-fold. With this enormous accumulation there is also potential for huge errors. Now consider a PCR reaction that operates with an efficiency of 95%. In this instance, the original amount of DNA or cDNA will only be amplified approximately 400,000-fold. That is a 60% decrease in amplification compared to the reaction operating with 100% efficiency. Therefore, accurate DNA quantification using the qPCR techniques requires that samples have an amplification efficiencies as close to 100% as possible [92] .

Quantitative End Point PCR

Although it was one of the first techniques developed to quantify DNA, there are major limitations associated with quantitative end point PCR (end point qPCR). In end

point qPCR, DNA (either genomic or cDNA derived from RNA) is amplified for a discrete number of cycles and the resulting products are then subjected to analysis. Typically, the products are visualized through agarose gel electrophoresis and ethidium bromide staining (Figure 10). This is both time consuming and not reliably quantitative. Examination of a PCR amplification plot (Figure 11) shows the reaction going through exponential and linear phases in which the PCR is initially not limited by enzymatic activity or substrates. Eventually, the enzyme activity and/or nucleotide substrates become limiting or exhausted. At this point, the reaction reaches a plateau and, theoretically, all of the samples will reach the same total amount of amplified DNA. This obscures any difference in initial DNA or cDNA abundance. Also, by quantifying PCR products at the end of the reaction after a high number of cycles, any small difference in reaction efficiencies between samples is magnified. For these reasons, the use of the end point qPCR for quantitative analysis is inappropriate [92].

Quantitative Real-Time PCR

The standard for quantitative PCR (qPCR) has become real-time qPCR, which avoids many of the pitfalls of end point qPCR; however, real-time qPCR also has its own caveats [92]. The major difference between real-time PCR and endpoint PCR is the addition of a fluorescence dye to the reaction mixture that binds to DNA and, consequently, emits a fluorescent light. This fluorescent light is then measured after every temperature cycle by a thermocycling instrument. Typical fluorescence measurements for a real-time qPCR assay are shown in Figure 11. While end point qPCR requires that PCR products be detected and quantified after completion of the 40-cycle reaction, real-time qPCR technology allows quantification of PCR products in "real time" during each PCR cycle, yielding a quantitative measurement of PCR products accumulated during the course of the reaction. The real-time PCR approach requires less DNA than end point assays and can more accurately quantity small differences in sample

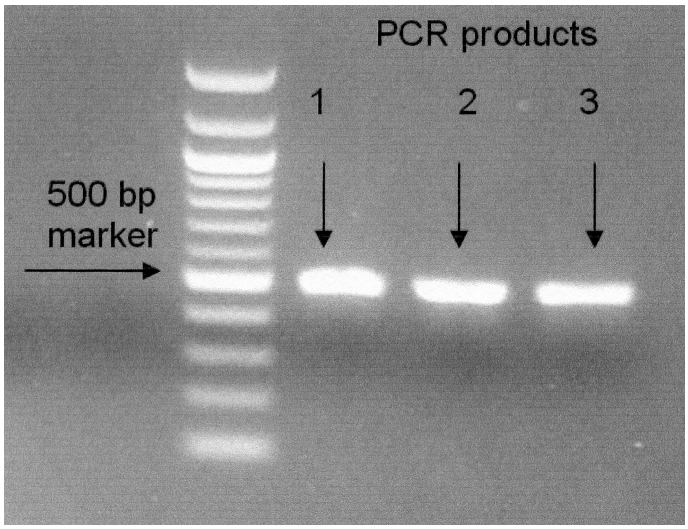

Figure 10: Visualization of end point PCR products via agarose gel electrophoresis and ethidium bromide staining.

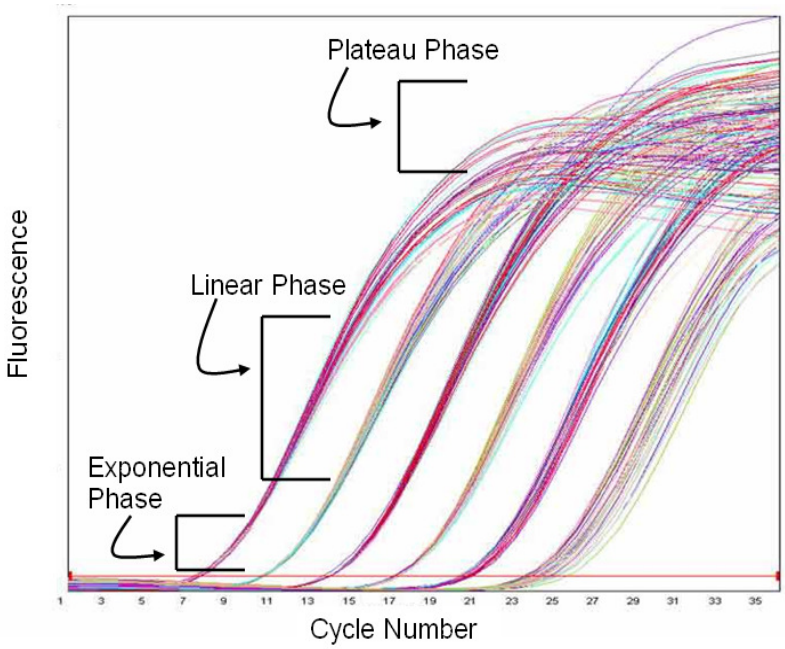

Figure 11: Amplification plot of a real-time qPCR assay showing the exponential, linear, and plateau stages of PCR amplification. This amplification plot also demonstrates that with each additional PCR cycle the mass of DNA in each reaction increases and, subsequently, so also does the amount of fluorescent light emitted by each reaction.

DNA concentrations [92].

SYBR Green Technology

Real-time reactions are carried out in a thermocycler that permits measurement of fluorescence emitted from a detector molecule. One such detector molecule, SYBR Green, is an intercalating dye that fluoresces upon binding to double-stranded DNA. Following primer-mediated replication of the target sequence during PCR, molecules of SYBR Green bind to the product and emit a strong fluorescent signal that is easily detected [92]. As a result, the amount of fluorescence emitted by the SYBR Green dye is directly related to the mass of DNA present in the PCR reaction. Thus, after every cycle of a PCR reaction containing SYBR Green, the mass of DNA in the reaction increases and, consequently, the amount of fluorescent light emitted by the detector molecules also increase.

Intercalating dyes are inexpensive, simple to use and, because they are not sequence-specific, can be used for any reaction. However, because these molecules do not discriminate between gene sequences, it is possible for non-specific PCR products and primer dimer artifacts to contribute to the fluorescence detection captured by the thermocycling instrument [92], ultimately resulting in inaccurate quantification of sample target DNA. Non-specific PCR products are sequences produced when primers bind non-specifically to template DNA that is not the targeted sequence of interest. Primer dimer artifacts occur when weak interactions between primer pairs cause binding and amplification of short PCR products called primer dimers [93].

To ensure that neither primer-dimers nor non-specific PCR products are contributing to sample quantifications, a dissociation curve is required when using SYBR Green. A dissociation curve is produced at the end of a real-time PCR cycle by ramping up the temperature in each reaction tube by small increments and, after each temperature increase, measuring the florescence emitted from a specific reaction. At a certain

temperature, the PCR products produced during the 40-cycle amplification process will denature causing the fluorescence in that reaction to drastically decrease. Due to the chemistry of DNA, double-stranded nucleotides will separate at specific temperatures based on their exact sequence. Thus, if neither primer-dimers nor non-specific PCR products are being produced, then there will only be one DNA sequence present in a given PCR reaction. Consequently, the resulting dissociation curve for that reaction will only show a single peak temperature (Figure 12). However, if there are non-specific products being produced, then multiple DNA sequences will be present in the PCR reaction and the resulting dissociation curve will show several peak temperatures, each corresponding to a different PCR product sequence. Therefore, when using SYBR Green as a detection method in real-time qPCR, it is very important that the dissociation curve show only one peak.

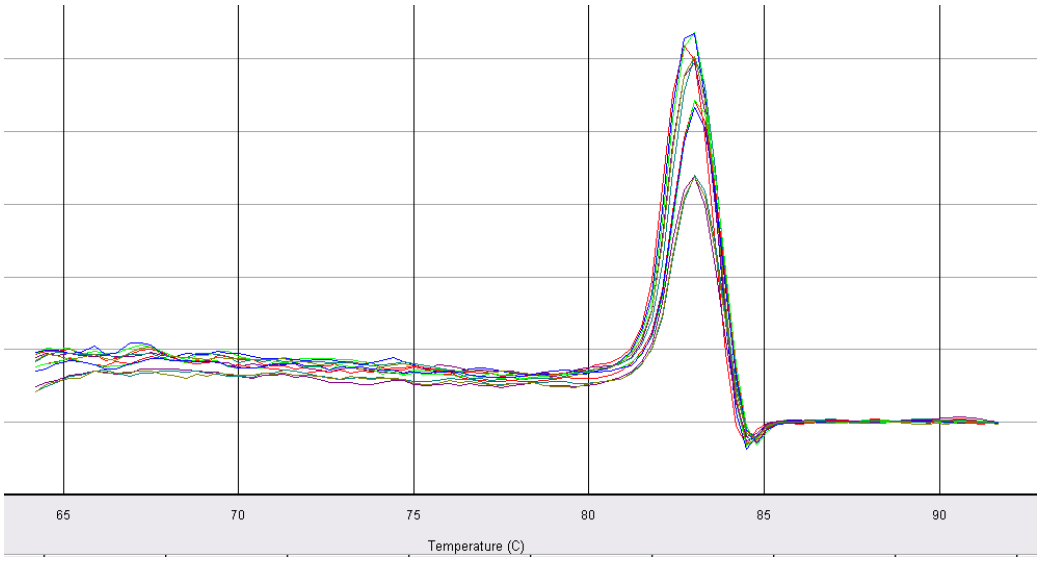

Figure 12: Ideal dissociation curve for a qPCR reaction. As demonstrated by the single peak temperature of the dissociation curve, this PCR reaction only contained PCR products from the targeted DNA sequence. Primer dimers and non-specific PCR products were not formed during this reaction.

Quantitative Real-Time PCR Standard Curves

For absolute quantifications, a DNA standard curve of the gene of interest is required in order to calculate the number of copies. In this case, a serial dilution of a known amount (number of copies) of pure DNA is diluted and subjected to amplification. Like a protein assay, the unknown signal is compared with the curve to extrapolate the starting concentration. Figure 13 demonstrates a typical qPCR standard curve.

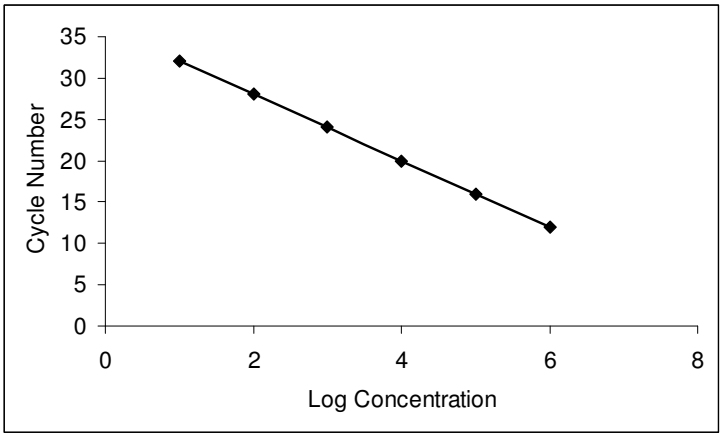

Figure 13: Standard curve plot for a typical qPCR assay. The plot demonstrates that as the standard concentration increases, the cycle at which the instrument is able to measure fluorescence in that reaction is lowered.

Degenerate Primers and Primer Bias

Primer bias is a phenomenon that occurs during PCR when a primer binds and amplifies certain sequences preferentially to others. This bias is attributed to differences in primer binding energy. For example, if a primer has one mismatch base pair with a target sequence, the amplification efficiency will be very low, and consequently, a large bias in the amplification process will occur. To avoid this phenomenon, PCRs containing multiple template sequences (such as those in environmental samples) should use a degenerate primer. Degenerate primers are obtained by using a mixture of primers with

nucleotide sequences corresponding to various homologs of the target sequence. Although degenerate primers lower the chance of primer bias, they do not eliminate the phenomenon completely [94].

DNA, Proteins, and Messenger RNA Transcript

DNA is a linear, double-helical structure whose biological role is to carry information, in the form of genes, which specify the chemical composition of proteins. Proteins play an important role in the cell as active agents, such as enzymes, in cellular processes. The first step taken by the cell to make a protein is to transcribe, or copy, a DNA sequence into a complimentary single stranded RNA molecule known as messenger RNA (mRNA). Messenger RNA is then used by ribosomes in the cell to synthesize protein. Since mRNA is only present in cells when the protein is being synthesized, the presence and abundance of these transcripts can be indicative of the enzymatic activity of a cell. For this reason, mRNA transcripts pMMO and sMMO are of interest in this research, as they will be able to demonstrate that methanotrophs are actively synthesizing the pMMO and sMMO enzymes that are capable of VC oxidation. In the lab, mRNA transcripts are converted to DNA by a process known as reverse transcription. The product of mRNA reverse transcription is a DNA molecule known as cDNA [95].

Pyrosequencing

Pyrosequencing is a DNA sequencing technique that is based on the detection of released pyrophosphate (PPi) during DNA synthesis. In a cascade of enzymatic reactions, visible light is generated that is proportional to the amount of PPi released, which in turn is proportional to the number of DNA nucleotides that are incorporated into a sequence. The cascade starts with a nucleic acid polymerization reaction in which inorganic PPi is released as a result of nucleotide incorporation by polymerase. The released PPi is subsequently converted to adenosine triphosphate (ATP) by ATP sulfurylase, which provides the energy to luciferase to oxidize luciferin and generate

light. Because the added nucleotide is known, the sequence of the template can be determined. Pyrosequencing can be used at contaminated sites to help elucidate the microbial ecology of the pollutant degrading bacteria, as well as corroborate qPCR data [96]. Figure 14 shows the reaction cycle of the pyrosequencing process.

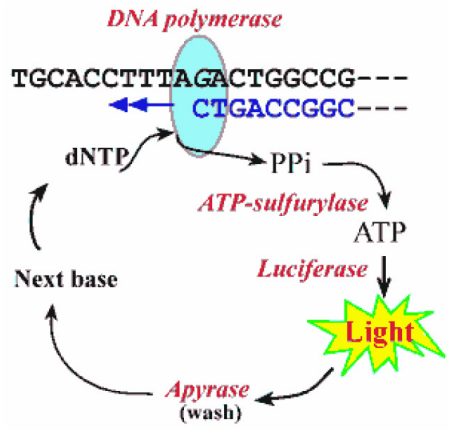

Figure 14: Enzymes and process flow for pyrosequencing technique. Apyrase is an enzyme that catalyzes the hydrolysis of ATP to adenosine monophosphate (AMP). This step of the process ensures that leftover ATP from a previous reaction will not falsely elevate light production in the next cycle [97].

Contaminated site info

Soldotna, Alaska

The River Terrace RV Park (RTRVP) site is located in Soldotna, Alaska, adjacent to the Kenai River, a renowned sport fishing location on the Kenai Peninsula. From the mid-1960s to the late 1980s, a dry cleaning facility operated at this site. Due to inappropriate storage of the dry cleaning solvent PCE, the groundwater below this site became contaminated with PCE [98].

The remedial strategy chosen at this site was bioremediation using Hydrogen Releasing Compound (HRC). It was anticipated that the use of HRC would drive the

aquifer anaerobic and promote reductive dechlorination of PCE to ethene prior to migrating off site. HRC was injected in six phases at the site, in October 2000, June 2001, October 2003, August 2005, October 2006 and August 2009. After each injection, groundwater monitoring showed a significant drop in PCE concentrations; however, it was discovered that, although some ethene was generated, a majority of the reductive dechlorination occurring at this site was stalling at the VC daughter product. This stall resulted in the accumulation of VC in the groundwater system. In addition to the generation of ethene and VC, the injection of HRC into the groundwater system also resulted in the production of large amounts of methane [99]. The resulting VC plume, containing methane, ethene, and VC, migrated towards the Kenai River where dissolved oxygen is present. Since methane, ethene, oxygen and VC are present, Soldotna provides an excellent environmental site where groundwater samples can be evaluated for the presence of methanotrophs and their role in VC oxidation.

A series of C-radiotracer-based microcosm experiments were conducted in 2004 to assess, among other things, the products being generated by microbial dechlorination of TCE, DCE, and VC in sediments at the River Terrace RV Park [100, 101]. In these experiments, the mechanism of TCE biodegradation was primarily reductive dechlorination to the reduced products, DCE and VC, whereas biodegradation of DCE and VC involved net oxidation to CO2 [100]. This aerobic VC oxidation was measured in microcosms contained sediment collected down gradient from MW6. This evidence would suggest a possible role for oxidative degradation of VC by methanotrophs. Figure 15 shows the Soldotna contaminated site and the location of sampling wells tested in this research. For more photos of the Soldotna site, see APPENDIX B: Figure B 1and Figure B 2.

Naval Air Station Oceana, Virginia

Naval Air Station (NAS) Oceana, located in Virginia Beach, Virginia, was

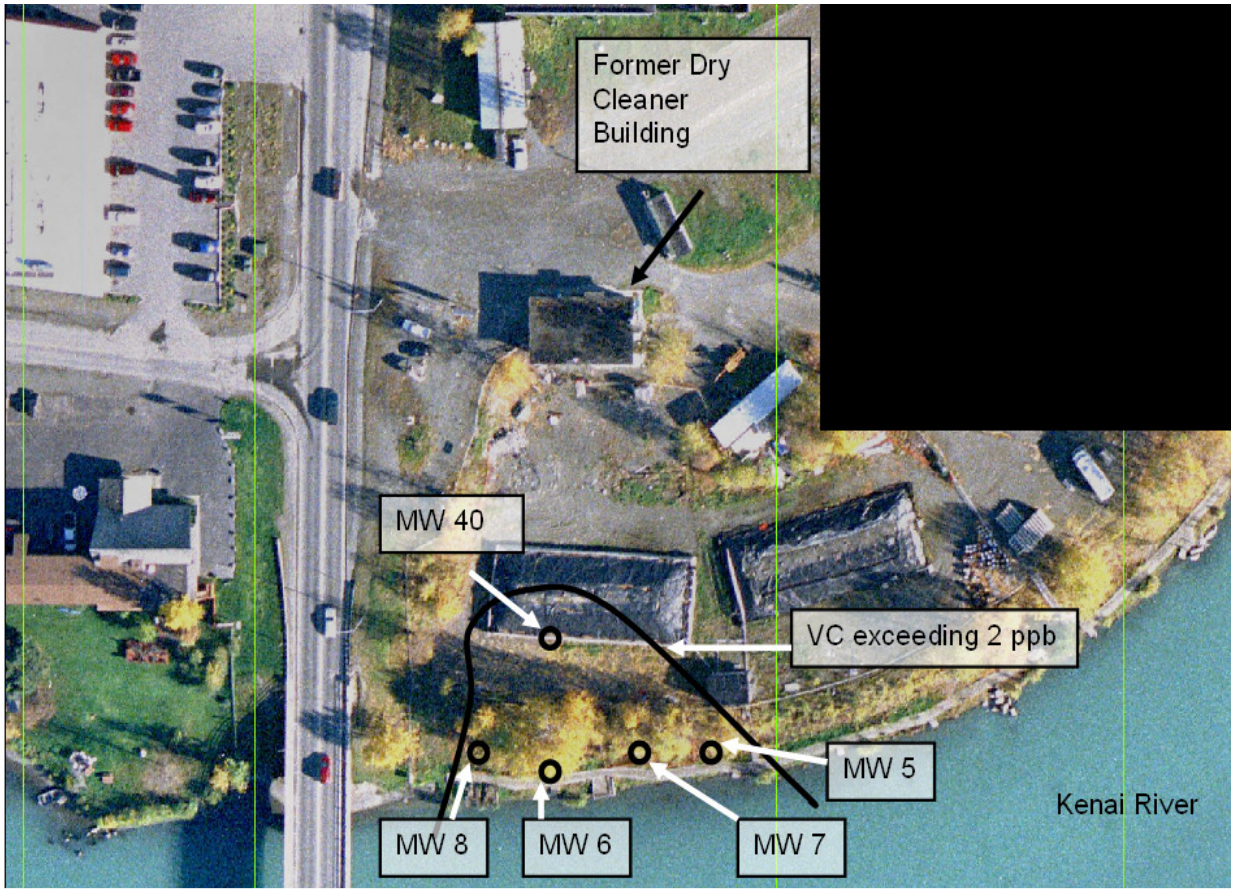

Figure 15: VC Contaminated groundwater site in Soldotna, Alaska. Monitoring wells 5, 6, 7, and 8 are near the rivers edge where oxygen is present, and oxidative degradation is likely to occur [99].

established in 1940 as a small auxiliary airfield. Since then, NAS Oceana has grown to more than 16 times its original size and is now a 6,000-acre master jet base supporting a community of nearly 20,000 Navy personnel and dependents. The operational growth of this facility coupled with historical disposal of various maintenance and cleaning chemicals, many of which contained TCE, resulted in VC contamination at the NAS Oceana site. The area of contamination, located near solid waste management unit 2C (SWMU 2C), has been and is currently being used for aircraft maintenance and cleaning. Two areas of the SWMU 2C site, a north and a south plume, contained substantially elevated levels of VC. Utilizing these two dilute VC plumes, a field study was conducted which compare the outcome of aerobic and anaerobic enhanced bioremediation [102].

The remedial strategy for the north plume was aerobic degradation of VC. Accordingly, Oxygen Releasing Compound (ORC) was injected into the contaminated groundwater [103]. Although methane was not monitored in all of the north plume wells, monitoring well 18 showed the presence of methane in its waters (Figure 16). The remedial strategy for this plume, along with the presence of methane, made it an interesting environmental site for this research. Since methanotrophs are aerobic oxidizers of VC, the injection of oxygen in the presence of methane may be stimulating these microbes to degrade VC. The remedial strategy for the south plume was anaerobic degradation of VC. Accordingly, emulsified vegetable oil was used as an electron donor to promote reductive dechlorination of VC. Results showed that the average VC concentrations in the north plume area were reduced by 67%. For the south plume, the average VC concentrations were reduced by 69% [103, 104]. Figure 16 shows the NAS Oceana contaminated site and the location of sampling wells tested in this research.

Carver, Massachusetts

A landfill waste disposal facility, located in Carver, Massachusetts, is the site of VC contamination that resulted from the dumping of polymer-concrete landing-strip

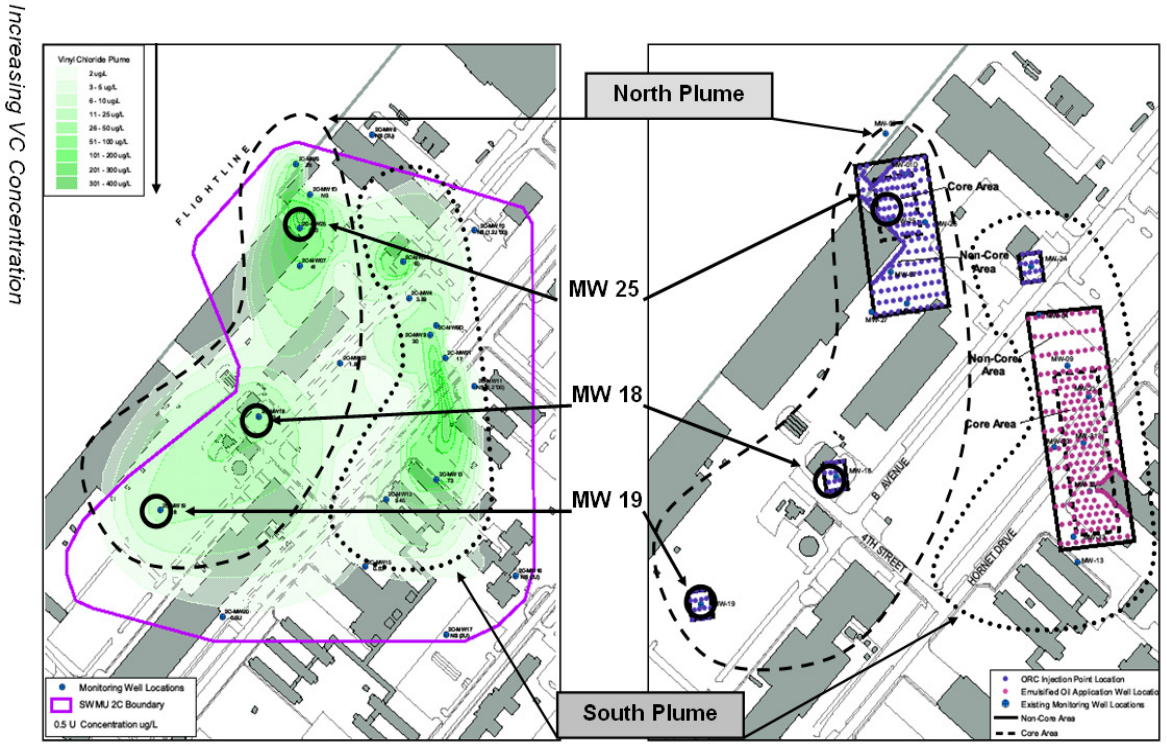

Note: For more information on NAS Oceana site, see APPENDIX B: Figure B 3, Figure B 4, and Figure B 5.

Figure 16: VC Contaminated groundwater at Naval Air Station Oceana. Monitoring wells 18, 19, and 25 are in the north plume aerobic treatment zone, where methanotrophs may be playing a role in VC degradation. The left hand side of the figure illustrates the extent of the VC plume. The purple dots on the right hand side of the figure indicate the oxygen injection points.

materials from a local Air Force Base in the 1970's [105]. It was discovered later that the polymer-concrete contained PCE. Disposal of the polymer in the landfill caused groundwater contamination with PCE and a subsequent VC plume. The remedial strategy chosen at this site was bioremediation using direct injection of oxygen. It was anticipated that the supplemental oxygen would stimulate aerobic degradation of VC. The remedial strategy for this plume, along with the presence of methane at this site [106, 107], made it an ideal environmental location for this research. Since methanotrophs are aerobic oxidizers of VC, the injection of oxygen in the presence of methane may be stimulating cometabolic degradation of VC by these microbes. Figure 17 shows the Carver contaminated site and the location of sampling wells tested in this research.

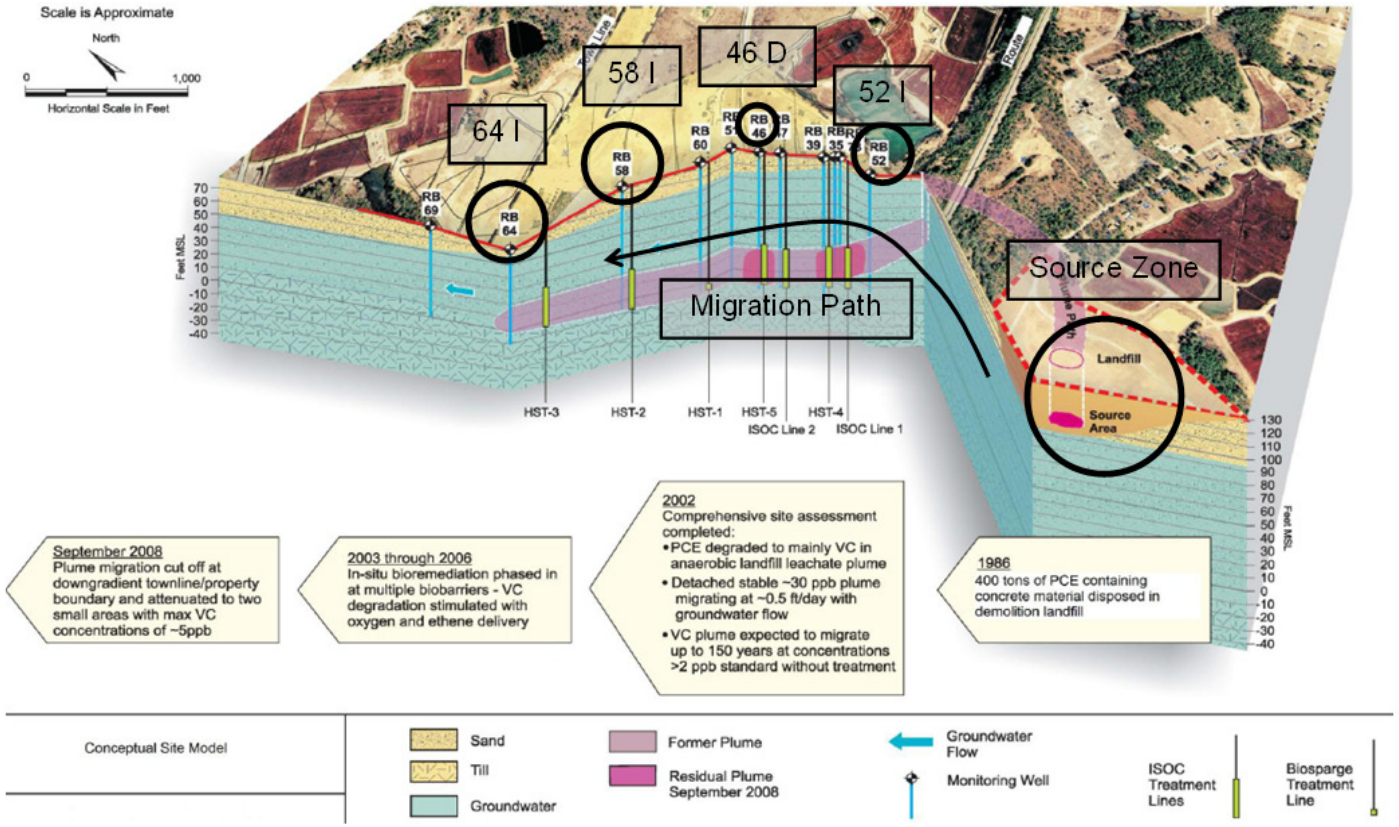

Figure 17: VC Contaminated groundwater in Carver, Massachusetts [107]. The presence of methanotrophs in monitoring wells 46 D, 52 I, 58 I, and 64 I was evaluated in this research.

CHAPTER 3

MATERIALS AND METHODS

Chemicals and Growth Media

Methane (99.995%) was from Airgas, and all other chemicals were reagent grade or better. One liter of minimal salts medium (MSM) was prepared as follows: 0.95 g KH_2PO_4, 2.27 g K_2HPO_4, 0.67 g $(NH_4)SO_4$ per liter of deionized water. MSM was autoclave sterilized at 121 degrees Celsius (°C) for 30 minutes. One liter of trace metals solution (TMS) was prepared as follows: 60 g $MgSO_4 \cdot 7H_2O$, 6.37 g EDTA ($Na_2(H_2O)_2$), 1 g $ZnSO_4 \cdot 7H_2O$, 0.5 g $CaCl_2 \cdot 2H_2O$, 2.5 g $FeSO_4 \cdot 7H_2O$, 0.1 g $NaMoO_4 \cdot 2H_2O$, 0.1 g $CuSO_4 \cdot 6H_2O$, 0.2 g $CoCl_2 \cdot 6H_2O$, 0.52 g $MnSO_4 \cdot H_2O$ per liter of deionized water. TMS was not autoclaved and was stored at 4°C in a foil wrapped container to prevent photodegradation.

Bacterial Strains, Culture Conditions, and Cell Line Maintenance

Two species of methane oxidizing bacteria, *Methylococcus capsulatus* (ATCC 33009, Type I methanotroph) and *Methylocystis* sp. strain Rockwell (ATCC 49242, TypeII methanotroph), were used in this study. Methanotroph cultures were grown in modified 1 liter Erlenmeyer flasks containing MSM (250 mL, Figure 18), filter-sterilized TMS (500 µL), and filter-sterilized methane (60 mLs). Polyvinylidene fluoride (PVDF) filters from Millpore (Millex, 0.22 µm) were used for filter sterilizations. M. *capsulatus* cultures were incubated at 37 °C while *Methylocystis* sp. cultures were grown at room temperature (RT, ~25°C). Both cultures were agitated on a circular shaker operating at 200 revolutions per minute (rpm). For cell line maintenance, frozen stocks were made of each bacterial strain. When cultures reached mid-exponential growth phase, they were pelleted via centrifugation (5 min, 5000 rpm), resuspended in either MSM or MSM/glycerol (50% MSM, 50% glycerol), and stored at -80°C. M. *capsulatus* required

the added glycerol while *Methylocystis* sp. strain Rockwell did not. To revive the *Methylocystis* cell line, thawed frozen-stock was added directly to fresh media. Due to the presence of glycerol in the M. *capsulatus* frozen stocks, it was necessary to wash them twice in sterile MSM before cells could be added to growth media. A single wash step consisted of the following: (1) resuspending frozen stock in 25 mLs sterile MSM, (2) pelleting cells in centrifuge (5 min, 5000 rpm), (3) removing supernatant.

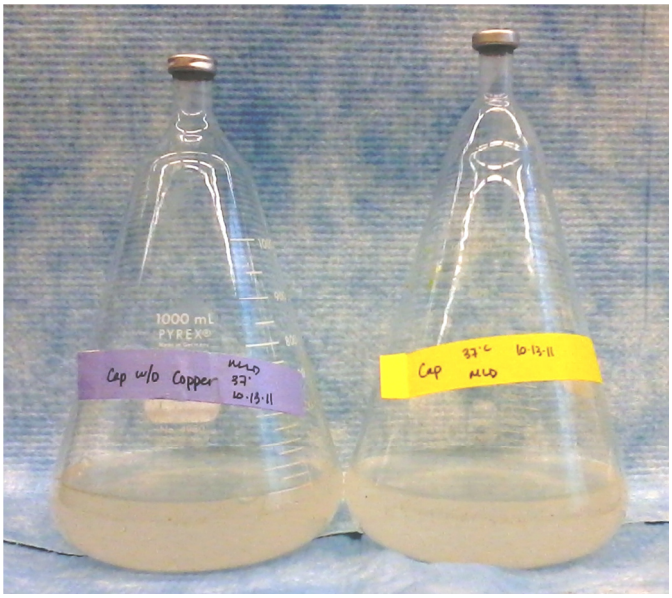

Figure 18: Modified Erlenmeyer flasks used to culture methanotroph bacterium.

DNA Extraction from Pure Cultures and Sterivex Filters

DNA was extracted from methanotroph pure cultures using the MO BIO Ultra Clean Soil DNA kit (MoBio, #12800-50) according to the manufacturer's protocol or using a previously reported bead-beating extraction method [42] with the cells grown on MSM and methane (0.44 mg/mL) instead of trypticase soy agar and glucose (TSAG). DNA extracted from pure cultures was used as a template in endpoint PCR procedures.

Removal of genomic DNA from Sterivex filters was performed using the MO BIO PowerSoil DNA extraction kit and a modified manufacturer's protocol, as earlier reported [89], or using the MO BIO PowerWater DNA extraction kit according to the manufacturer's protocol. The modified PowerSoil protocol increased DNA yield by 43% [89] as compared to the un-altered PowerSoil protocol [42].

To monitor DNA losses during the extraction process, a Luciferase gene control was used. Luciferase is used as an external gene control because it is a very rare gene only found in fireflies, therefore, it would not be mistaken for any other gene in the methanotroph genome. After genomic DNA or RNA is removed from the sterivex filter, $7.5x10^7$ copies of the Luciferase gene were added to each environmental sample. At the end of the extraction process, the copies of Luciferase gene were measured using a qPCR standard curve (as described in Real-time PCR Procedures Section), and a percent recovery was calculated. That percent recovery was then used to adjust gene abundance calculations from environmental samples [108]. For more information regarding the use of Luciferase percent recoveries to calculate gene abundance see Real-time PCR Procedures Section.

End Point PCR Procedures

PCR mixtures (50 µL) contained 25 µL of Qiagen HotStart PCR Master Mix, 2 µm of each primer, and 100 ng of template DNA. The thermocycling protocol consisted of one cycle at 95°C (5 min), 55°C (1 min), 72°C (30 sec), followed by 40 cycles of 94°C (1 min), 55°C (1 min), 72°C (30 sec), and concluded with a final extension cycle (72°C, 10 min). Agarose gel electrophoresis was used to visualize the PCR products, which were then purified using the Qiagen PCR purification kit (#28104). DNA concentrations were measured on a Qubit fluorometer (Invitrogen) using the Quanti-IT dsDNA BR assay (Invitrogen). Selected PCR products were used as the template for qPCR standard curves.

Real-time PCR Procedures

Real-time PCR was performed by the DNA Facility at the University of Iowa using an ABI 7000 Sequence Detection System (Applied Biosystems). Each assay consisted of a 3 stage process. Stage 1: 1 cycle of 95°C for 10 min (DNA denaturing), stage 2: 40 cycles of 95°C (15 sec, denaturation step) and either 60°C for 1 min (annealing, elongation, and data collection), and stage 3: a PCR product dissociation curve. For construction of the dissociation curve, the temperature inside each reaction was increased in small intervals (0.3 – 0.4°C) from 65-95°C. After each temperature increase, fluorescence in each reaction well was measured and plotted (for more information on dissociation curves see SYBR Green Technology Section). PCR mixtures were prepared in 25 µL volumes using 12.5 µL of Power SYBR Green PCR Master Mix (Applied Biosystems), 100 nM to 800 nM of primer (as determined in qPCR Primer Optimization Experiments), 2 µL of DNA template (DNA concentration varied 0.16 – 19.48 ng/ µL), and 400 ng/µL Bovine Serum Albumin (BSA; New England Biolabs). Environmental samples may contain humic substances that can interfere with the PCR process. BSA was added to alleviate this PCR inhibition [109, 110]. Standard curves were constructed for each primer set using PCR products as template. The number of gene copies per µL of PCR product was calculated by the following equation (Applied Biosystems):

$$\frac{copies}{uL} = \frac{\left[DNA\ concentration\ \left(\frac{pg}{uL}\right)\right] \times \left[6.023 \times 10^{23}\ \left(\frac{bp}{mole\ bp}\right)\right]}{\left[PCR\ product\ size\ \left(\frac{bp}{copy}\right)\right] \times \left[660\ \left(\frac{g}{mole\ bp}\right)\right] \times \left[10^{12}\ \left(\frac{pg}{g}\right)\right]}$$

Avogadro's number is 6.023 x 10^{23} molecules per 1 mole, and the average molecular weight of double stranded DNA is 660 g/mole. ABI 7000 System SDS Software (Applied Biosystems) was used to analyze real-time PCR fluorescence data.

Data analysis was performed using the proprietary software provided for the Applied Biosystems 7000 System. The "auto" function was used to determine the threshold fluorescence values (used for determining the threshold cycle Ct) for each set of standards and samples analyzed.

To normalize gene copy quantifications to the amount of groundwater tested, the following equations were used:

Reference DNA Recovery Ratio

$$RDRR = \frac{[Quantified\ Gene\ Copies/PCR\ Rxn)] \times [DNA\ Elution\ Volume\ (uL)]}{[Total\ Gene\ Copies\ Added\ before\ Extraction] \times [Template\ DNA\ (uL)]}$$

RNA Transcript Copies per Liter Groundwater

$$\frac{RNA\ TC}{L\ GW} = \frac{[Transcript\ Copies/PCR\ Rxn] \times 4 \times [RNA\ Elution\ Volume\ (uL)]}{[RDRR] \times [Template\ cDNA\ (uL)] \times [GW\ Sample\ Volume\ (L)]}$$

DNA Gene Copies per Liter Groundwater

$$\frac{DNA\ GC}{L\ GW} = \frac{[Quantified\ Gene\ Copies/PCR\ Rxn] \times [DNA\ Elution\ Volume\ (uL)]}{[RDRR] \times [Template\ DNA\ (uL)] \times [GW\ Sample\ Volume\ (L)]}$$

PCR efficiency was calculated using the following equation. An ideal slope of -3.32 cycle #/ Log [concentration] would yield an efficiency of 100%.

$$PCR\ Efficiency = \left[\left(10^{-1/slope}\right) - 1\right] \times 100$$

Real-time PCR Primer Sets

A list of all primers used in this study can be found in Table 8. Eight primer sets from the literature were compiled and evaluated to determine which pairs most accurately detected methanotroph populations in groundwater qPCR assays. Four primer sets targeted the *pmoA* gene encoding β-subunit of the particulate methane monooxygenase enzyme (pMMO), three targeted the 16S rRNA gene, and one targeted the *mmoX* gene encoding a subunit of the soluble MMO enzyme (sMMO). The specific pmoA primer sets were as follows: A189 F (GGN GAC TGG GAC TTC TGG) and Mb661 R (GGT AAR GAC GTT GCN CCG) [8], pmof1 (GGG GGA ACT TCT GGG GIT GGA C) and pmor (GGG GGR CIA CGT CIT TAC CGA A) [111], pmof2 (TTC TAY CCD RRC AAC TGG CC) and pmor [111], and A189 F and mb661r (CCG GMG CAA CGT CYT TAC C) [112, 113]. Hereafter, these primer sets will be referred to as Kolb, pmoA 330, pmoA 178 and pmoA 472, respectively.

The 16S primer sets each targeted a separate conserved region of the rRNA gene which allowed for identification of distinct bacterial populations. One primer set detected bacteria universally, while the other two sets amplified the rRNA gene of either type 1 or type 2 methanotrophs. The specific 16S primer sets were as follows: 16S universal primers – 16SU f (TCC TAC GGG AGG CAG CAG T) and 16SU r (GGA CTA CCA GGG TAT CTA ATC CTG TT) [114], 16S type 1 methanotroph primers – U785F (GGA TTA GAT ACC CTG GTA G) [115] and MethT1bR (GAT TCY MTG SAT GTC AAG G) [116], 16S type 2 methanotroph primers – U785F and MethT2R (CAT CTC TGR CSA YCA TAC CGG) [116]. Hereafter, these primer sets will be referred to as 16S U, 16S T1 and 16S T2, respectively. The mmoX primer set was as follows: 536f (CGC TGT GGA AGG GCA TGA AGC G) and 898r (GCT CGA CCT TGA ACT TGG AGC C) [113, 117], and hereafter will be referred to as mmoX.

It should be noted that based on the phylogenetic trees in the literature review, these primer sets will likely be biased against the Methylacidophilium and Crenothrix

methanotrophs because their sequences appear far removed from the rest of the methanotroph family. Primer bias occurs when primers do not efficiency bind to certain species sequence and therefore, do not show a true picture of the microbial population based on those primers.

Optimization of Real-time PCR Primer Concentrations

The pmoA 178, pmoA 330, 16S T1, and 16S T2 primer sets were assayed to find their optimal working concentrations. For pmoA 178 and pmoA 330, approximately 15 qPCR plates were run amplifying template NDA with primer concentrations ranging from 200 nM to 1000 nM. Both pmoA primer sets (pmoA 178 and pmoA 330) were used to amplify both our isolated methanotroph DNA templates (*Methylococcus* sp. and *Methylocystis* sp.). The goal of this experiment was to determine the optimal standard templates, primer set, and primer concentration for these specific primer sets.

For 16S T1 and 16S T2, approximately 5 qPCR plates were run amplifying template DNA with primer concentrations ranging from 200 nM to 1000 nM. The 16S T1 primer set amplified from the Type I methanotroph DNA (*Methylococcus* sp.); while the 16S T2 primers amplified form the Type II methanotroph DNA (*Methylocystis* sp.). The goal of this experiment was to determine the optimal primer concentration for these specific primer sets.

Primer Validation and Comparison

In order to validate each primer set, known amounts of methanotroph DNA were quantified using the pmoA 178, 330, 16S T1, and T2 primer sets and subsequently compared. Assuming there is one copy of each gene per organism genome, then this technique would be expected to validate the qPCR primers because the gene abundance derived from them would be with in the same order of magnitude. Genomic DNA was extracted from *Methylococcus capsulatus* (Type I) and *Methylocystis* sp. strain Rockwell (Type II) and used to assemble 5 different mixtures of Type I and Type II methanotroph

Table 8: Oligonucleotides used in this study.

Primer Set	Sequence	Target Gene	Product Length	Reference
Kolb		**pMMO**	**472**	**[8]**
A189 F	GGN GAC TGG GAC TTC TGG			
Mb661 R	GGT AAR GAC GTT GCN CCG			
pmoA 330		**pMMO**	**330**	**[111]**
pmof1	GGG GGA ACT TCT GGG GIT GGA C			
pmor	GGG GGR CIA CGT CIT TAC CGA A			
pmoA 178		**pMMO**	**178**	**[111]**
pmof1	GGG GGA ACT TCT GGG GIT GGA C			
pmof2	TTC TAY CCD RRC AAC TGG CC			
pmoA 472		**pMMO**	**472**	**[112, 113]**
A189 F	GGN GAC TGG GAC TTC TGG			
mb661r	CCG GMG CAA CGT CYT TAC C			
16S U		**16S Universal**	**466**	**[114]**
16SU f	TCC TAC GGG AGG CAG CAG T			
16SU r	GGA CTA CCA GGG TAT CTA ATC CTG TT			

Table 8 continued

Primer Set	Sequence	Target Gene	Product Length	Reference
16S Type 1		**16S Type 1**	**221**	**[115, 116]**
U785F	GGA TTA GAT ACC CTG GTA G	**Methanotroph**		
MethT1bR	GAT TCY MTG SAT GTC AAG G			
16S Type 2		**16S Type 2**	**232**	**[115, 116]**
U785F	GGA TTA GAT ACC CTG GTA G	**Methanotroph**		
MethT2R	CAT CTC TGR CSA YCA TAC CGG			
mmoX		**sMMO**	**362**	**[113, 117]**
536f	CGC TGT GGA AGG GCA TGA AGC G			
898r	GCT CGA CCT TGA ACT TGG AGC C			

DNA. The mixtures were as follows: 100% (T1); 75:25 (T1:T2); 50:50 (T1:T2); 25:75 (T1:T2); 100% (T2). The concentration of each mixture was 5 ng/uL, with a total of 15 ng used per reaction. The mixtures were as follows: 100% (T1); 75:25 (T1:T2); 50:50 (T1:T2); 25:75 (T1:T2); 100% (T2). The concentration of each mixture was 5 ng/uL and 3 uL were used per reaction for a total of 15 ng/rxn.

Pyrosequencing Analysis and Phylogenetic Trees

Sequence data was collected from the Carver, MA site using the Pyrosequencing technique. This sequence data was then used to construct phylogenetic trees of the methanotroph populations in these tested wells. Phylogenetic trees were constructed using Silva and Seaview software programs. Sequences were uploaded to the Sina aligner on the Silva website where they were aligned using the default alignment parameters. The Silva browser was then used to retrieve appropriate methanotroph references sequences as well as an out group from the *Bacteroides* genus. Sequences alignments were manually trimmed in Seaview, and the final alignment sequences contained 620 nucleotides. Within Seaview, the PhyML program was run using the GTR+G model to construct a maximum likelihood phylogeny. Trees were edited in Archaeopteryx. Data analysis and phylogenetic tree construction was done in collaboration with Josh Livermore.

CHAPTER 4

RESULTS AND DISCUSSION

One of the objectives of this research was to develop a qPCR method for detecting the abundance and activity of methanotrophs in dilute VC groundwater plumes. To accomplish this task, literature articles were reviewed to find qPCR specific primers targeting the methanotroph pMMO functional gene. Particulate MMO was targeted due to the fact that it is present in nearly all methanotrophs [6] and because it is the functional gene in the methanotroph VC degradation pathway. Thus, measuring levels of pMMO genomic DNA and mRNA in groundwater would allow for estimations of methanotroph abundance and activity. Specifically, primers targeted the gene encoding for the β-subunit (*pmoA*) of the pMMO gene.

Initially, the only qPCR-specific primers targeting *pmoA* found in the literature were designed by Kolb et al [8]. However, reliable amplification of *pmoA* from pure culture methanotroph DNA using end point PCR techniques was not possible with these primers and thus, they were not used in the remainder of this study. For Kolb primer results, see APPENDIX A. Other *pmoA* primers sets, pmoA 178 and pmoA 330, were discovered in the literature and, though not specifically designed for qPCR, were rigorously evaluated to determine their usefulness in such assays. The first step was to evaluate the PCR efficiencies of standard curves constructed using these primer sets. Initially, PCR efficiencies were inconsistent from assay to assay, ranging from 70% to 125%. It was discovered that this inconsistency was most likely attributed to the freshness of the serial dilutions. In order to increase their reproducibility, the serial dilutions were made fresh for every experiment, and the primer concentrations were optimized as well. PCR inconsistencies for pmoA 178 and pmoA 330 are discussed further in APPENDIX A. Furthermore, using two primer sets to amplify two sets of pure culture template DNA resulted in four separate standard curves. Since only one standard

curve is necessary to detect *pmoA* in environmental samples, creating four standards curves for every experiment would not only waste valuable time and resources, but would also be needless. Thus, in addition to optimizing primer concentrations, it was also necessary to determine the optimal standard templates and primer set.

Primer Optimization

Optimizing pmoA 178 and pmoA 330 Primer Concentrations

The goal of this experiment was to determine the optimal standard templates, primer set, and primer concentration so that a single standard curve can be used in the remainder of our methanotroph qPCR experiments. To that end, standard curves were constructed using both pmoA 178 and pmoA 330 primer sets, amplifying from both isolates of methanotroptophs (*Methylococcus* and *Methylocystis*), and with primer concentrations varying from 200 nM to 1000 nM. To ensure equal comparison between primer sets, template species, and primer concentrations, the standard curve dynamic ranges were limited to 100-10^6 copies per reaction and data was analyzed using the "auto CT analysis" function of the proprietary Applied Biosystems 7000 System software.

The results of this experiment revealed that, when *Methylocystsis* sp. and *Methylococcus* sp. template DNA was amplified, the optimal standard curves for the pmoA 178 primer set occurred when the primer concentrations were 300*[1] nM and 200

[1] Throughout the course of this study, attempts were made to optimize experimental conditions and increase PCR efficiencies. One such attempt included manual analysis of CTs. This analysis altered the PCR efficiencies such that the optimal primer concentration for pmoA 178/*Methylocystis* was thought to be 300 nM. The 300 nM concentration was used for all remaining experiments, including the assessment of environmental samples. It was later decided that, due to the unknown effects of the manual CT analysis, the auto CT analysis was most appropriate. Upon reanalyzing with auto CT, the optimal PCR efficiency was found to be 200 nM. Table 9 and Figure 19 represent the latter auto CT analysis; however, the highlighted primer concentrations in those tables and figures are those used in the assessment of environmental samples. Thus, the highlighted primer concentrations are not the optimal concentration demonstrated by Table 9 and Figure 19.

nM, respectively, yielding PCR efficiencies of 107%* and 103% (Table 9, Table 10, Figure 19, and Figure 20). For the pmoA 330 primer set, when *Methylocystsis* sp. and *Methylococcus* sp. template DNA was amplified, the optimal standard curves for both species occurred when the primer concentrations were 300 nM, yielding PCR efficiencies of 100% for both (Table 11, Table 12, Figure 21, Figure 22).

When comparing results between species, there was no noticeable difference between standard curves amplified using *Methylocystis* sp. or *Methylococcus* sp. template DNA. Due to the lack of discernable variation, and because the *Methylocystis* sp. is easier to culture in the lab, it was decided that *Methylocystis* sp. would be the best choice for template DNA in standard curves. Table 9 and Figure 19 contain the standard curve results for the pmoA 178 primer set amplifying *Methylocystis* sp. template DNA, while Table 10 and Figure 20 contain the standard curve results for *Methylococcus* sp. template DNA. Table 11 and Figure 21 contain the standard curve results for the pmoA 330 primer set amplifying *Methylocystis* sp. template DNA, while Table 12 and Figure 22 contain the standard curve results for *Methylococcus* sp. template DNA. Dissociation curves for pmoA 178 and 330 qPCR assays can be found in APPENDIX C: Figure C 1, Figure C 2, Figure C 3, and Figure C 4.

Optimizing 16S Type I and 16S Type II Primer Concentrations

After the appropriate primer concentrations and template species were determined, the pmoA 178 and pmoA 330 primer sets needed to be validated. In order to do this, a set of 16S qPCR primers specific to Type I and Type II methanotrophs were taken from the literature [115]. However, before performing the validation experiment, the 16S qPCR primer concentrations were also optimized.

Standard curves were constructed using both 16S T1 and 16S T2 primer sets, amplifying from *Methylococcus* sp. (Type I methanotroph) and *Methylocystis* sp. (Type II

Table 9: Average standard curve characteristics for primer set pmoA 178 amplifying template DNA from *Methylocystis* sp. strain Rockwell.

nM	Dynamic Range	Slope	R^2	PCR Efficiency (%)	Y-intercept (cycle #)
200	100 - 10^6	-3.34	0.993	99.3	38.0
300	100 - 10^6	-3.16	0.994	107	36.1
400	100 - 10^6	-2.97	0.988	117	34.4
500	na	na	na	na	na
600	na	na	na	na	na
700	100 - 10^6	-3.00	0.994	115	34.2
800	100 - 10^6	-2.89	0.989	121	33.7
900	100 - 10^6	-2.86	0.987	123	33.5
1000	100 - 10^6	-2.75	0.981	131	33.3

Note: Cells marked "na" were not included in these result due to the 10^3 portion of the standard curve amplifying poorly, resulting in standard curves that were unusable.

Note: Values represent the average of triplicate measurements.

methanotroph), respectively. Primer concentrations varied from 200 nM to 1000 nM. To ensure equal comparisons between primer concentrations, the standard curve dynamic ranges were limited to 100-10^6 copies per reaction and were analyzed using the "auto CT analysis". The results of this experiment revealed that the optimal standard curve for the 16S T1 primer set occurred when the primer concentration was 800 nM, yielding a PCR efficiency of 101% (Table 13 and Figure 23). For the 16S T2 primer set, the optimal standard curve occurred when the primer concentration was 300 nM, yielding a PCR efficiency of 100% (Table 14 and Figure 24). Table 13 and Figure 23 contain the standard curve results for the 16S T1 primer set, and Table 14 and Figure 24 contain the standard curve results for the 16S T2 primer set. Dissociation curves for 16S T1 and T2 qPCR assays can be found in APPENDIX C: Figure C 5 and Figure C 6.

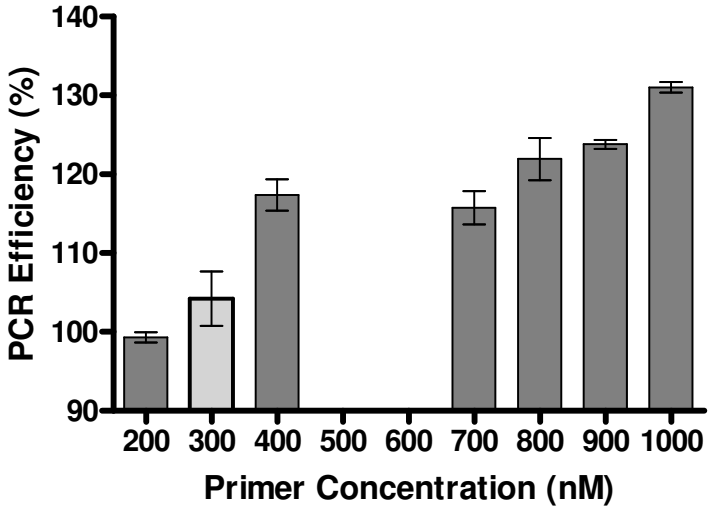

Figure 19: Comparison of pmoA 178 PCR efficiencies as related to varying primer concentrations. Template DNA was from *Methylocystis* sp. strain Rockwell. Bolded borders indicate optimal primer concentration, and light grey bars represent chosen template species for the indicated primer set. The bar heights at each concentration are the average of triplicate measurements and error bars represent standard deviations.

Table 10: Average standard curve characteristics for primer set pmoA 178 amplifying template DNA from *Methylococcus capsulatus*.

nM	Dynamic Range	Slope	R^2	PCR Efficiency (%)	Y-intercept (CT)
200	100 - 10^6	-3.23	0.994	104	36.5
300	100 - 10^6	-3.14	0.995	108	35.5
400	100 - 10^6	-2.91	0.984	121	33.5
500	100 - 10^6	-3.08	0.993	111	34.5
600	100 - 10^6	-3.03	0.991	114	34.2
700	100 - 10^6	-2.93	0.986	120	33.9
800	100 - 10^6	-2.87	0.979	123	33.7
900	100 - 10^6	-2.78	0.968	129	33.3
1000	100 - 10^6	-2.68	0.959	136	32.9

Note: Values represent the average of triplicate measurements.

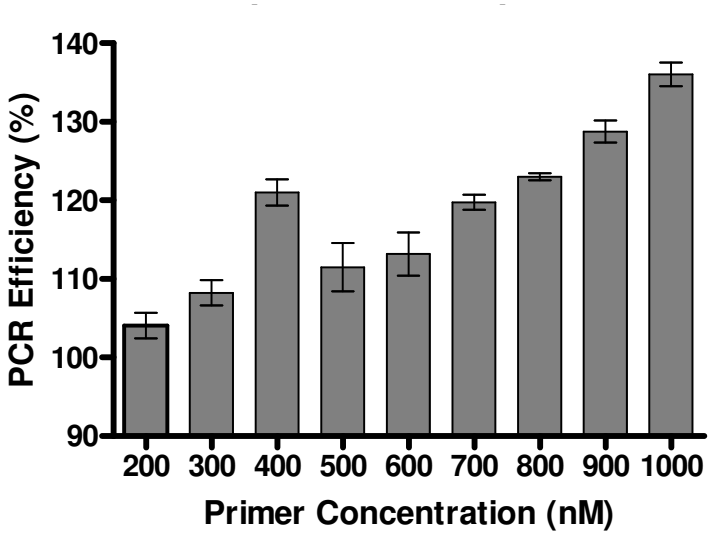

Figure 20: Comparison of pmoA 178 PCR efficiencies as related to varying primer concentrations. Template DNA was from *Methylococcus capsulatus*. Bolded borders indicate optimal primer concentration. The bar heights are the average of triplicate measurements and the error bars represent standard deviations.

Table 11: Average standard curve characteristics for primer set pmoA 330 amplifying template DNA from *Methylocystis* sp. strain Rockwell.

nM	Dynamic Range	Slope	R^2	PCR Efficiency (%)	Y-intercept (CT)
200	100 - 10^6	-3.35	0.998	98.9	35.9
300	100 - 10^6	-3.31	0.999	101	35.6
400	100 - 10^6	-3.26	0.998	103	35.5
500	100 - 10^6	-3.20	0.995	105	35.3
600	100 - 10^6	-3.22	0.997	105	35.4
700	100 - 10^6	-3.22	0.999	104	35.2
800	100 - 10^6	-3.14	0.998	108	35.1
900	100 - 10^6	-3.05	0.999	113	34.9
1000	100 - 10^6	-3.09	0.998	111	35.4

Note: Values represent the average of triplicate measurements.

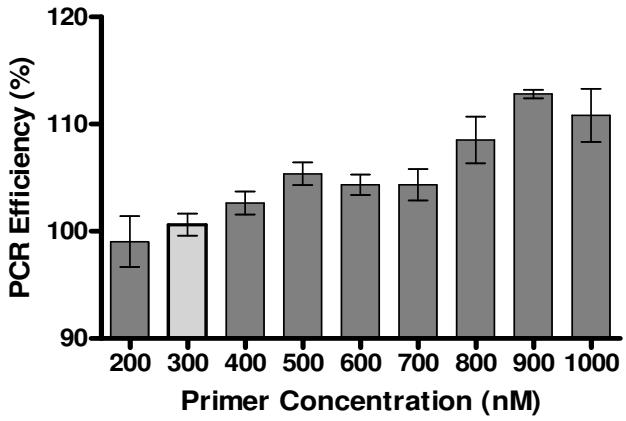

Figure 21: Comparison of pmoA 330 PCR efficiencies as related to varying primer concentrations. Template DNA was from *Methylocystis* sp. strain Rockwell. Bolded borders indicate optimal primer concentration, and light grey bars represent chosen template species for the indicated primer set. The bar heights at each concentration are the average of triplicate measurements and error bars represent standard deviations.

Table 12: Average standard curve characteristics for primer set pmoA 330 amplifying template DNA from *Methylococcus capsulatus.*

nM	Dynamic Range	Slope	R^2	PCR Efficiency (%)	Y-intercept (CT)
200	100 - 10^6	-3.32	0.999	100	35.5
300	100 - 10^6	-3.31	0.999	101	35.3
400	100 - 10^6	-3.23	0.999	104	35
500	na	na	na	na	na
600	na	na	na	na	na
700	100 - 10^6	-3.20	0.997	106	35.1
800	100 - 10^6	-3.15	0.995	108	35.2
900	100 - 10^6	-3.03	0.997	114	34.4
1000	100 - 10^6	-3.08	0.994	111	35.0

Note: Cells marked "na" were not included in these result because the 10^3 portion of the standard curve amplified poorly, resulting in standard curves that were unusable.

Note: Values represent the average of triplicate measurements.

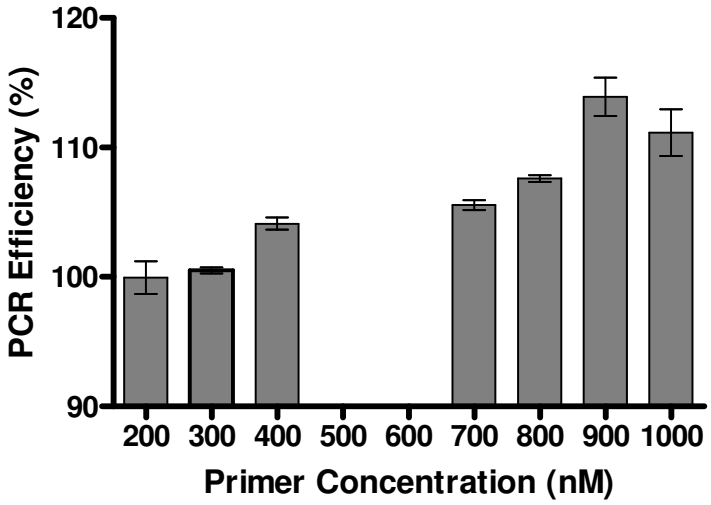

Figure 22: Comparison of pmoA 330 PCR efficiencies as related to varying primer concentrations. Template DNA was from *Methylococcus capsulatus*. Bolded borders indicate optimal primer concentration. The bar heights at each concentration are the average of triplicate measurements and error bars represent standard deviations.

Table 13: Average standard curve characteristics for 16S T1 primer set amplifying template DNA from *Methylococcus capsulatus*.

nM	Dynamic Range	Slope	R^2	PCR Efficiency (%)	Y-intercept (CT)
200	100 - 10^6	-3.96	0.998	78.8	42.8
300	100 - 10^6	-3.62	0.999	88.9	39.2
400	100 - 10^6	-3.46	0.999	94.7	37.3
500	100 - 10^6	-3.46	0.999	94.7	36.5
600	100 - 10^6	-3.42	1.000	96.0	35.9
700	100 - 10^6	-3.35	0.999	99.0	35.6
800	100 - 10^6	-3.30	0.999	101	35.1
900	100 - 10^6	-3.31	0.999	101	34.8
1000	100 - 10^6	-3.34	0.999	99.3	35.0

Note: The standard curve at each concentration was run in triplicate.

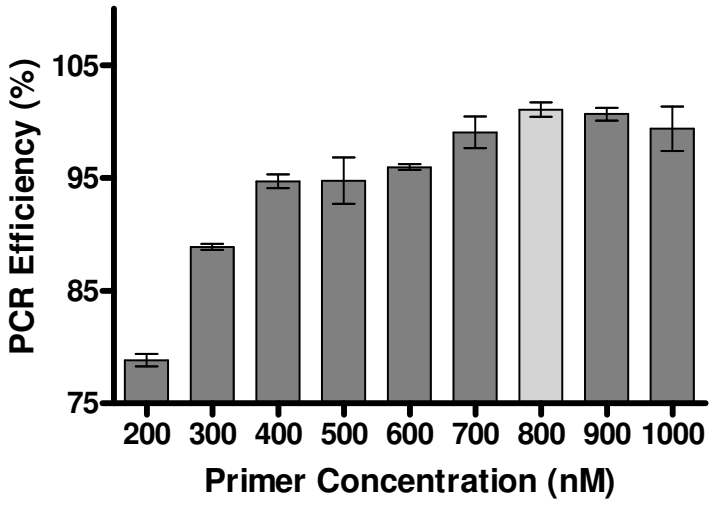

Figure 23: Comparison of 16S T1 PCR efficiencies as related to varying primer concentrations. Template DNA was from *Methylococcus capsulatus*. Light grey bars indicate optimal primer concentration. The bar heights at each concentration are the average of triplicate measurements and error bars represent standard deviations.

Table 14: Average standard curve characteristics for 16S T2 primer set amplifying template DNA from *Methylocystis* sp. strain Rockwell.

nM	Dynamic Range	Slope	R^2	PCR Efficiency (%)	Y-intercept (CT)
200	100 - 10^6	-3.36	0.999	98.6	35.8
300	100 - 10^6	-2.97	0.989	117	33.2
400	100 - 10^6	-3.05	0.994	113	33.1
500	100 - 10^6	-3.27	0.999	102	34.2
600	100 - 10^6	-3.26	0.994	103	34.0
700	100 - 10^6	-3.16	0.997	108	33.7
800	100 - 10^6	-3.18	0.998	107	33.2
900	100 - 10^6	-3.24	0.999	104	34.1
1000	100 - 10^6	-3.24	0.999	103	34.1

Note: The standard curve at each concentration was run in triplicate.

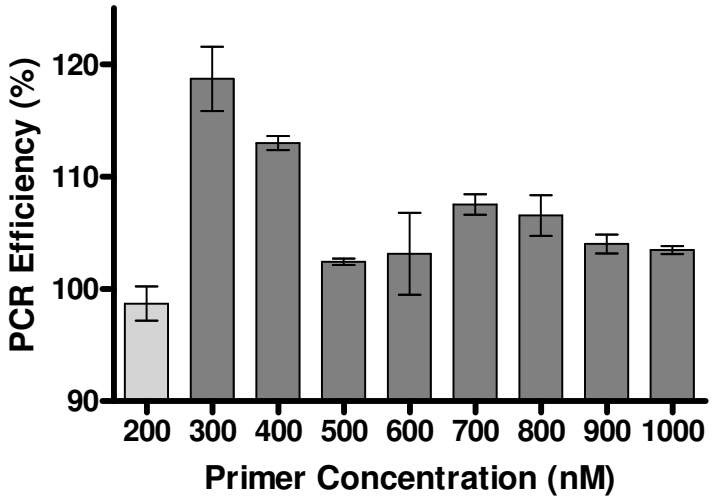

Figure 24: Comparison of 16S T2 PCR efficiencies as related to varying primer concentrations. Template DNA was from *Methylocystis* sp. strain Rockwell. Light grey bars indicate optimal primer concentration. The bar heights at each concentration are the average of triplicate measurements and error bars represent standard deviations.

Primer Validation

To validate the pmoA primer sets for qPCR, known amounts of methanotrophic DNA were quantified using the pmoA 178, 330, 16S T1, and T2 primer sets and subsequently compared. Assuming there is one copy of each gene per organism genome, this technique would be expected to validate the qPCR primers because the gene abundance derived from them would be with in the same order of magnitude. Genomic DNA was extracted from *Methylococcus capsulatus* (Type I) and *Methylocystis* sp. strain Rockwell (Type II) and used to assemble 5 different mixtures of Type I and Type II methanotroph DNA. The mixtures were as follows: 100% (T1); 75:25 (T1:T2); 50:50

pmoA 178 and pmoA 330 Primer Validation

The standard curve PCR efficiencies for the pmoA 178, pmoA 330, 16S T1, and 16S T2 primer sets were 95.8%, 94.5%, 95.5%, and 87.3%, respectively. The primer sets

were used at 300 nM, 300 nM, 800 nM, and 200 nM, respectively (for more standard curve characteristics for this experiment, see APPENDIX A: Table A 1) Although the 16S T2 standard curve PCR efficiency is outside of the desirable range (95% to 105%) [118], the most important issue raised by this experiment is the inefficient amplification of pure culture methanotroph template DNA by both pmoA primer sets. Dissociation curves for pmoA 178, pmoA 330, 16S T1, and 16S T2 qPCR assays can be found in APPENDIX C: Figure C 7, Figure C 8, Figure C 9, and Figure C 10.

The experimental results revealed that neither pmoA 178 nor pmoA 330 could robustly amplify methanotroph DNA when compared to the 16S T1 and T2 primers. In comparison, pmoA 178 and 330 produced quantifications one to three orders of magnitude lower than the 16S primers. This was serious cause for concern because DNA extractions from environmental samples typically have low yields. As a result, to be able to detect methanotrophs in environmental samples, a primer set that can vigorously amplify from small quantities of DNA is necessary. Furthermore, the pmoA 178 primers seemed to be biased towards Type I methanotrophs. As the amount of Type I methanotroph DNA decreased in each sample, so also did the pmoA 178 quantifications ($1.2x10^4$ copies per ng DNA down to $2.0x10^2$ copies per ng DNA). For both of these reasons, it was decided that neither the pmoA 178 nor the pmoA 330 were adequate primer sets for use in qPCR detection of methanotrophs. Full results of the pmoA 178 and 330 validation experiments are listed in Table 15 and shown in Figure 25.

Conversely, the 16S T1 and 16S T2 primer sets efficiently amplified methanotroph template DNA (Table 15, Figure 25). As expected, when the amount of Type I methanotroph DNA decreased in each samples, so also did the 16S T1 quantifications ($4.3x10^4$ copies per ng DNA down to 0 copies per ng DNA). Likewise, as the amount of Type II methanotroph DNA increased in each samples, so also did the 16S T2 quantifications (0 copies per ng DNA up to $1.2x10^5$ copies per ng DNA). These results demonstrated that 16S Type I and Type II primers were functioning as expected.

Table 15: Average quantification results for known amounts of methanotrophic DNA amplified with 16S T1, 16S T2, pmoA 178, and pmoA 330 primer sets.

Sample	**16S T1**	**16S T2**	**pmoA 178**	**pmoA 330**
T1:T2	copies/ng DNA	copies/ng DNA	copies/ng DNA	copies/ng DNA
100 : 0	$4.3x10^4$	2	$1.2x10^3$	$6.8x10^2$
75 : 25	$3.0x10^4$	$8.7x10^4$	$1.3x10^3$	$3.4x10^2$
50 : 50	$2.1x10^4$	$1.4x10^5$	$9.3x10^2$	$2.5x10^2$
25 : 75	$1.1x10^4$	$1.4x10^5$	$6.2x10^2$	$1.9x10^2$
0 : 100	0	$1.2x10^5$	$2.1x10^2$	$1.0x10^2$

Note: Values represent the average of replicate measurements.

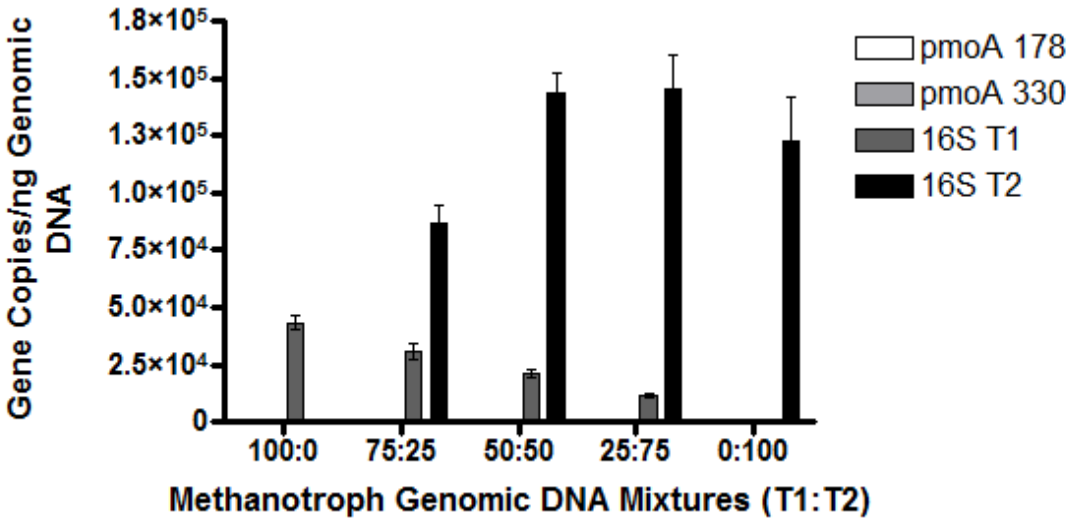

Figure 25: Comparisons of average quantifications between pmoA 178, pmoA 330, 16S T1, and 16S T2 primer sets amplifying known amounts of genomic DNA. Type I DNA was extracted from *Methylococcus capsulatus* pure culture. Type II DNA was extracted from *Methylocystis* sp. strain Rockwell. The bar heights for each sample are the average of replicate measurements and error bars represent the range of data.

It should be noted that, although the 16S T1 primers were able to produce significant levels of quantification, they were small when compared to the 16S T2 quantifications. This could be explained by primer bias. Since only one species of methanotroph Type I DNA was used in these mixtures, if the primer set does not amplify that species well, then the quantifications will be lower. This hypothesis would need to be confirmed in lab experiments.

pmoA 472 and mmoX Primer Validation

Fortunately, a more recent literature review revealed a new set of pmoA qPCR primers, pmoA 472 [112, 113], which could potentially be used in this research. In that same publication were qPCR primers that amplify a subunit of the soluble methane monooxygenase (sMMO). Another publication was found to have qPCR primers for universal detection of Bacteria [114]. Standard curves were constructed using the new pmoA 472, mmoX, and the 16S gene (16S U) primers. The primers were used at the same concentrations as stated in the original papers (300 nM for all) and were validated using the same technique as previously described. The standard curve PCR efficiencies for the pmoA 472, mmoX, 16S T1, and 16S T2 primer sets were 98.0%, 94.2%, 103%, and 101%, respectively (for more standard curve characteristics for this experiment, see APPENDIX A: Table A 2). Dissociation curves for pmoA 472, 16S T1, and 16S T2 qPCR assays can be found in APPENDIX C: Figure C 11, Figure C 12, and Figure C 13. Dissociation curves for the mmoX experiment can be seen in Figure 27.

Results, listed in Table 16, show that the *Methylocystis* sp. did not have *mmoX* (an sMMO gene). As the mass of *Methylocystis* DNA increased in each sample, the *mmoX* quantifications decreased from $1.3x10^5$ copies per ng DNA to 0 copies per ng DNA. This was confirmed by inspection of the recently published genome sequence of this strain

[119]. The new pmoA 472 and mmoX primers did not produce the same quantification disparity as did the previous *pmoA* primer sets and were able to detect similar amounts of genomic DNA as the 16S T1 and T2. In fact, the *pmoA* detection level was approximately 35% greater than the 16S T2 detection when the 100% T2 sample was probed (T2 ~ $8.8x10^5$ copies; pmoA ~ $1.2x10^6$ copies). This result would be easily explained by the fact that there are two copies of *pmoA* present in this methanotroph's genome. We concluded that both 16S primer sets and the *pmoA* primers were suitable for use evaluating environmental samples from contaminated groundwater.

With regard to the *mmoX* primers, it should be noted that there are two areas of concern. First, although the mmoX primers were able to produce significant levels of quantification, they were small when compared to the other primer sets. This could be explained by primer bias. Since only one species of methanotroph with the sMMO gene was used in these mixtures, if the primer set does not amplify that species well, then the quantifications will be lower. As mentioned before, this hypothesis would also need to be confirmed using lab experiments.

The second area of concern arose upon inspection of the *mmoX* dissociation curve, which showed two peak temperatures, 76.3°C and 85.8°C (Figure 27). Although the 76.3°C peak was much weaker than the 85.8°C peak, its presence implies possible primer-dimer artifacts or non-specific amplicons. Upon further inspection, it appeared that the 76.3°C peak only occurred in the dissociation curve related to the standard curve PCR products, while the dissociation curve associated with the Type I/Type II sample mixtures contained only the 85.8°C peak. Furthermore, it was observed that the no-template control contained only the 76.3°C peak. Since the no-template control is void of genetic material that would produce non-specific amplification, this peak implies a primer-dimer artifact. To confirm this suspected caveat, PCR products from these reactions should be gel analyzed and sequenced. Evaluation of environmental samples using the mmoX primers proceeded with caution. Full results of the pmoA 472 and

mmoX validation experiments are listed in Table 16 and shown in Figure 26 and Figure 27.

16S T1, T2 and Universal

Finally, the 16S T1 and 16S T2 primer sets were validated using the 16S universal qPCR primers and the same technique as previously stated. The standard curve PCR efficiencies for the 16S T1, 16S T2, and 16S U primer sets were 101%, 99.2%, and 102%, respectively. The primer sets were used at 800 nM, 200 nM, and 300 nM, respectively (for all standard curve characteristics for this experiment, see APPENDIX A: Table A 3). Dissociation curves for the 16S T1, 16S T2, and 16S U primer assays can be found in APPENDIX C: Figure C 14, Figure C 15, and Figure C 16.

Experimental results showed that the 16S T2 primer quantifications matched well with the 16S U quantifications (Table 17). This shows that the 16S T2 primers are efficiently amplifying the methanotroph DNA. However, the 16S T1 primer set was producing much smaller quantifications than the 16S U. This means that either the primer set is not good for use in qPCR or that the primer set is biased against the specific species of methanotroph that we have used in these mixtures. Full results of the 16S T1 and T2 validation experiments are listed in Table 17 and shown in Figure 28.

The overall results from the pmoA 472, mmoX, 16S T1, 16S T2, and 16 U validation experiments suggest that the mmoX and 16S T1 primer sets should be used with caution until they can be further validated. However, quantifying environmental DNA with several sets of primers would be of benefit. Therefore, these five primer sets used to evaluate environmental samples from contaminated groundwater.

Table 16: Average quantification results for known amounts of methanotrophic DNA amplified using 16S T1, 16S T2, pmoA 472, and mmoX primer sets.

Sample	**16S T1**	**16S T2**	**pmoA 472**	**mmoX**
T1:T2	copies/ng DNA	copies/ng DNA	copies/ng DNA	copies/ng DNA
100 : 0	$3.2x10^4$	0	$7.7x10^5$	$1.3x10^5$
75 : 25	$1.3x10^4$	$2.1x10^5$	$6.6x10^5$	$6.8x10^4$
50 : 50	$1.3x10^4$	$4.5x10^5$	$1.1x10^6$	$6.4x10^4$
25 : 75	$8.5x10^3$	$7.7x10^5$	$1.1x10^6$	$3.2x10^4$
0 : 100	3	$8.8x10^5$	$1.2x10^6$	0

Note: Values represent the average of replicate measurements.

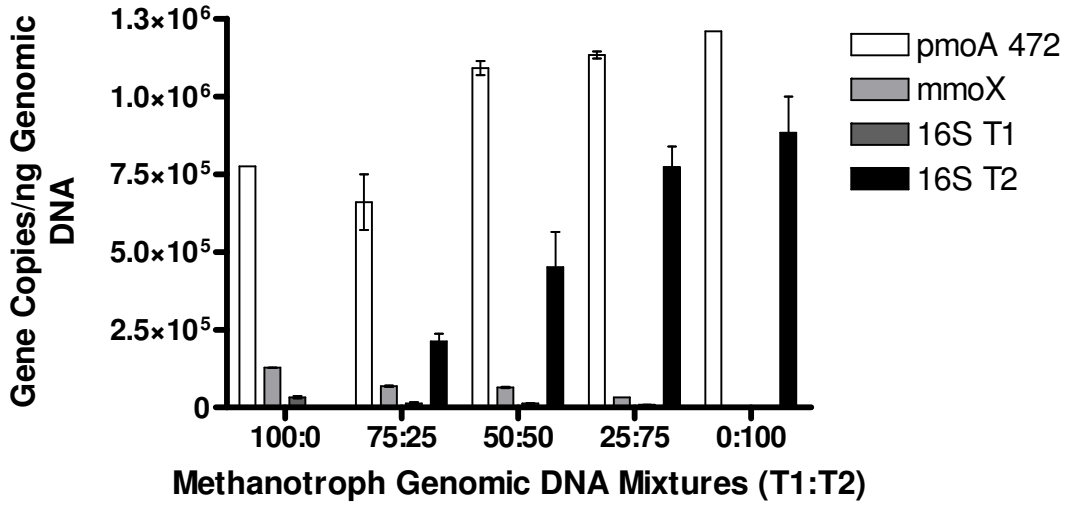

Figure 26: Comparison of average quantifications between pmoA 472, mmoX, 16S T1, and 16S T2 primer sets amplifying known amounts of genomic DNA. Type I DNA was extracted from *Methylococcus capsulatus* pure culture. Type II DNA was extracted from *Methylocystis* sp. strain Rockwell. The bar heights for each sample are the average of replicate measurements and error bars represent the range of data.

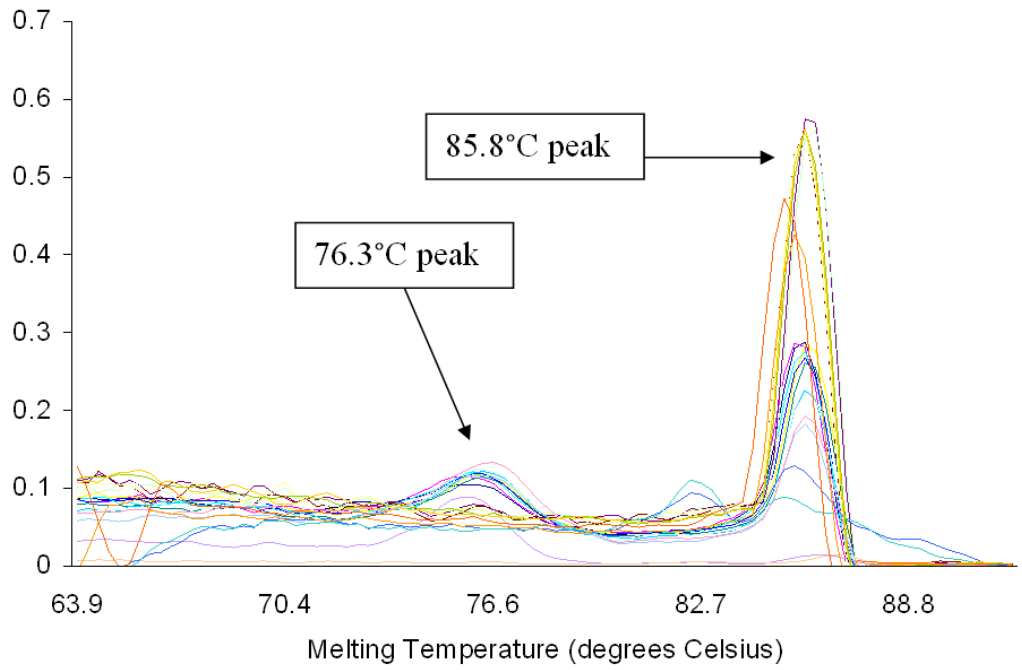

Figure 27: Dissociation curve for *mmoX* primer set amplifying *Methylococcus* sp. (Type I) and *Methylocystis* sp. (Type II). Multiple peaks were observed, implying primer-dimer artifacts or non-specific amplification.

Table 17: Average quantification results for known amounts of methanotrophic DNA amplified using 16S T1, 16S T2, and 16S U primer sets.

Sample T1:T2	**16S T1** copies/ng DNA	**16S T2** copies/ng DNA	**16S U** copies/ng DNA
100 : 0	6.0×10^4	0	9.7×10^5
75 : 25	2.3×10^4	1.6×10^5	6.9×10^5
50 : 50	1.7×10^4	4.1×10^5	6.5×10^5
25 : 75	1.2×10^4	6.9×10^5	1.0×10^6
0 : 100	1	9.5×10^5	9.5×10^5

Note: Values represent the average of replicate measurements.

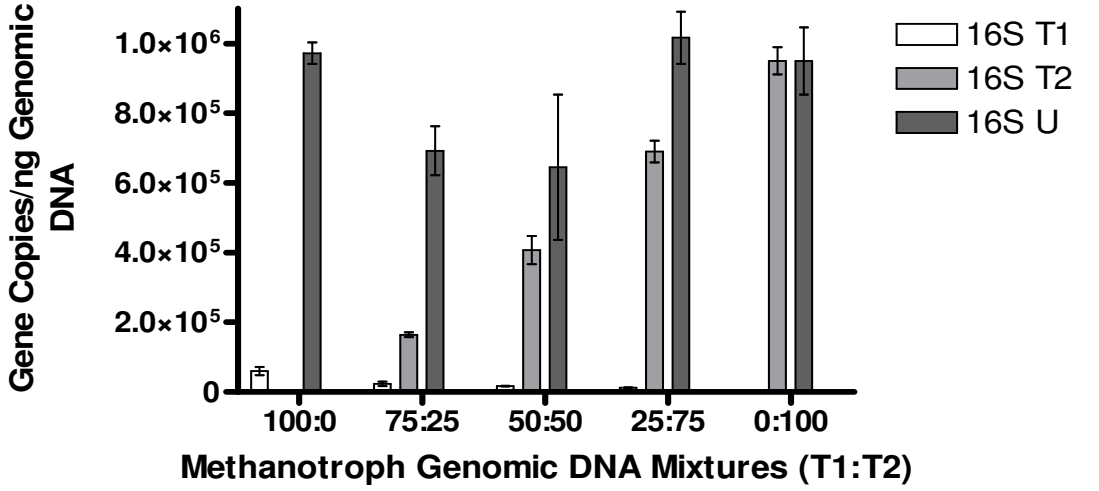

Figure 28: Comparison of average quantifications between 16S T1, 16S T2 and 16S U primer sets amplifying known amounts of genomic DNA. Type I DNA was extracted from *Methylococcus capsulatus* pure culture. Type II DNA was extracted from *Methylocystis* sp. strain Rockwell. The bar heights for each sample are the average of replicate measurements and error bars represent the range of data.

Methanotroph qPCR Method Validation Using

Environmental Samples

Soldotna, AK[2]

In order to evaluate the presence of methanotrophs in contaminated groundwater at the Soldotna, AK site (Site map – Figure 29), first genomic DNA was extracted from groundwater samples. The DNA was then qPCR assayed using pmoA 472 and mmoX primers at a concentration of 300 nM. Standard curve PCR efficiencies for each primer set were 101 % and 97.6 %, respectively (for more standard curve characteristics, see

[2] DNA and RNA extractions for the Soldotna site were performed by Yang Oh Jin.

APPENDIX A: Table A 4 and Table A 5). Dissociation curves for the pmoA 472 primer assays can be found in APPENDIX C: Figure C 17.

Results for this experiment showed that all wells tested contained detectable amount of both genes, although in some wells gene abundances were detected in quantities both above and below the dynamic range of the standard curves. Monitoring well 40 (MW40), which is located in an area considered to be favorable for reductive dechlorination, experienced a 99% decrease in gene abundance; down from $3.9x10^7$ copies/L groundwater (copies/LGW) to $1.7x10^5$ copies/LGW. Generally, these results would seem to fit with the overall geochemical data trends of this well, which indicate high concentrations of methane, low concentrations of dissolved oxygen (1.29 mg/L in 2008), and are typically indicative of anaerobic conditions. As a result, aerobic methanotrophs would not be expected to thrive in this well under such environmental circumstances. Specific geochemical data for this well illustrated a decrease in both VC (20.7 µg/L to 9.4 µg/L) and methane (12,400 µg/L to 4,380 µg/L) from 2008 to 2009, and the presence of ethene (90 µg/L and 72 µg/L) at both time points. The decrease in methane, if being consumed by methanotrophs, would point towards a growing methanotroph population and, consequently, would seemingly contradict the qPCR data. Yet, the presence of ethene could indicate possible methanotroph inhibition and, thus, would tend to corroborate the qPCR data. Another alternative analysis could be that a decrease in methanotroph food source (i.e. decreasing methane concentrations) would lead to a decreasing population, which would coincide with the geochemical data. The ultimate conclusion being that, because there are very few groundwater and geochemical samples being considered, it is extremely difficult to draw any definitive conclusions, or links, between the specific geochemical data and the qPCR gene abundance results.

Regarding MW6, although quantifications at both time points were within the same order of magnitude, MW 6, which is located on an aerobic/anaerobic boundary, experienced an increase in the *pmoA* gene abundance by 438%. From 2008 to 2009,

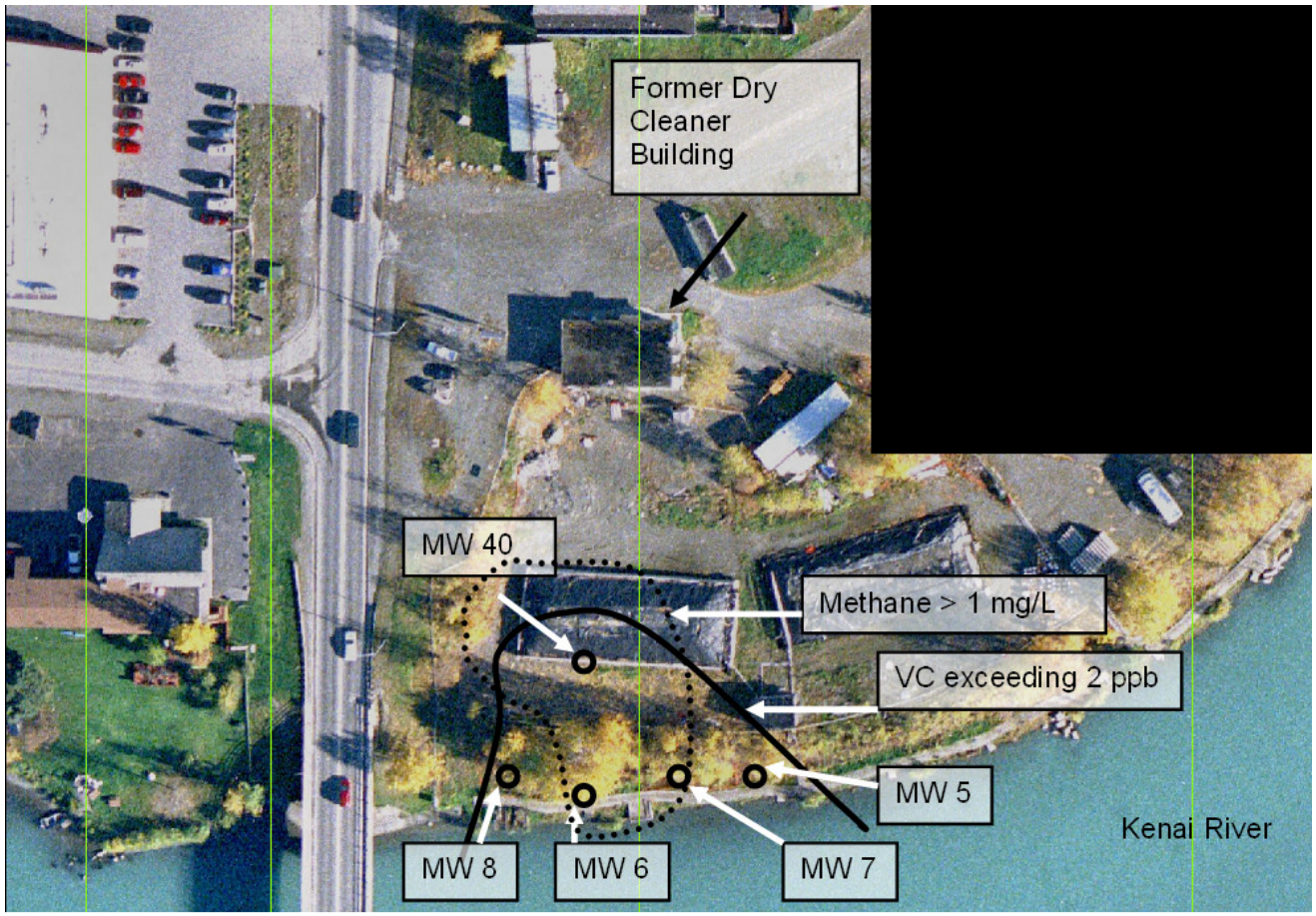

Figure 29: Bird's eye view of Soldotna site with methane and VC plumes delineated.

pmoA gene abundance in MW 6 increased from $1.6x10^4$ copies/LGW to $6.3x10^4$ copies/LGW. Again, these results would seem to generally fit with the overall geochemical data trends of this well, which indicate MW 6 to be near an aerobic/anaerobic interface. These aerobic/anaerobic interfaces are thought to be conducive to methanotrophic VC oxidation, because they are likely to contain ample amounts of methane, VC, and O_2. Specific geochemical data for this well illustrated a steady presence of VC (8.89 µg/L to 9.64 µg/L) from 2008 to 2009, a dissolved oxygen concentration of 0.35 mg/L in 2008, and methane and ethene concentrations of 7,650 µg/L and 50 µg/L, respectively, in 2009.

For the *mmoX* gene, from 2008 to 2009, MW 6 and MW 40 experienced a 170% increase ($1.5x10^3$ copies/LGW to $2.6x10^3$ copies/LGW) and a 52% decrease ($2.0x10^5$ copies/LGW to $9.7x10^4$ copies/LGW) an in gene abundance, respectively. As previously stated, these results coincide with the overall trends of these wells; however, it is extremely difficult to draw any definitive conclusions, or links, between the specific geochemical data and the qPCR gene abundance results. Full results for Soldotna are displayed in Table 18, Figure 30, Figure 31, Figure 32, and Figure 33. In addition to geochemical data, Soldotna results were also compared to data from a tracer study conducted at the site. Real-time PCR results coincide with the tracer study, which demonstrated DCE and VC were being oxidized to CO_2 near MW 6 [100, 101]. The presence of *pmoA* and *mmoX* genes in these wells could indicate that methanotrophs producing pMMO and sMMO enzymes are responsible for the oxidative degradation of VC.

With regard to the mmoX dissociation curve, results showed the presence of the standard-curve double peak that was previously mentioned; however, in this instance the 76°C peak was much large than those observed in the previous experiment (Figure 34). The presence of this suspected primer-dimer artifact in the standard curve would falsely elevate the fluorescence in these wells, ultimately leading to decreased sample

quantification. The environmental sample melt curve contained a single peak at the 86°C (Figure 35).

Table 18: Average methanotroph gene abundance at the Soldotna, Alaska contaminated site.

Monitoring Well	*pmoA 472*		*mmoX*	
	2008	**2009**	**2008**	**2009**
	copies/L groundwater		copies/L groundwater	
MW 6	$1.6x10^4$	$6.3x10^4$	$1.5x10^3$ **	$2.6x10^3$ **
MW 40	$3.9x10^7$ *	$1.7x10^5$	$2.0x10^5$	$9.7x10^4$

Note: Samples marked with "**" were detected at quantities below the dynamic range of the standard curve (100 copies/reaction). Samples marked with "*" were detected at quantities above the dynamic range of the standard curve ($1.0x10^5$ copies/reaction).

Note: Each sample was run in duplicate.

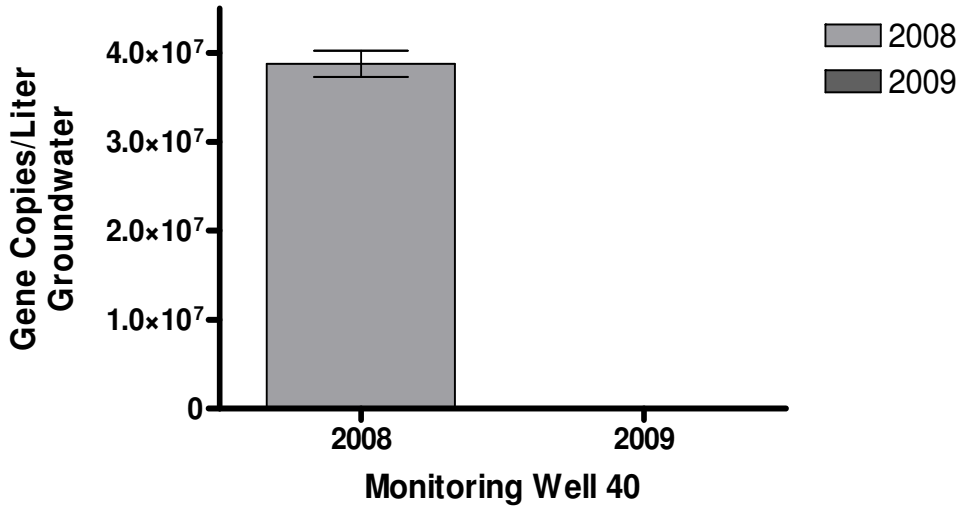

Figure 30: Change in average *pmoA* gene abundance in contaminated groundwater from MW 40 in Soldotna, AK. The bar heights for each sample are the average of replicate measurements and error bars represent the range of data.

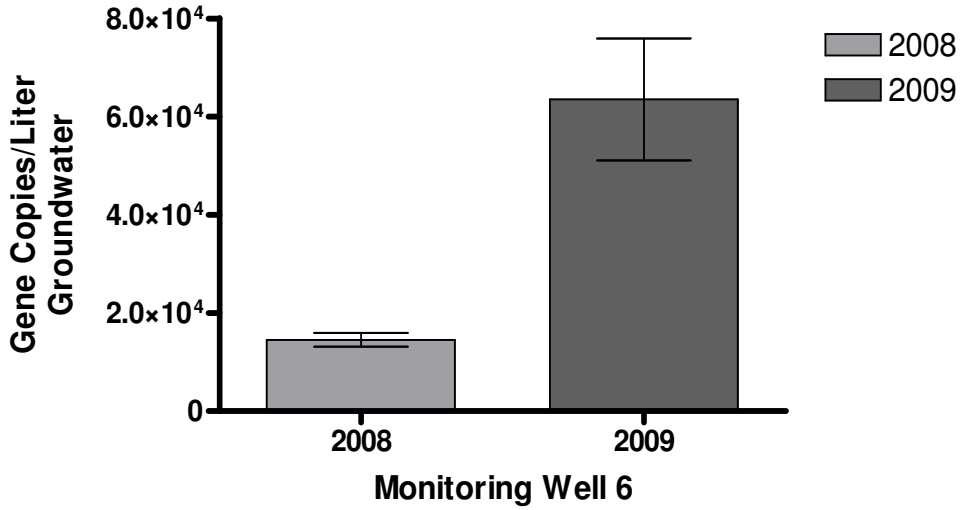

Figure 31: Change in average *pmoA* gene abundance in contaminated groundwater from MW 6 in Soldotna, AK. The bar heights for each sample are the average of replicate measurements and error bars represent the range of data.

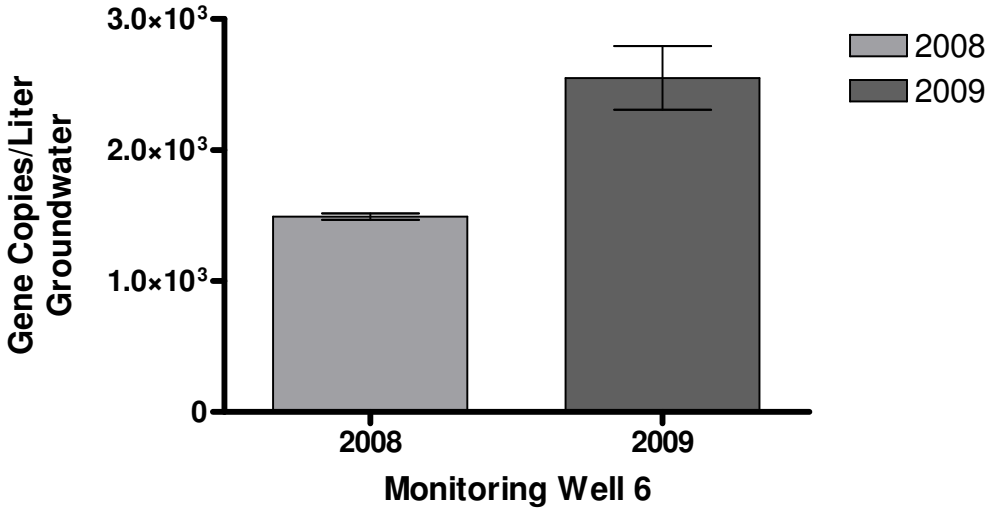

Figure 32: Change in average *mmoX* gene abundance in contaminated groundwater from MW 6 in Soldotna, AK. The bar heights for each sample are the average of replicate measurements and error bars represent the range of data.

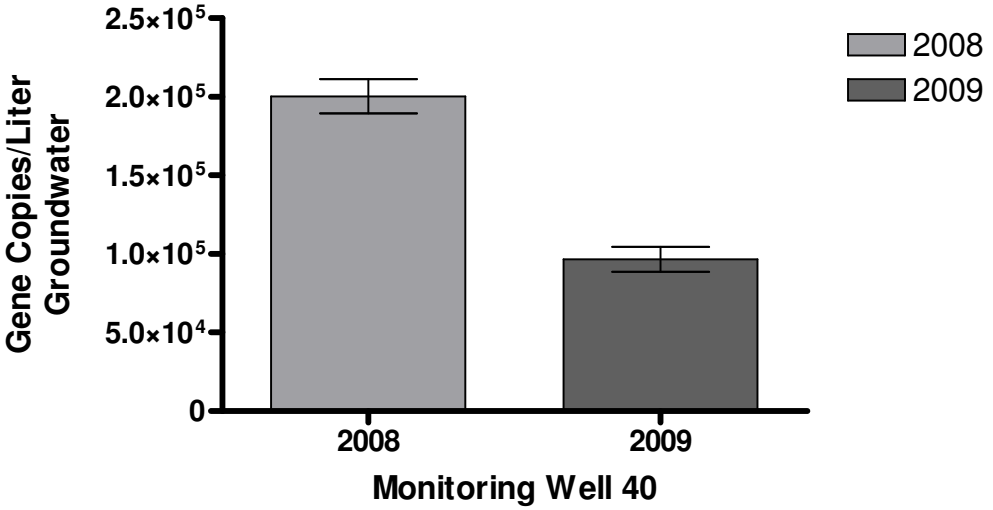

Figure 33: Change in average *mmoX* gene abundance in contaminated groundwater from MW 40 in Soldotna, AK. The bar heights for each sample are the average of replicate measurements and error bars represent the range of data.

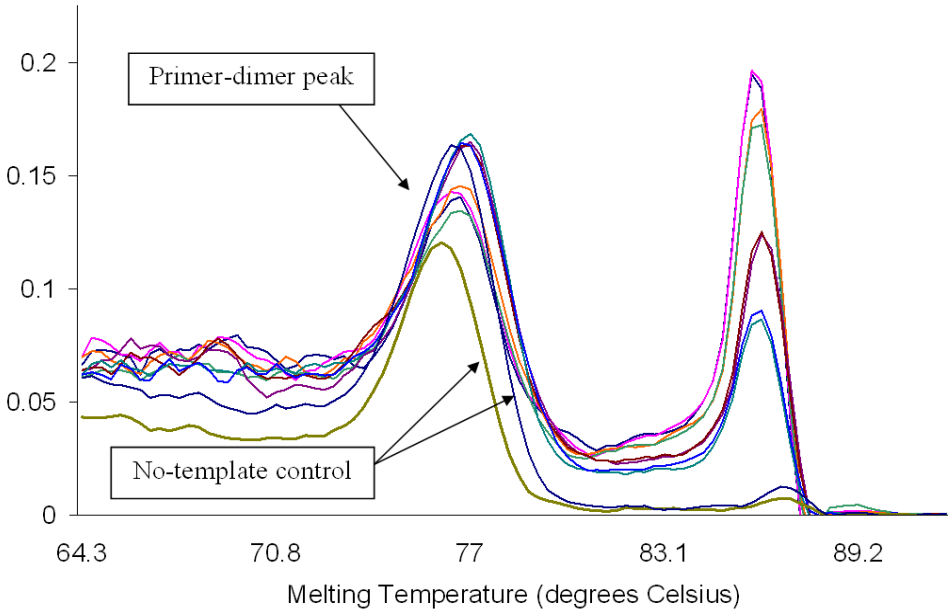

Figure 34: Dissociation curve for *mmoX* primer set standard curve. Multiple peaks were observed and appear to be primer-dimer artifacts since the no-template control contains only one peak.

quantification. The environmental sample melt curve contained a single peak at the 86°C (Figure 35).

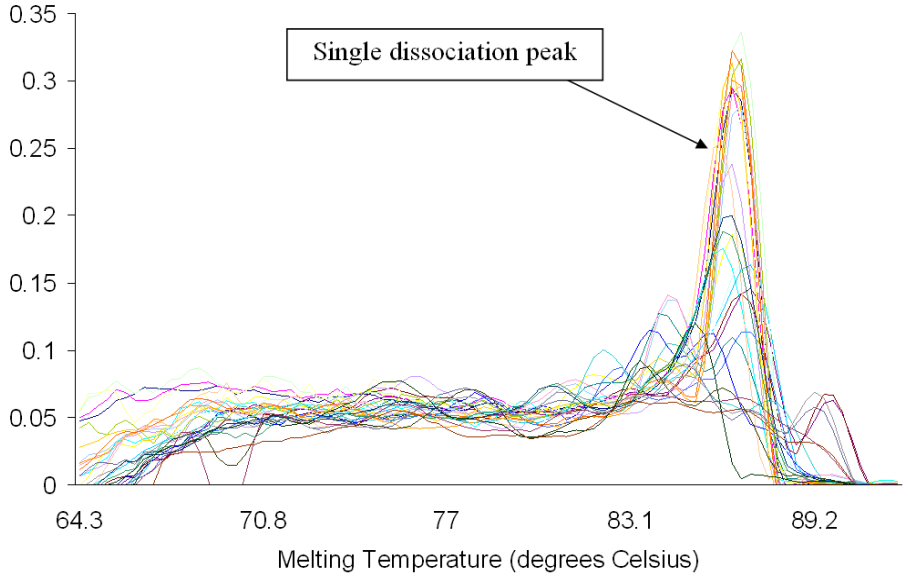

Figure 35: Dissociation curve for *mmoX* primer set amplifying environmental samples from Soldotna site. The single dissociation peak demonstrates absence of primer-dimer artifacts.

NAS Oceana, VA[3]

Environmental samples from the Naval Air Station Oceana contaminated site in Virginia Beach, VA were also tested (Site map – Figure 36). To evaluate the presence of methanotrophs, genomic DNA from groundwater samples were qPCR assayed using the pmoA 472, mmoX, 16S T1, and 16S T2 primer sets. Primer concentrations were 300 nM, 300 nM, 800 nM, and 200 nM, respectively, and produce standard curve PCR efficiencies of 100 %, 99.4 %, 102 %, and 94.5 %, respectively. The 16S T2 PCR

[3] DNA and RNA extractions for the NAS Oceana site were performed by Yang Oh Jin.

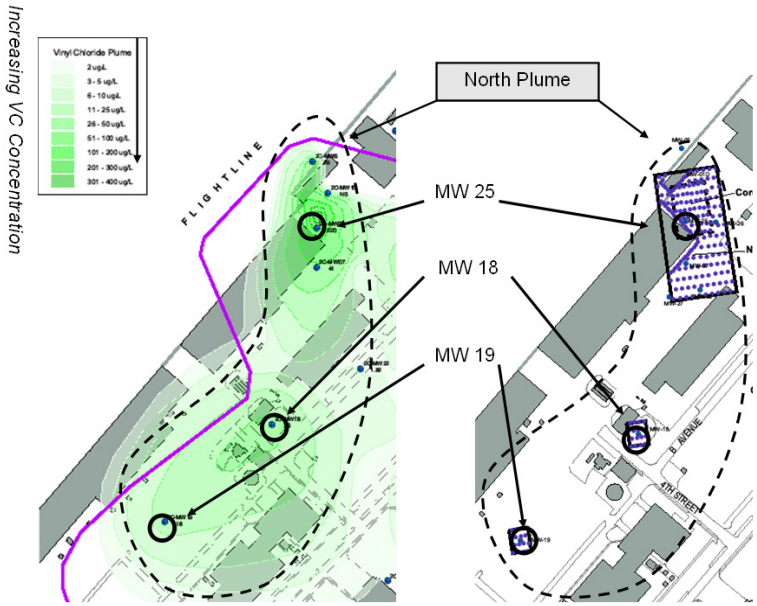

Figure 36: The north VC plume at NAS Oceana containing monitoring wells 18, 19, and 25 [103]. The left hand side of the figure illustrates the extent of the VC plume. The purple dots on the right hand side of the figure indicate the oxygen injection points.

efficiency falls below the desired range (95% to 105%) and implies slightly decreased amplification efficiency for that primer set. This decrease in efficiency will cause the 16S T2 quantifications to appear smaller than they would otherwise in a qPCR reaction amplifying at 100%. For more standard curve characteristics, see APPENDIX A: Table A 6 and Table A 7.

Results for this experiment showed that nearly all wells tested contained detectable amounts of *pmoA*, *mmoX*, 16S T1, and 16S T2 genomic DNA, and imply that methanotrophs are present at this site. Geochemical data from well 18, spanning 2008 to 2009, showed a decrease in CH_4 and VC (2.8 mg/L – 1.0 mg/L and 22 µg/L – 0.83 µg/L, respectively), and a steady presence of dissolved O_2 (1.28 mg/L – 1.89 mg/L). From 2008 to 2009, samples from well 18 saw a decrease in *pmoA*, *mmoX*, and 16S T1 gene abundance by 99%, 98%, and 83%, respectively. These results would seem to contradict the geochemical data trends of this well. If methanotrophs are the VC degrading

microbes at this site, the aerobic treatment scheme, along with falling methane and VC concentrations, would point towards a growing methanotroph population. Yet this is not what the qPCR data shows. These results could indicate that methanotrophs are not the microorganism responsible for VC and methane degradation in this well. However, again, an alternative analysis could be that a decrease in methanotroph food source would lead to a decreasing methanotroph population, which would coincide with the geochemical data. As stated previously, it is extremely difficult to draw any definitive conclusions, or links, between the specific geochemical data and the qPCR gene abundance results, due to the limited scope of the sampling.

Differing from well 18, geochemical data for well 19, spanning 2008 to 2009, showed an increase in CH_4 and VC (1.8 mg/L – 5.8 mg/L and 7.2 µg/L – 11.2 µg/L, respectively) and steady presence of dissolved O_2 (1.3 mg/L – 1.26 mg/L). Samples from well 19 also saw an increase in abundance for all targeted genes by 3 orders of magnitude. Again, these results could have more than one explanation. A decreasing methanotroph population, and the subsequent decrease in methane consumption, could explain the increase in methane concentrations, but would contradict the qPCR results. Alternatively, an increase in methane, the methanotroph food source, could initiate a growth in methanotroph populations. Again, it should be noted that, because very few groundwater and geochemical samples are being considered, it is extremely difficult to draw any definitive conclusions, or links, between the specific geochemical data and the qPCR gene abundance results.

Geochemical data for well 25, years 2008 to 2009, showed an increase in CH_4 and VC (2.5 mg/L – 7.6 mg/L and 19 µg/L – 46 µg/L, respectively) and steady presence of dissolved O_2 (1.2 mg/L – 1.44 mg/L). Likewise, samples from well 25 saw an increase in *pmoA*, *mmoX*, and 16S T1 gene abundance by 1 order of magnitude and steady presence of the 16S T2 methanotroph gene, with abundances varying from $2.0x10^5$ copies/L GW to $4.2x10^5$ copies/L GW. These results could have similar explanations as previously

stated; however, it is difficult to draw any definitive conclusions between the specific geochemical data and the qPCR gene abundance results, due to the limited scope of the sampling. Full results for NAS Oceana are displayed in Table 19.

Regarding the mmoX dissociation curve, results mirrored those of Soldotna, with the presence of the standard-curve double peak at 76°C and 86°C. Likewise, environmental samples contained only a single peak melting temperature at 86°C. Since the sample PCRs do not seem to contain the primer-dimer artifact, and since each sample is being quantified using the same standard curve, the effect of the primer-dimer artifact on sample results is uncertain. Dissociation curves for this experiment are located in APPENDIX C: Figure C 18 and Figure C 19.

Carver, MA

Pyrosequencing Comparison[4]

Environmental samples from the Carver, Massachusetts were also tested (Site map – Figure 17). To evaluate the presence of methanotrophs at this contaminated site, genomic DNA from groundwater samples were qPCR assayed using the 16S universal, 16S T1, 16S T2, and Luciferase primers [108] . Primer concentrations were 300 nM, 800 nM, 200 nM, and 100 nM, respectively, and produce standard curve PCR efficiencies of 99.4 %, 99.3 %, 99.9 %, and 99.8 %, respectively. Percent recoveries for the Luciferase control gene for each sample ranged from 1.6 % to 13.6 %. For more standard curve characteristics and detailed Luciferase recovery ratios, see APPENDIX A: Table A 8, Table A 9, and Table A 10. Dissociation curves for the 16S T1, 16S T2, 16S U, and

[4] Pyrosequencing experiments, raw data analysis and construction of the phylogenetic tree in this section were performed by Josh Livermore.

Table 19: Average methanotroph gene abundance at NAS Oceana contaminated site.

Monitoring Well	*pmoA*		*mmoX*		16S T1		16S T2	
	2008	**2009**	**2008**	**2009**	**2008**	**2009**	**2008**	**2009**
	copies/L groundwater		copies/L groundwater		copies/L groundwater		copies/L groundwater	
18	$9.6x10^5$	$1.2x10^4$	$4.3x10^3$	$1.3x10^2$ **	$1.9x10^4$ **	$3.0x10^3$ **	$6.5x10^5$	$5.3x10^3$
19	$1.4x10^4$	$1.9x10^7$*	0	$4.3x10^4$	$1.0x10^3$ **	$1.6x10^6$	$9.4x10^3$	$5.2x10^6$
25	$2.1x10^5$	$1.1x10^6$	$6.6x10^4$	$4.8x10^5$	$1.0x10^4$	$4.8x10^5$	$2.0x10^5$	$4.2x10^5$

Note: Samples marked with "*" were detected at quantities above the dynamic range of the standard curve (10^5 copies/reaction).
Samples marked with "**" were detected at quantities below the dynamic range of the standard curve (100 copies/reaction).

Note: Values are the average of replicate measurements.

Luciferase primer assays can be found in APPENDIX C: Figure C 20, Figure C 21, Figure C 22, and Figure C 23.

All wells tested contained detectable amounts of 16S U, 16S T1, and 16S T2 genomic DNA. These results indicate methanotroph presence in all wells from the Carver, MA site. The relative abundance of methanotrophs was calculated and then compared to the relative abundances obtained through pyrosequencing of the same samples. This comparison was yet another way to validate the methanotroph qPCR method used in this study.

The relative abundance was calculated by adding the Type I methanotroph rRNA quantifications with the Type II methanotroph rRNA quantifications and then dividing by the universal bacterial quantifications (16S T1+16S T2/16S U). For each monitoring well, the relative abundance was as follows: 46D – 0.95%, 52I – 0.18 %, 58I – 6.56%, and 64I – 0.48% (well 63I was not analyzed due to lack of available sample). This data suggests that methanotrophs make up a very small portion of the total microbial community in these wells, with MW 58I having the highest presence of methanotrophs. Full quantification results for methanotroph relative abundances are presented in Table 20 and Table 21.

The relative abundance of Type I versus Type II methanotrophs was calculated by dividing the Type I or Type II quantifications be the sum total of Type I and Type II methanotrophs (16S T1 or 16S T2/ 16S T1+16S T2). For each monitoring well, the relative abundance of Type I and Type II methanotrophs were as follows: 46D – 98% and 2%, respectively; 52I – 44% and 56%, respectively; 58I – 76% and 24%, respectively; and 64I – 35% and 65%, respectively. This data suggests the methanotroph populations in MW 46D and 58I consisted of a majority of Type I methanotrophs, while the populations in MW 52I and 64I were majority Type II methanotrophs. Full quantification results for methanotroph relative abundances are presented in Table 20 and Table 21.

Table 20: Average methanotroph gene abundance at Carver contaminated site.

Monitoring Well	16S U	16S T1	16S T2
	copies/L groundwater		
46 D	$6.1x10^7$	$5.3x10^5$	$5.3x10^5$ *
52 I	$5.0x10^9$ *	$3.9x10^6$	$3.9x10^6$
58 I	$1.0x10^8$ *	$5.1x10^7$	$5.1x10^7$
64 I	$9.2x10^8$ *	$1.4x10^6$	$1.4x10^6$

Note: Samples marked with "*" were detected at quantities above the dynamic range of the standard curve (10^5 copies/reaction).

Note: Values are the average of replicate measurements.

To corroborate these results, methanotroph relative abundances were determined using pyrosequencing techniques. In order to do this, first the actual base pair sequences from the pyrosequencing results were blasted to determine their likely taxonomical identity. Next, the *Gammaproteobacterium* and the *Alphaproteobacterium* methanotrophs were separated as Type I and Type II, respectively. Finally, relative abundance was calculated by taking the number of Type I and Type II sequences and dividing by the total number of sequences obtained.

Pyrosequencing relative abundance results showed that the methanotroph population in MW 46D was 1.13%, in MW 52I was 1.71%, in MW 58I – 54.73%, in MW 63I was 24.10%, and in MW 64I was 2.70%. This data suggests that methanotrophs make up a significant portion of the total microbial community in MW 58I and 63I. Although the qPCR and pyrosequencing data did not match exactly, they did follow the same trend, which showed the largest relative abundance of methanotrophs occurring in well 58I. Table 21 and Table 22 contain the relative abundance data for each technique.

The relative abundance of Type I versus Type II methanotrophs was calculated by dividing the number of Type I or Type II sequences by the sum total of these sequences

Table 21: Methanotroph relative abundances as determined by qPCR.

Monitoring Well	Methanotroph Population as a % of Total Organisms	Type I Methanotrophs as a % of Total Methanotrophs	Type II Methanotrophs as a % of Total Methanotrophs
46 D	0.95	97.7	2.31
52 I	0.18	43.7	56.3
58 I	6.56	76.0	24.0
64 I	0.48	34.8	65.2

Note: Each sample was quantified in duplicate and quantifications were averaged before calculating relative abundances.

Table 22: Methanotroph relative abundance as determined by pyrosequencing.

Monitoring Well	Methanotroph Population as a % of Total Organisms	Type I Methanotrophs as a % of Total Methanotrophs	Type II Methanotrophs as a % of Total Methanotrophs
46 D	1.13	60.6	39.4
52 I	1.71	0.00	100
58 I	54.7	47.4	52.6
63 I	24.1	0.75	99.3
64 I	2.70	0.80	99.2

Note: Each sample was quantified in duplicate and quantifications were averaged before calculating relative abundances.

(16S T1 or 16S T2/ 16S T1+16S T2). Pyrosequencing results for the relative abundance of Type I and Type II methanotrophs were as follows: 46D – 61% and 39%, respectively; 52I – 0% and 100%, respectively; 58I – 47% and 53%, respectively; 63I – 1% and 99%; and 64I – 1% and 99%, respectively. This data suggested that the methanotroph populations in MW 46D consisted of a majority of Type I methanotrophs, while the populations in MW 52I, 58I, 63I, and 64I were majority Type II methanotrophs. Although this data does not match the qPCR data exactly, wells 46D, 52I, and 64I exhibited the same trend in both techniques. Overall, these results suggest that pyrosequencing may be biased towards the more abundant microbial species in an environmental sample, and that qPCR may be a more sensitive at detecting genes present in small quantities. Table 21 and Table 22 contain the relative abundance data for each technique. A phylogenetic tree was constructed using pyrosequencing data (Figure 37). This tree demonstrates an additional method for evaluating relative abundance of Type I versus Type II methanotrophs. Geochemical data for these wells is listed in Table 23.

Transcripts per Gene Ratios[5]

Samples well 64I, 63I, and 46D were subject to simultaneous RNA and DNA extractions. For these samples, the quantity of functional gene transcripts per gene copy was compared for *pmoA* and *mmoX*. Primer concentrations were 300 nM for both functional genes (pmoA 472 and mmoX) and 100 nM for the Luciferase control gene. Standard curve PCR efficiencies for each primer set were of 98.6 %, 96.7 %, and 100 %, respectively. Percent recoveries for the Luciferase control gene ranged from 9.3 % to 60.1 %. For more standard curve characteristics and detailed Luciferase recovery ratios, see APPENDIX A: Table A 11, Table A 12, and Table A 13. Results from this

[5] DNA and RNA extractions for the Carver site were performed by Yang Oh Jin.

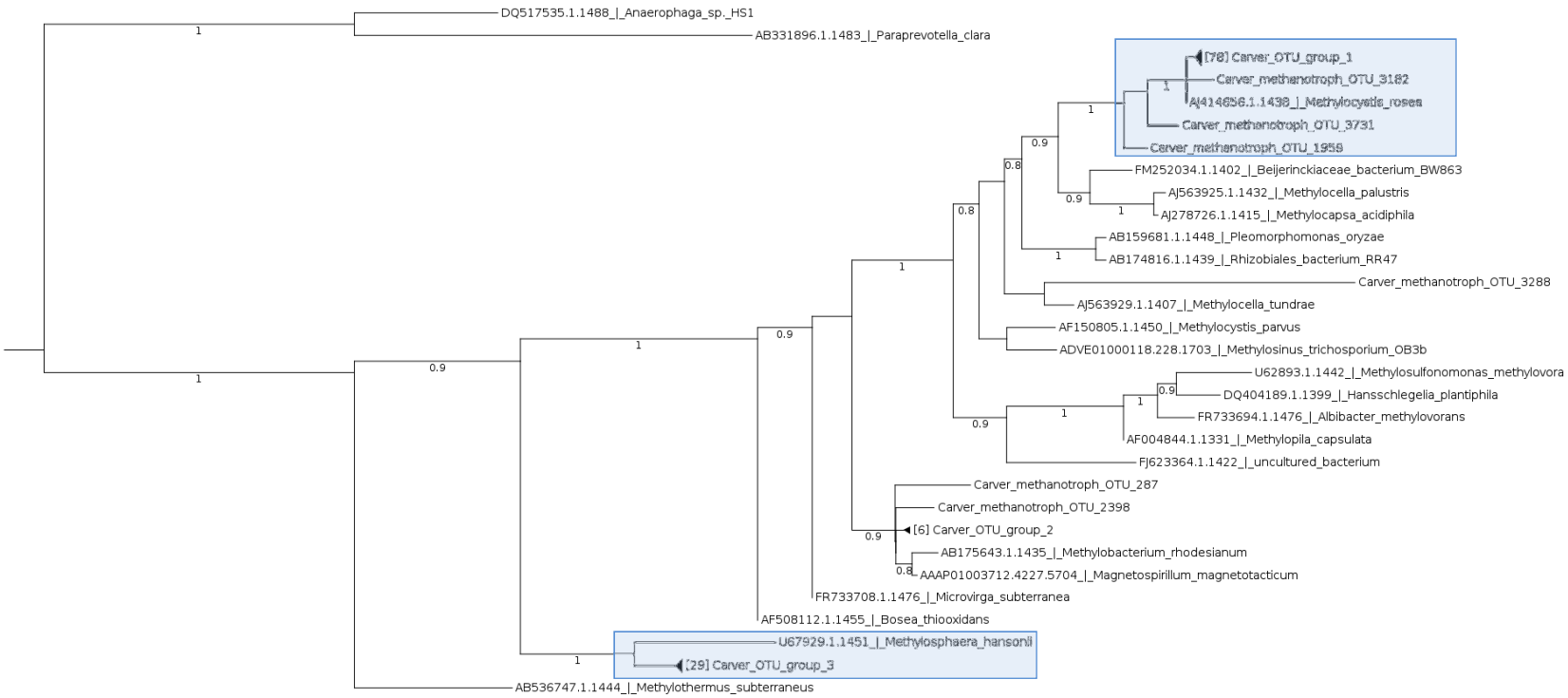

Figure 37: Phylogenetic Tree constructed from methanotroph pyrosequencing data. Sixty nine percent (78 of 114) of sequences gathered by this technique were closely related to *Methylocystis rosea*, a Type II methanotroph. Twenty five percent (29 of 114) of sequences gathered by this technique were closely related to *Methylosphaera hansoni*, a Type I methanotroph. These results could indicate limited diversity of methanotroph species in these samples; however, biases suggested by the qPCR/pyrosequencing comparison could indicate that *Methylocystis rosea* and *Methylosphaera hansoni* are more abundant than other methanotroph species, but not nearly as abundant as would be suggested by this phylogenetic tree.

Table 23: Geochemical data for Carver, MA pyrosequencing experiment.

Wells	Methane (ìg/L)	Vinyl Chloride (ìg/L)	Ethene (ìg/L)
46D	640	1.6	0.4
52I	na	na	na
58I	99	0.8	0.1
64I	0.8	< 1	< 0.1

Note: Samples marked "na" were not analyzed for that specific geochemical maker.

experiment showed that for both *pmoA* and *mmoX*, the transcripts/gene ratio was less than one for all wells (Table 24). Based on previous, non-published, experiments conducted by Yang Oh Jin in the Mattes Lab, a transcript per gene ratio of less than one indicates low levels of functional gene activity. Thus, the VC oxidation occurring in these wells is not likely attributed to methanotrophic bacteria, since their functional gene expression is very low. Geochemical data for these wells is listed in Table 25.

With regard to the mmoX dissociation curve, results mirrored those of Soldotna, with the presence of the standard-curve double peak at 76°C and 86°C. Environmental samples contained two peak temperatures as well. It is suspected that the primer-dimer artifact in environmental samples is due to low target gene abundance. Dissociation curves for the pmoA 472, mmoX, and Luciferase primer assays can be found in APPENDIX C: Figure C 24, Figure C 25, Figure C 26, and Figure C 27

Table 24: *pmoA* and *mmoX* transcript per gene ratios.

Monitoring Well	Transcripts per Gene Ratio			
	pmoA 472		mmoX	
64I	0.18	0.10	0.27	0.26
63I	0.02	0.01	0.00	0.00
46D	0.02	0.01	0.28	0.20

Note: Each sample was quantified in duplicate and quantifications were averaged before calculating relative abundances.

Table 25: Geochemical data for Carver, MA cDNA experiment.

Wells	Methane (ìg/L)	Vinyl Chloride (ìg/L)	Ethene (ìg/L)
46D	363	0.6	0.1
63I	217	1.5	0.5
64I	117	1.1	0.2

CHAPTER 5

SUMMARY AND CONCLUSIONS

In this work, we evaluated several PCR primer sets from the literature for use in methanotroph qPCR assays of groundwater samples. PCR primers targeting two functional genes involved in VC cometabolism, *pmoA* (sub-unit of pMMO) and *mmoX* (sub-unit of sMMO), as well as 16S rRNA gene primers that targeted Bacteria, and Type I and Type II methanotrophs were tested. These assays were made quantitative by constructing standard curves with DNA from *Methylococcus capsulatus* (Type I) and *Methylocystis* sp. strain Rockwell (Type II). Primer sets were evaluated by comparing gene abundance estimated against known amounts of Type I and Type II methanotroph DNA. Results of the validation experiments showed that two of the *pmoA* primer sets (pmoA 178 and pmoA 330) could not robustly amplify methanotroph DNA in such a way that would make them adequate for use in environmental sample qPCR assays. However, one pmoA (pmoA 472) and mmoX primer set, as well as three 16S primer sets (16S T1, 16S T2, 16S U) were tested and found to be suitable for qPCR environmental applications.

After primer validation, an effort to substantiate this methanotroph qPCR method was made by attempting to investigate methanotroph populations in groundwater samples from VC-contaminated sites. Some samples studied were also subjected to 16S rRNA gene pyrosequencing, allowing for relative abundance comparisons with qPCR analyses, and further substantiation of the method. Results from all environmental sites showed that each primer set was able to amplify from genomic DNA extracted from contaminated groundwater samples. This was an important confirmation because groundwater samples typically yield low concentrations of genomic DNA which in turn could present an obstacle in the qPCR amplification of such samples. Comparison of qPCR and pyrosequencing analyses of relative methanotroph abundance revealed that,

although the actual quantifications produced were not the same, the data trends were similar. On the other hand, comparison of qPCR and pyrosequencing analyses of relative abundances of Type I and Type II methanotrophs revealed that the data produced by these techniques did not always follow the same trend. This suggests there are biases in either one or both of these evaluation techniques. In groundwater samples where both DNA and RNA was extracted, the quantities of functional gene transcripts per gene copy was compared, revealing that the transcripts/gene ratio for both *pmoA* and *mmoX* was less than one, implying relatively low methanotroph activity.

Ultimately our data suggests that the qPCR method used in this study can adequately detect the abundance and functionality of methanotrophs in a rapid, convincing and more cost effective manner than the current enrichment culture technique. Our data also suggests that, at least at the Carver site, methanotrophs are not actively expressing their VC-oxidizing functional genes, casting uncertainty on their role in the VC biodegradation occurring at that site.

CHAPTER 6
ENGINEERING SIGNIFICANCE AND RECOMMENDATIONS FOR FUTURE RESEARCH

The research presented in this thesis supports the premise that real-time quantitative PCR can be used to assess the abundance and functionality of VC-degrading methanotrophs in a rapid, convincing, and more cost effective manner. Identification of genes associated with enzymatic pathways directly related to the degradation of specific groundwater contaminants via real-time PCR is as persuasive at demonstrating the presence of VC oxidizing microbes as the current enrichment-culture technique. Furthermore, obtaining environmental results with real-time PCR can take a matter of days as compared to the several weeks or months needed for enrichment cultures. This technique, when coupled with rate studies, has the potential to improve the ability to evaluate, demonstrate and measure natural and enhanced attenuation of dilute VC plumes. The resulting improved VC bioremediation approach would thereby improve decision making, save time, and ultimately, reduce the life cycle costs for remediation of dilute VC plumes.

Despite the insight this research provides, there is still much work that needs to be done before real-time qPCR can be utilized to its full potential at a contaminated site. The most immediate use of this technique would in a controlled lab setting where the interactions between methanotrophs and other microorganisms that co-exist at many of these contaminated sites can be elucidated. Armed with the knowledge of microbial-substrate interactions, this qPCR technique could be used in conjunction with geochemical data to rapidly and accurately evaluate the in-situ remediation capacity of indigenous bacteria at contaminated sites, and could also provide insight as to which bacteria will play major roles in the bioremediation process. This knowledge will help

remediation officials determine how to stimulate those specific bacteria to accelerate the biodegradation process.

APPENDIX A

QPCR STANDARD CURVE SUPPORTING DOCUMENTS

Kolb Primer Results

When used to amplify *Methylocystis* sp. and *Methylococcus* sp. pure cultures genomic DNA, the Kolb primer set produced either two PCR products of no PCR product, respectively (Figure A 1). This was cause for concern. To begin to resolve the issue, the PCR products were excised from the agarose gel and then sequenced. Sequence data revealed the Kolb were amplifying non-specific PCR products. Due to the difficulties of amplifying from pure culture methanotrophs, coupled with the fact that, when able to amplify, these primers were amplifying non-specifically, the Kolb primers were not used in the remainder of this qPCR method development. These results suggest that we should abandon the Kolb primer set.

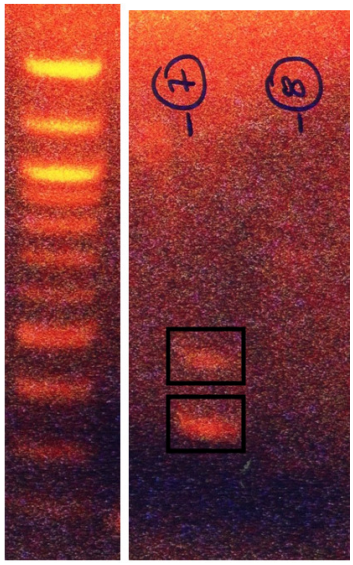

Figure A 1: End point PCR products of Kolb primers and Methylococcus (lane 7) and Methylocystis (lane 8) template DNA.

pmoA 178 and pmoA 330 PCR Efficiency Variations

Reproducibility of the methanotrophs standard curve on each plate was an issue of concern. The PCR efficiencies of the standard curves varied between plates

considerably, from 70% to 125%. One possible cause for this variation may be related to the freshness of the standard curve. Experiments show that when the standards are made with in 48 hrs of use, the PCR efficiencies are closer to 100% (115% for *Methylocystis* and *Methyloccocus* when amplifying with pmoA 178, 102% for *Methylocystis* and 107% for *Methyloccocus* when amplifying with pmoA 330 M, 98.8% for *Methylocystis* and 97.0% for *Methyloccocus* when amplifying with the pmoA 330 primer set). When an older standard curve was used (stored at -20 for 3 weeks) the PCR efficiencies were less than desirable (125% for *Methylocystis* and *Methyloccocus* when amplifying with pmoA 178, 70% for *Methylocystis* and *Methyloccocus* when amplifying with pmoA 330). In order to increase their reproducibility, the standards must be made fresh for every experiment.

Standard Curve Characteristics

Validation Experiments

Table A 1: Average standard curve characteristics for pmoA 178 and pmoA 330 primer validation experiments.

	Dynamic Range	Slope	R^2	PCR Efficiency (%)	Y-intercept (cycle #)
T1	100 - 10^7	-3.43	0.999	95.54	36.52
T2	100 - 10^6	-3.67	0.991	87.33	38.21
pmoA 178	100 - 10^7	-3.43	0.998	95.83	37.16
pmoA 330	100 - 10^7	-3.46	0.996	94.47	36.03

Note: Each standard curve was run in duplicate.

Table A 2: Average standard curve characteristics for pmoA 472 and mmoX primer validation experiment.

	Dynamic Range	Slope	R^2	PCR Efficiency (%)	Y-intercept (cycle #)
T1	1000 - 10^6	-3.25	0.997	102.93	34.75
T2	100 - 10^6	-3.30	0.999	100.94	35.43
pmoA 472	100 - 10^6	-3.37	0.998	98.05	36.36
mmoX	100 - 10^6	-3.47	0.999	94.18	35.80

Note: Each standard curve was run in duplicate.

Table A 3: Average standard curve characteristics for 16S T1 and 16S T2 primer validation experiment.

	Dynamic Range	Slope	R^2	PCR Efficiency (%)	Y-intercept (cycle #)
T1	100 - 10^6	-3.30	0.997	100.80	35.53
T2	100 - 10^6	-3.34	0.999	99.17	35.58
16S U	10^4 - 10^6	-3.27	0.999	102.22	34.79

Note: Each standard curve was run in duplicate.

Soldotna, AK Environmental Samples

Table A 4: Average standard curve characteristics for pmoA 472 and mmoX in Soldotna, AK environmental sample qPCR assay.

	Dynamic Range	Slope	R^2	PCR Efficiency (%)	Y-intercept (cycle #)
pmoA 472	100 - 10^5	-3.31	0.998	100.62	36.28
mmoX	100 - 10^6	-3.38	0.999	97.64	35.80

Note: Each standard curve was run in duplicate.

Table A 5: No Template Control (NTC) results for Soldotna, AK standard curves.

	No Template Control	
	Duplicate 1 (cycle #)	Duplicate 2 (cycle #)
pmoA 472	35.3	35.02
mmoX	35.69	33.61

Note: Each NTC was run in duplicate.

Naval Air Station Oceana, Virginia Environmental Samples

Table A 6: Average standard curve characteristics for pmoA 472, mmoX, 16 T1, and 16S T2 in NAS Oceana, VA environmental sample qPCR assay.

	Dynamic Range	Slope	R^2	PCR Efficiency (%)	Y-intercept (cycle #)
pmoA 472	100 - 10^5	-3.29	0.997	101.17	36.90
mmoX	100 - 10^6	-3.34	0.979	99.44	35.72
16S T1	1000 - 10^6	-3.28	0.998	101.88	35.31
16S T2	100 - 10^6	-3.46	0.999	94.53	38.66

Note: Each standard curve was run in duplicate.

Table A 7: No Template Control (NTC) results for NAS Oceana, VA standard curves.

	No Template Control	
	Duplicate 1 (cycle #)	Duplicate 2 (cycle #)
pmoA 472	36.37	undetectable
mmoX	undetectable	undetectable
16S T1	33.17	33.6
16S T2	36.93	36.76

Note: Each NTC was run in duplicate.

Carver, MA - Pyrosequencing Experiment

Table A 8: Luciferase gene recovery ratios for Carver, MA qPCR experiments.

Monitoring Well	Injected Reference Gene Copies	Reference Gene Copies Recovered	Recovery Ratio
46 D	75,000,000	10,114,966	0.134866
52 I	75,000,000	2,782,178	0.037096
58 I	75,000,000	3,750,655	0.050009
64 I	75,000,000	1,171,753	0.015623

Note: Each sample was run in duplicate and average quantifications were used to calculate recovery ratios.

Table A 9: Average standard curve characteristics for 16S U, 16 T1, 16S T2 and Luciferase in Carver, MA environmental sample qPCR assay.

	Dynamic Range	Slope	R^2	PCR Efficiency (%)	Y-intercept (cycle #)
16S U	100 - 10^6	-3.34	0.990	99.40	36.04
16S T1	100 - 10^6	-3.34	0.998	99.26	36.03
16S T2	100 - 10^6	-3.32	0.998	99.88	36.20
Luciferase	100 - 10^6	-3.33	0.998	99.80	35.91

Note: Each standard curve was run in duplicate

Table A 10: No Template Control (NTC) results for Carver, MA standard curves shown in Table A 9.

	No Template Controls	
	Duplicate 1 (cycle #)	Duplicate 2 (cycle #)
16S U	33.56	33.85
16S T1	34.37	33.79
16S T2	35.00	35.33
Luciferase	undetectable	undetectable

Note: Each NTC was run in duplicate.

Carver, MA – cDNA Experiment

Table A 11: Luciferase gene recovery ratios for Carver, MA qPCR experiments.

Monitoring Well	Injected Reference Gene Copies	Reference Gene Copies Recovered	Recovery Ratio
64I	225,000,000	25,392,468	0.112855
63I	225,000,000	20,950,970	0.093115
46D	225,000,000	21,836,357	0.09705
64I cDNA	225,000,000	61,151,264	0.271783
63I cDNA	225,000,000	31,010,226	0.137823
46D cDNA	225,000,000	135,332,755	0.601479

Note: Each sample was run in duplicate and average quantifications were used to calculate recovery ratios.

Table A 12: Average standard curve characteristics for 16S U, 16 T1, 16S T2 and Luciferase in Carver, MA environmental sample qPCR assay.

	Dynamic Range	Slope	R^2	PCR Efficiency (%)	Y-intercept (cycle #)
pmoA 472	100 - 10^6	-3.36	0.992	98.62	37.38
mmoX	100 - 10^6	-3.40	0.999	96.69	36.04
Luciferase	300 - $3x10^6$	-3.29	0.999	101.38	35.27

Note: Each standard curve was run in duplicate.

Table A 13: No Template Control (NTC) results for Carver, MA standard curves shown in Table A 12.

	No Template Controls	
	Duplicate 1 (cycle #)	Duplicate 2 (cycle #)
pmoA 472	34.02	35.49
mmoX	31.19	31.56
Luciferase	undetectable	undetectable

Note: Each NTC was run in duplicate.

APPENDIX B

CONTAMINATED SITE SUPPORTING DOCUMENTS

Additional Site Information for Soldotna, AK

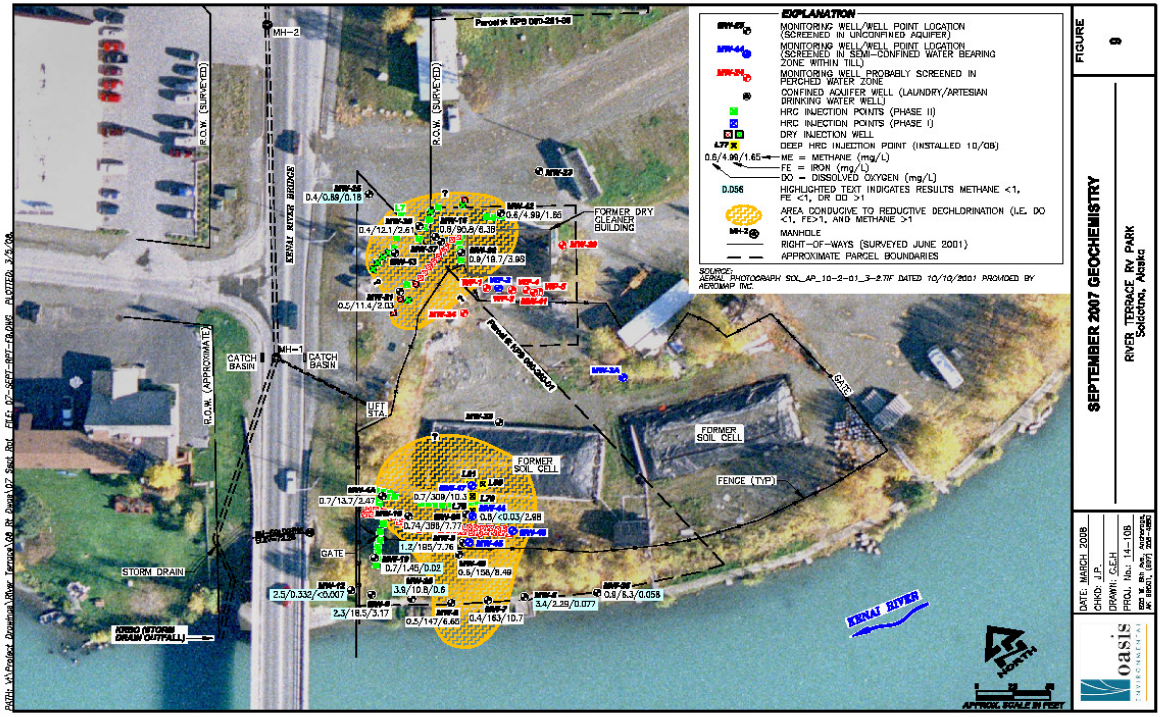

Figure B 1: Geochemical data from 2007 for Soldotna, AK contaminated site. Yellow areas indicate where methane is detected in groundwater at concentrations above 1 mg/L [99].

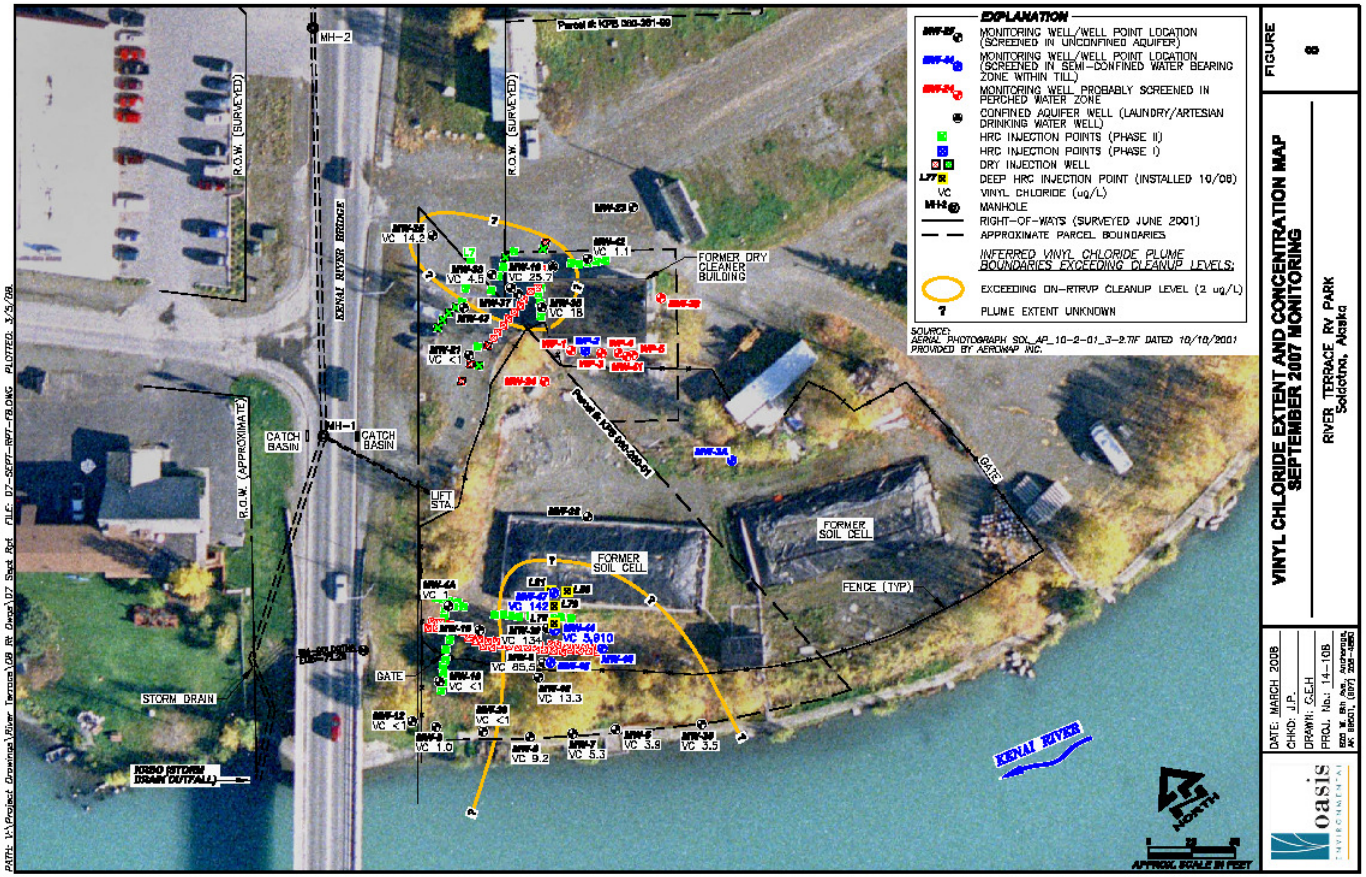

Figure B 2: Vinyl chloride concentration in 2007 at Soldotna, AK. Yellow lines indicate areas where VC is exceeding the 2 ppb MCL limit [99].

Additional Site Information for Naval Air Station

Oceana, Virginia

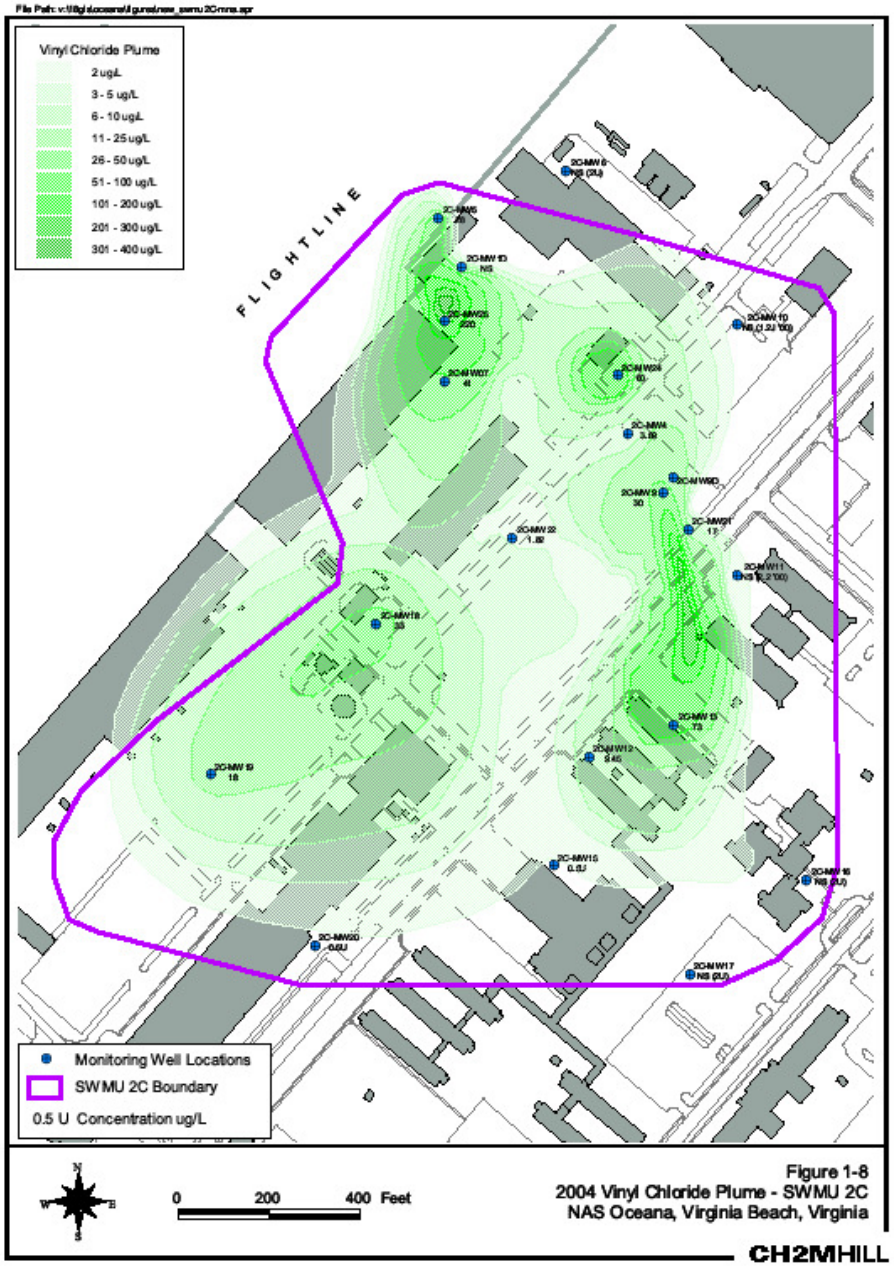

Figure B 3: VC plumes at NAS Oceana, VA [103].

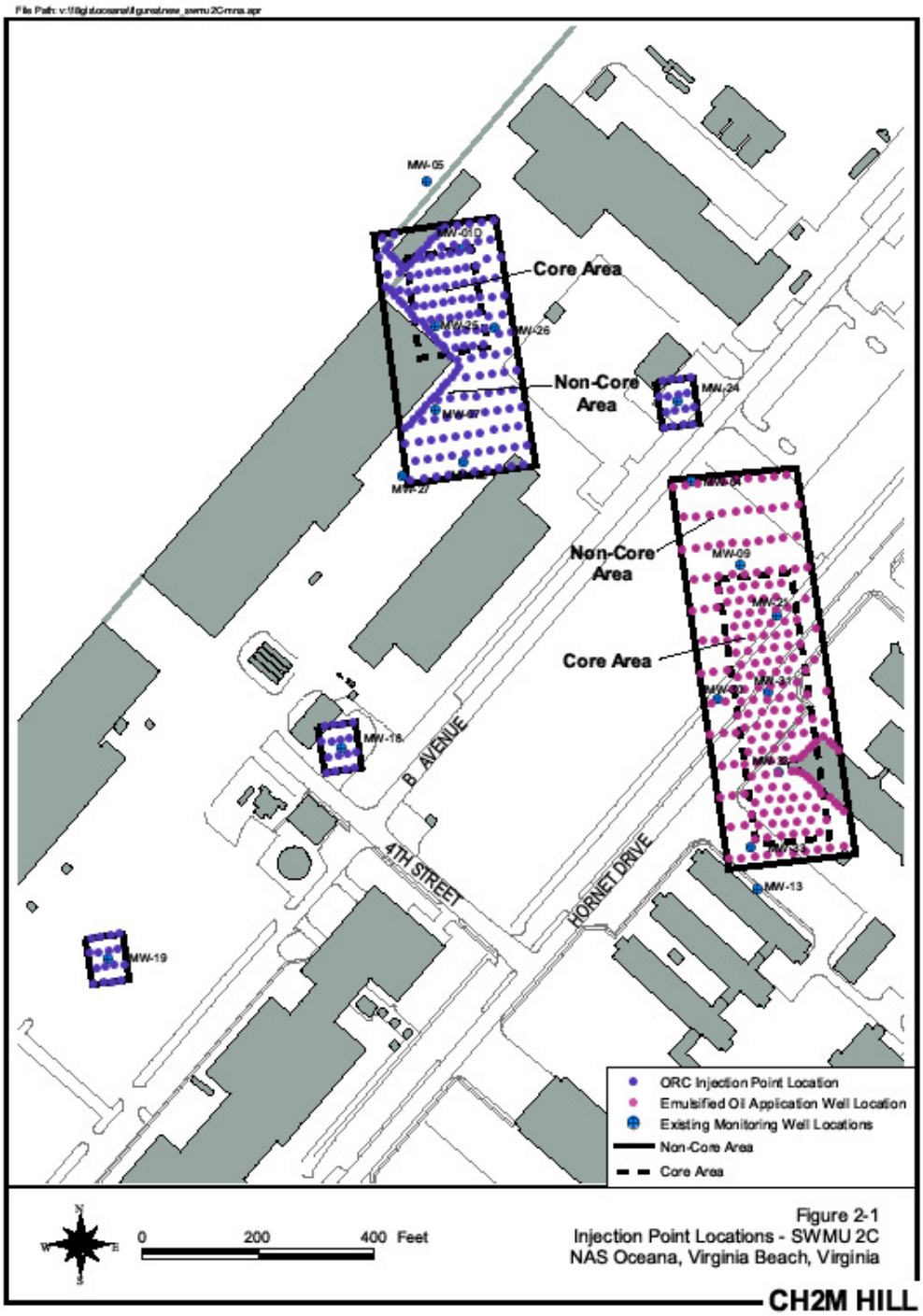

Figure B 4: Treatment set up for NAS Oceana. Purple dots represent ORC injections; pink dots represent emulsified oil injections [103].

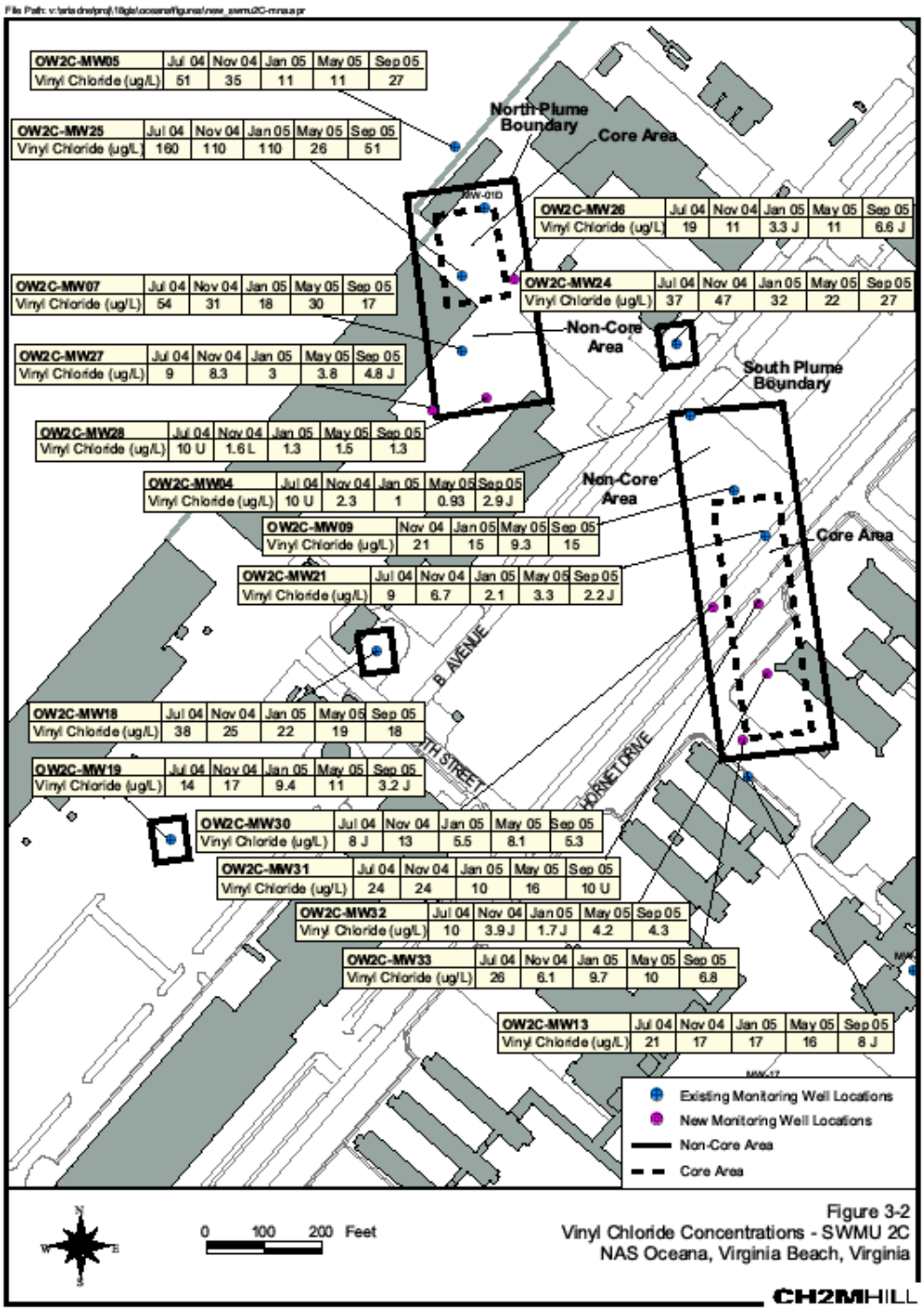

Figure B 5: Changes VC concentrations for NAS Oceana site from 2004 to 2005 [103].

APPENDIX C

DISSOCIATION CURVE SUPPORTING DOCUMENTS

Optimization Experiments:

pmoA 178/330 Dissociation Curves

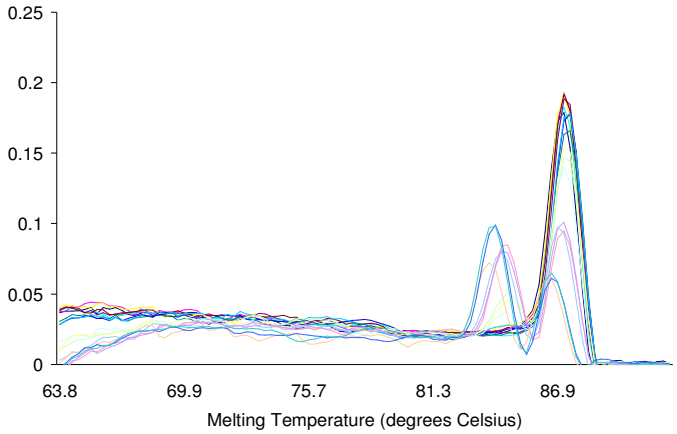

Figure C 1: Dissociation curve for primer set pmoA 178 amplifying template DNA from *Methylocystis* sp. strain Rockwell at a primer concentration of 300 nM. Double peaks are seen in samples containing little (10^2) to no (no-template control) template DNA, indicating probable primer-dimer artifacts.

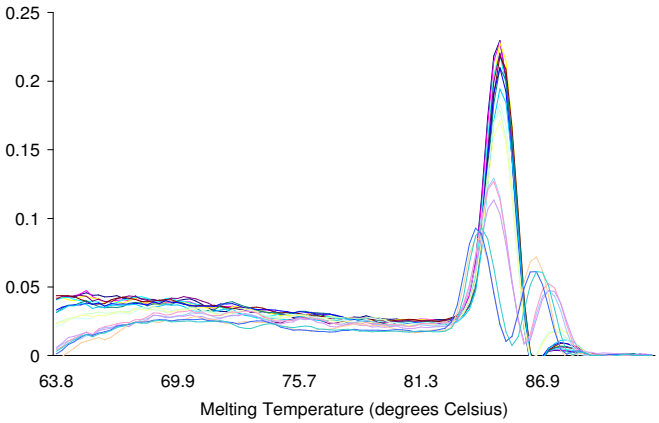

Figure C 2: Dissociation curve for primer set pmoA 178 amplifying template DNA from *Methylococcus capsulatus* at a primer concentration of 300 nM. Double peaks are seen in samples containing little (10^2) to no (no-template control) template DNA, indicating probable primer-dimer artifacts.

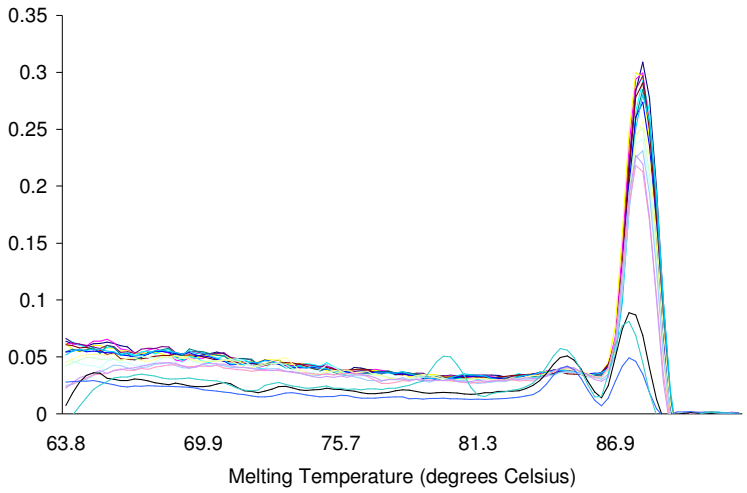

Figure C 3: Dissociation curve for primer set pmoA 330 amplifying template DNA from *Methylocystis* sp. strain Rockwell at a primer concentration of 300 nM. Double peaks are seen in no-template control samples indicating probable primer-dimer artifacts.

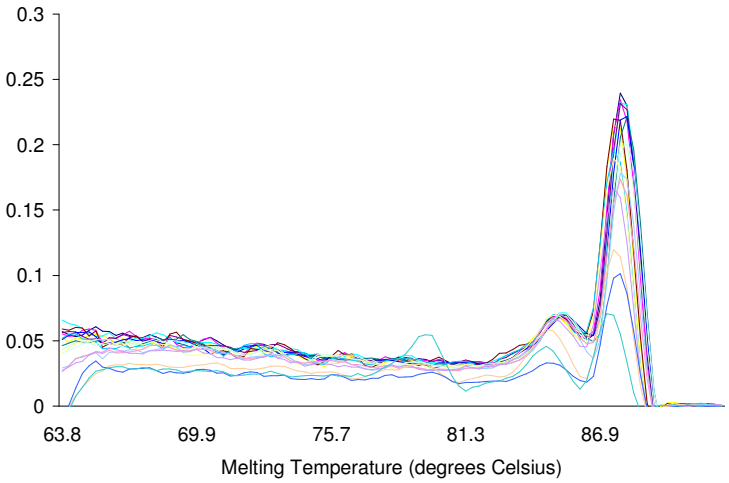

Figure C 4: Dissociation curve for primer set pmoA 330 amplifying template DNA from *Methylococcus capsulatus* at a primer concentration of 300 nM. Double peaks are seen in all samples. PCR products were purified and sequence results indicated that both peaks represented the *pmoA* gene.

Optimization Experiments:

16S T1 and 16S T2 Dissociation Curves

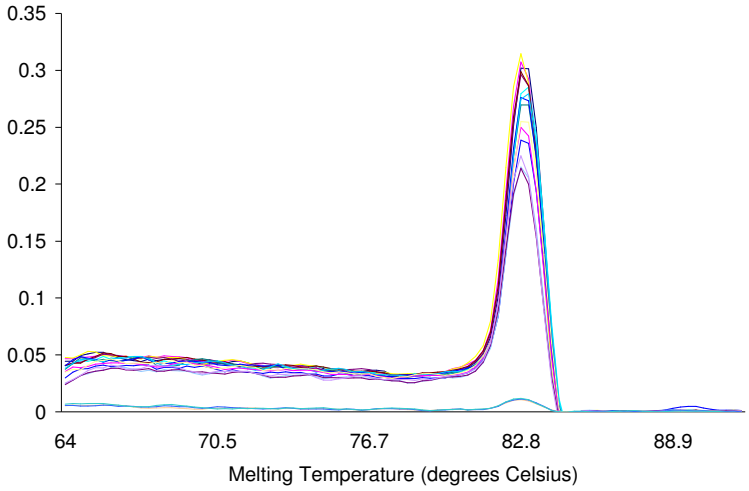

Figure C 5: Dissociation curve for primer set 16S T1 amplifying template DNA from *Methylococcus capsulatus* at a primer concentration of 800 nM.

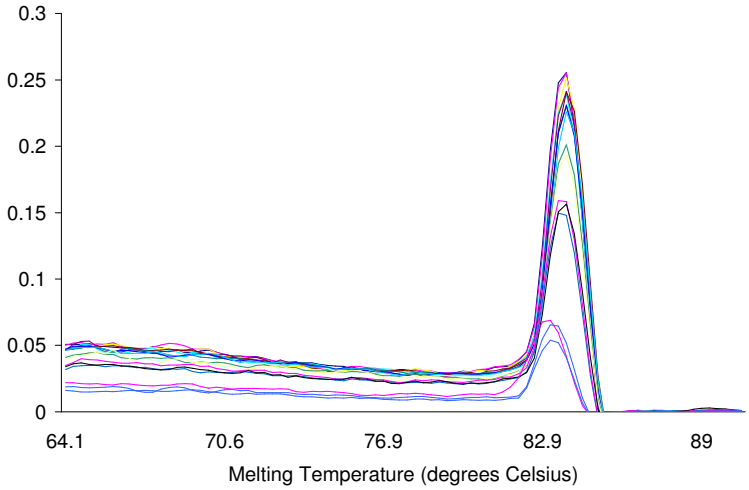

Figure C 6: Dissociation curve for primer set 16S T2 amplifying template DNA from *Methylocystis* sp. strain Rockwell at a primer concentration of 200 nM.

Validation Experiments:

pmoA 178/pmoA 330 Dissociation Curves

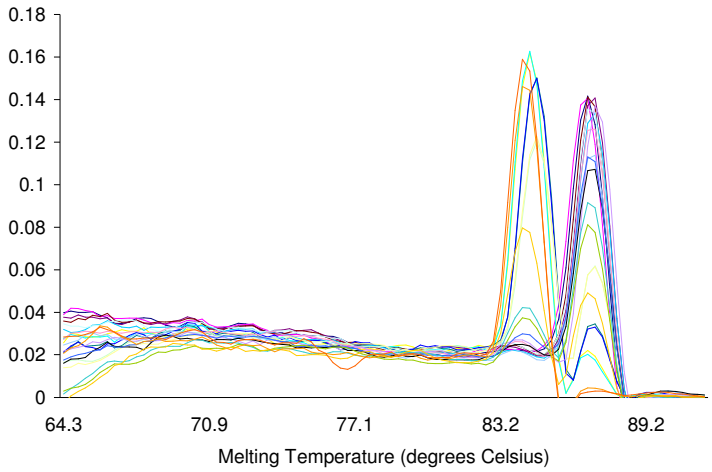

Figure C 7: Dissociation curve for primer set pmoA 178. The ~89°C peak represents standard curve melting temperatures, while the ~84°C peak represents melting temperature of the Type I/Type II sample mixtures.

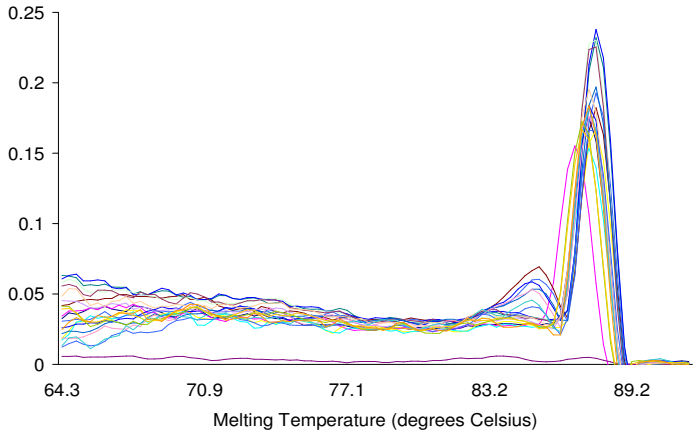

Figure C 8: Dissociation curve for primer set pmoA 330 amplifying standard curve template DNA and Type I/Type II sample mixtures at a primer concentration of 300 nM.

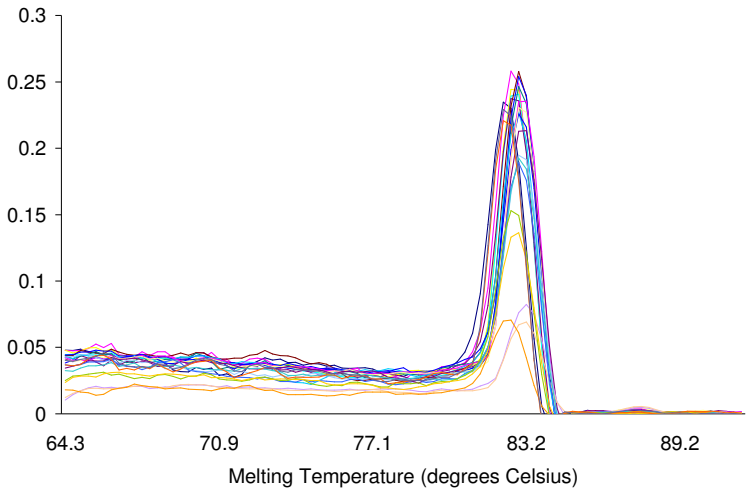

Figure C 9: Dissociation curve for primer set pmoA 16S T1 amplifying standard curve template DNA and Type I/Type II sample mixtures at a primer concentration of 800 nM.

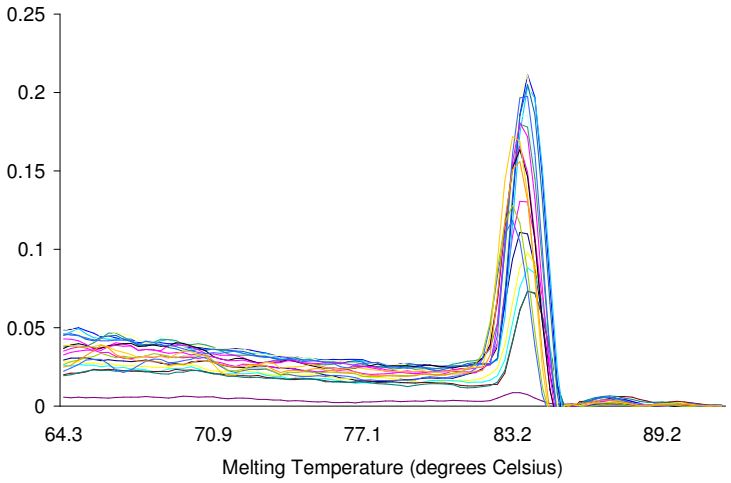

Figure C 10: Dissociation curve for primer set pmoA 16S T2 amplifying standard curve template DNA and Type I/Type II sample mixtures at a primer concentration of 200 nM.

Validation Experiments:

pmoA 472 and mmoX Dissociation Curves

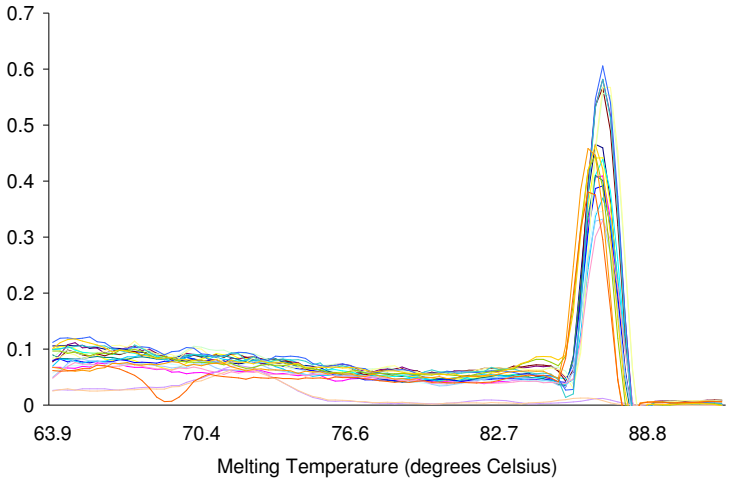

Figure C 11: Dissociation curve for primer set pmoA 472 amplifying standard curve template DNA and Type I/Type II sample mixtures at a primer concentration of 300 nM.

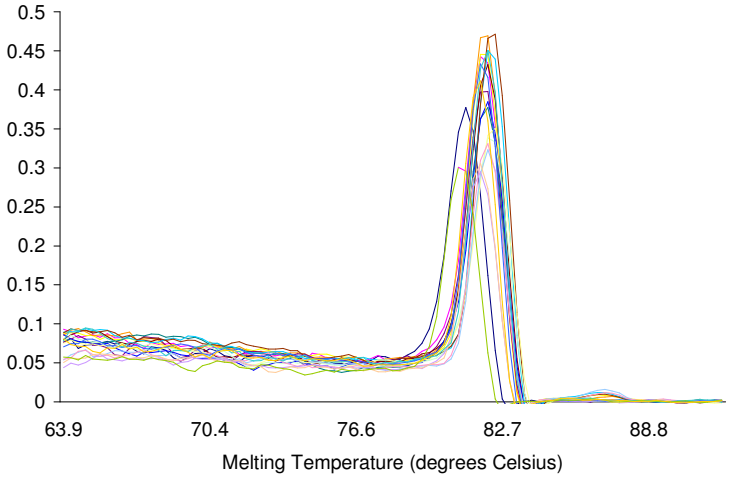

Figure C 12: Dissociation curve for primer set pmoA 16S T1 amplifying standard curve template DNA and Type I/Type II sample mixtures at a primer concentration of 800 nM.

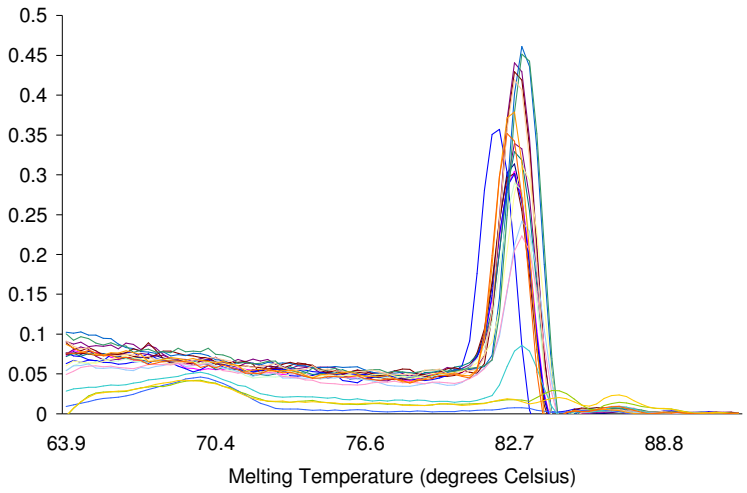

Figure C 13: Dissociation curve for primer set pmoA 16S T2 amplifying standard curve template DNA and Type I/Type II sample mixtures at a primer concentration of 200 nM.

Validation Experiments:

16S T1 and 16S T2 Dissociation Curves

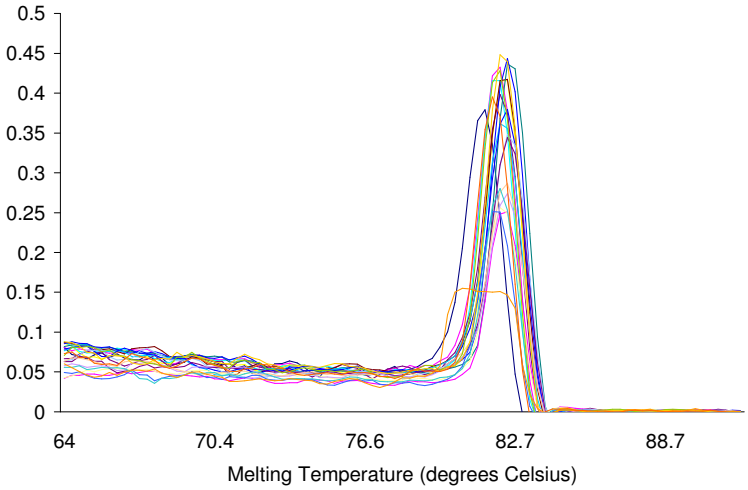

Figure C 14: Dissociation curve for primer set pmoA 16S T1 amplifying standard curve template DNA and Type I/Type II sample mixtures at a primer concentration of 800 nM.

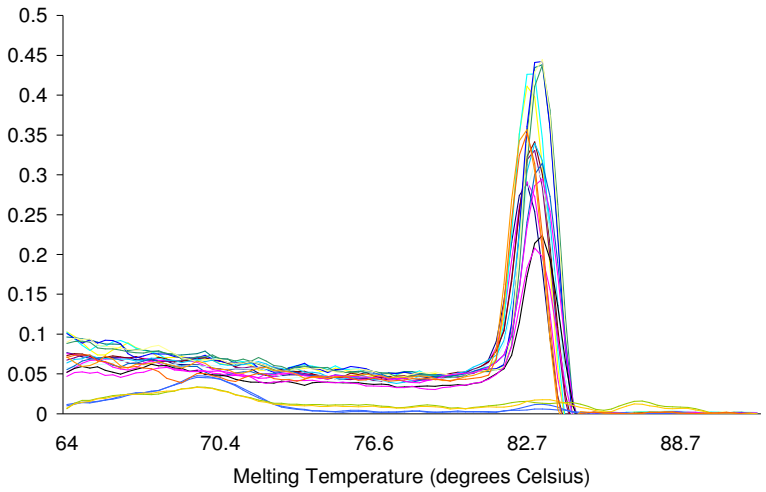

Figure C 15: Dissociation curve for primer set pmoA 16S T2 amplifying standard curve template DNA and Type I/Type II sample mixtures at a primer concentration of 200 nM.

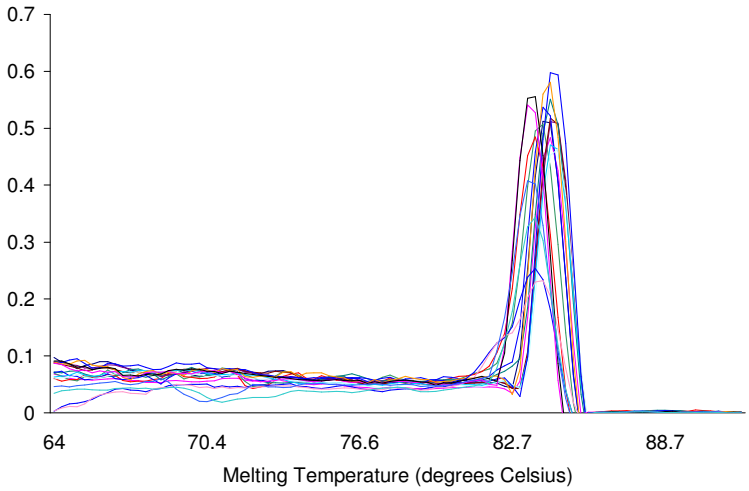

Figure C 16: Dissociation curve for primer set 16S U amplifying template DNA from *Methylocystis* sp. strain Rockwell at a primer concentration of 300 nM.

Environmental Site Evaluation:

Soldotna, AK Dissociation Curves

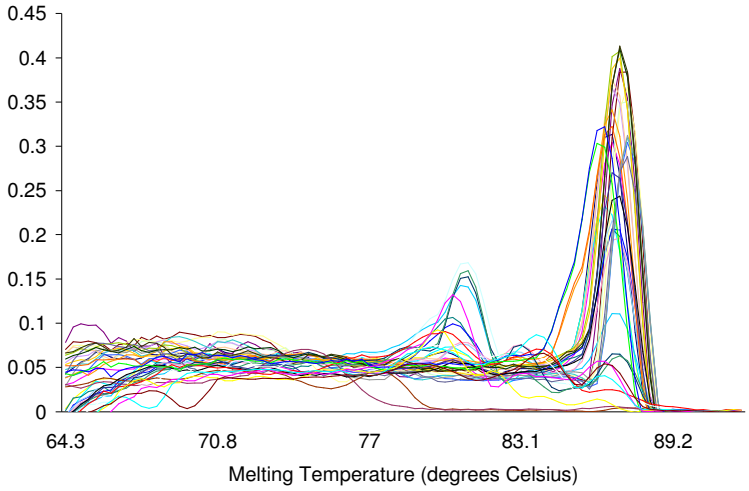

Figure C 17: Dissociation curve for primer set pmoA 472 amplifying standard curve template DNA and environmental samples from VC contaminated groundwater in Soldotna, AK.

Environmental Site Evaluation:

NAS Oceana, VA Dissociation Curves

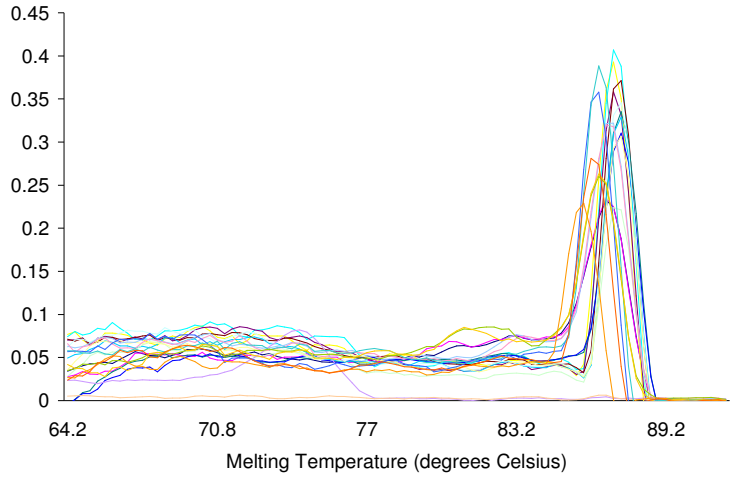

Figure C 18: Dissociation curve for primer set pmoA 472 amplifying standard curve template DNA and environmental samples from VC contaminated groundwater in NAS Oceana, VA.

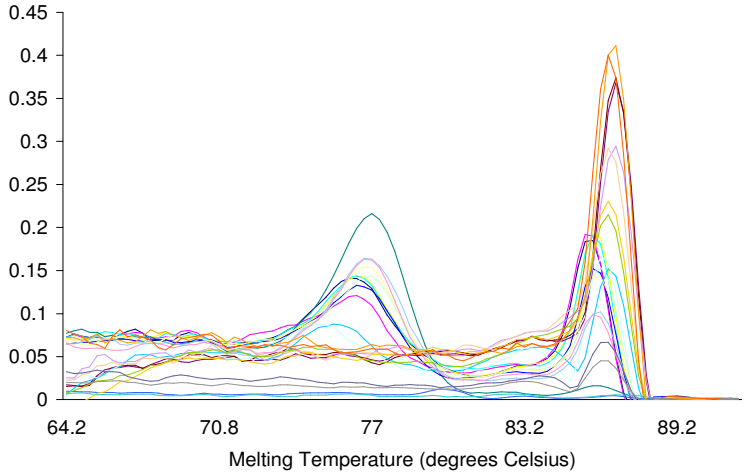

Figure C 19: Dissociation curve for primer set mmoX amplifying standard curve template DNA and environmental samples from VC contaminated groundwater in NAS Oceana, VA.

Environmental Site Evaluation:

Carver, MA Dissociation Curves

Pyrosequencing Experiment

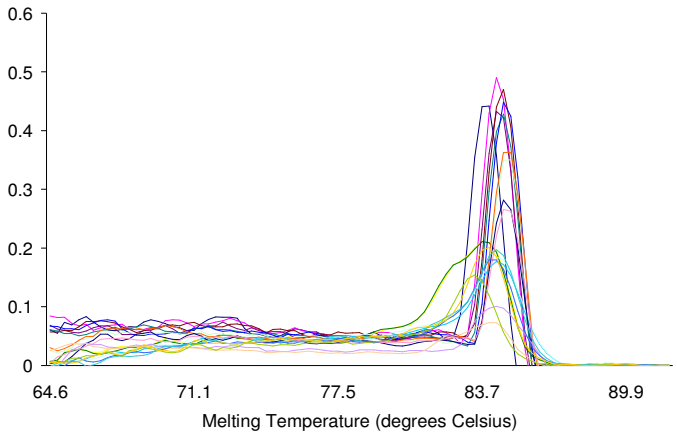

Figure C 20: Dissociation curve for primer set 16S U amplifying standard curve template DNA and environmental samples from VC contaminated groundwater in Carver, MA.

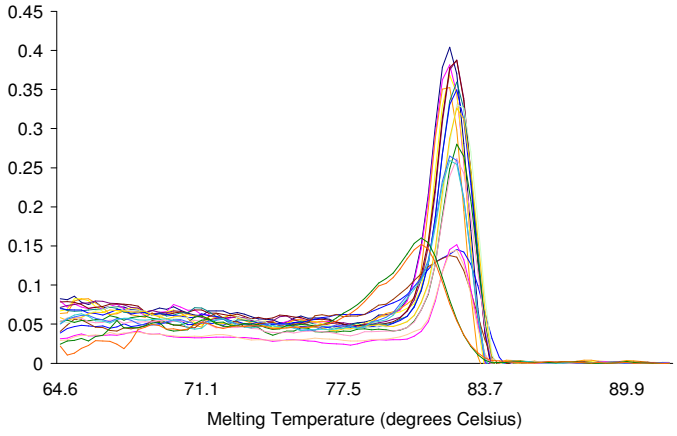

Figure C 21: Dissociation curve for primer set 16S T1 amplifying standard curve template DNA and environmental samples from VC contaminated groundwater in Carver, MA.

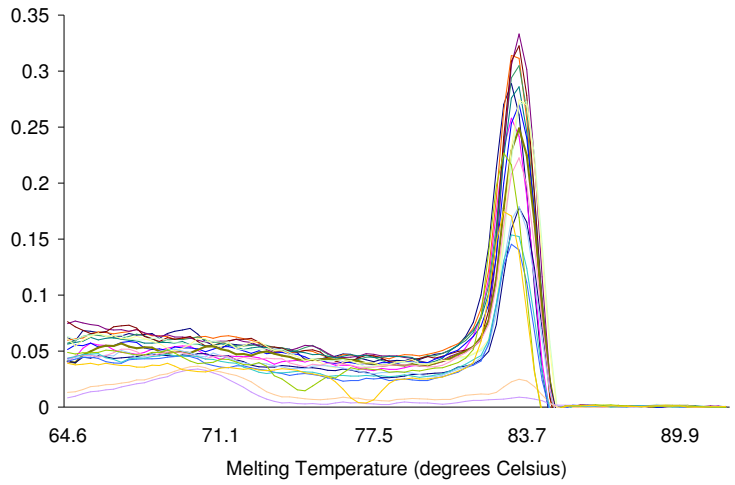

Figure C 22: Dissociation curve for primer set 16S T2 amplifying standard curve template DNA and environmental samples from VC contaminated groundwater in Carver, MA.

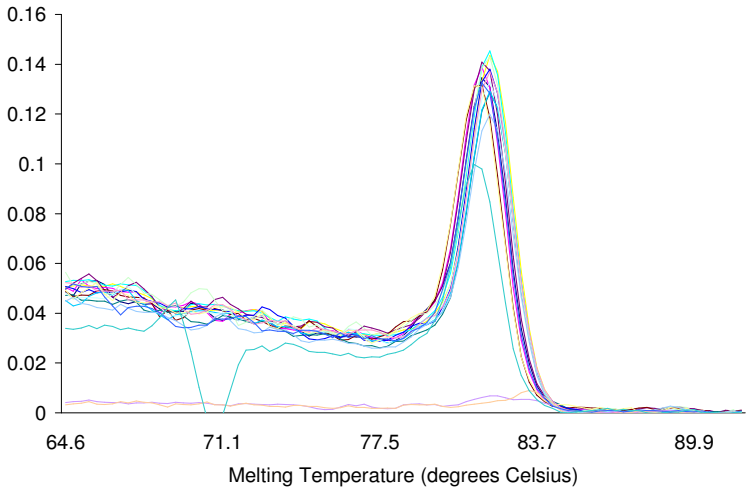

Figure C 23: Dissociation curve for Luciferase primer set amplifying standard curve template DNA and environmental samples from VC contaminated groundwater in Carver, MA.

cDNA Experiment

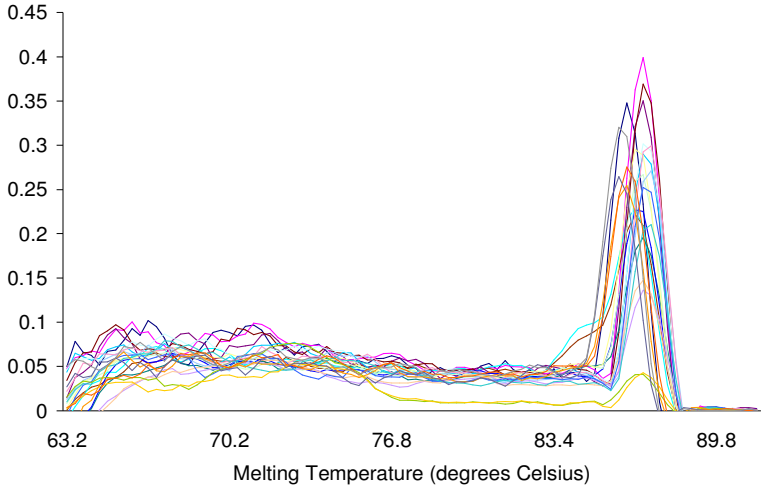

Figure C 24: Dissociation curve for pmoA 472 primer set amplifying standard curve template DNA and environmental samples from VC contaminated groundwater in Carver, MA.

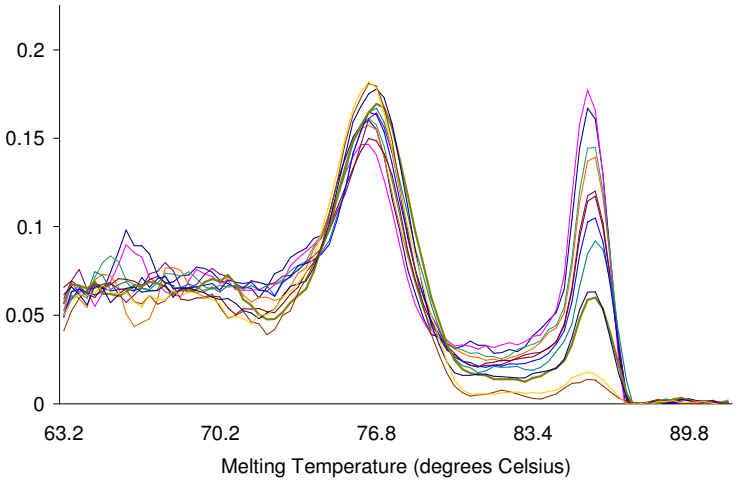

Figure C 25: Dissociation curve for *mmoX* primer set standard curve Carver, MA cDNA experiment. Multiple peaks were observed and appear to be primer-dimer artifacts since the no-template control contains only one peak.

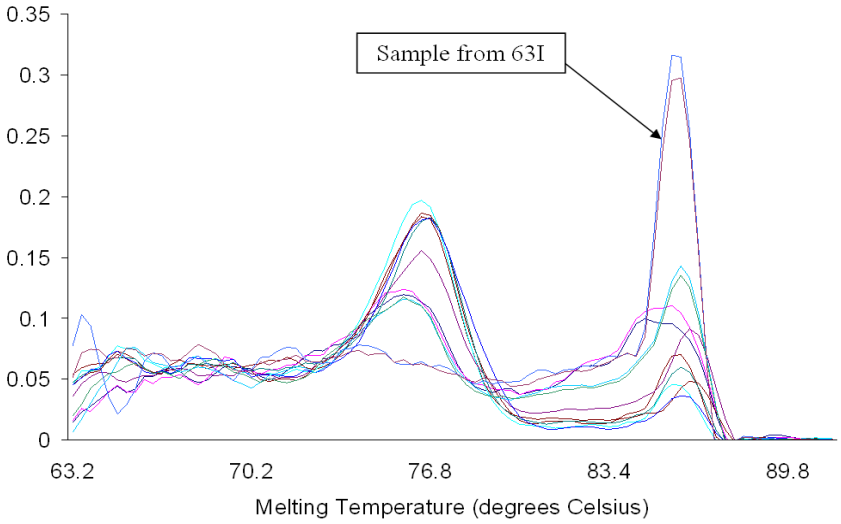

Figure C 26: Dissociation curve for *mmoX* primer set amplifying environmental samples from Carver, MA cDNA experiment. Multiple peaks were observed and appear to be primer-dimer artifacts caused by low target gene abundances. Sample 63I showed high quantities of the target gene, which could explain why it did not have a melting temperature associated with the primer-dimer peak.

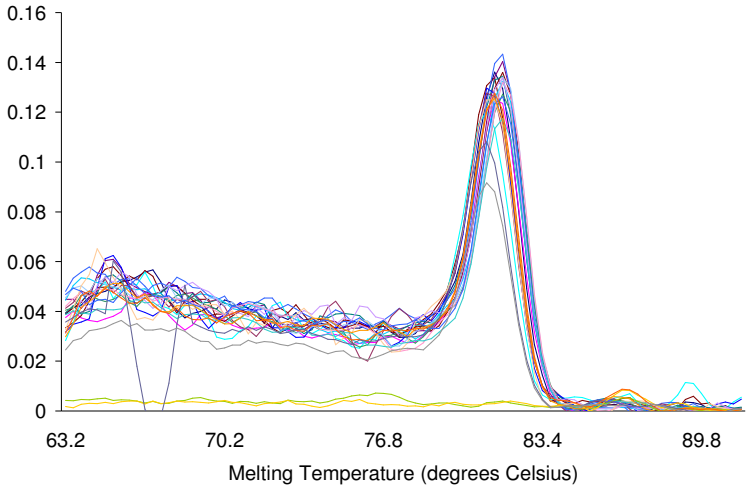

Figure C 27: Dissociation curve for Luciferase primer set amplifying standard curve template DNA and environmental samples from VC contaminated groundwater in Carver, MA.

REFERENCES

1. Bucher, J. R.; Cooper, G.; Haseman, J. K.; Jameson, C. W.; Longnecker, M.; Kamel, F.; Maronpot, R.; Matthews, H. B.; Melnick, R.; Newbold, R., Report on Carcinogens. In 12 ed.; U.S. Department of Health and Human Services, P. H. S. N. T. P., Ed. 2011.

2. Squillace, P. J.; Moran, M. J.; Lapham, W. W.; Price, C. V.; Clawges, R. M.; Zogorski, J. S., Volatile Organic Compounds in Untreated Ambient Groundwater of The United States, 1985-1995. *Environ Sci Technol* **1999,** *33*, (23), 4176-4187.

3. Davis, J. W.; Carpenter, C. L., Aerobic Biodegradation of Vinyl-Chloride in Groundwater Samples. *Appl Environ Microb* **1990,** *56*, (12), 3878-3880.

4. Lee, M. D.; Odom, J. M.; Buchanan, R. J., New Perspectives on Microbial Dehalogenation of Chlorinated Solvents: Insights From The Field. *Annu Rev Microbiol* **1998,** *52*, 423-452.

5. Fogel, M. M.; Taddeo, A. R.; Fogel, S., Biodegradation of Chlorinated Ethenes by a Methane-Utilizing Mixed Culture. *Appl Environ Microb* **1986,** *51*, (4), 720-724.

6. Semrau, J. D.; DiSpirito, A. A.; Yoon, S., Methanotrophs and Copper. *Fems Microbiol Rev* **2010,** *34*, (4), 496-531.

7. Kikuchi, T.; Iwasaki, K.; Nishihara, H.; Takamura, Y.; Yagi, O., Quantitative and Rapid Detection of The Trichloroethylene-Degrading Bacterium *Methylocystis* sp. M in Groundwater by Real-Time PCR. *Appl Microbiol Biot* **2002,** *59*, (6), 731-736.

8. Kolb, S.; Knief, C.; Stubner, S.; Conrad, R., Quantitative Detection of Methanotrophs in Soil by Novel pmoA-Targeted Real-Time PCR Assays. *Appl Environ Microb* **2003,** *69*, (5), 2423-2429.

9. Creech, J. L., Jr.; Johnson, M. N., Angiosarcoma of Liver in the Manufacture of Polyvinyl Chloride. *Journal of occupational medicine. : official publication of the Industrial Medical Association* **1974,** *16*, (3), 150-1.

10. Maltoni, C.; Lefemine, G., Carcinogenicity Bioassays of Vinyl-Chloride .1. Research Plan and Early Results. *Environ Res* **1974,** *7*, (3), 387-405.

11. ASTDR, Toxicological Profile for Vinyl Chloride. In Registry, A. f. T. S. a. D., Ed. 2006.

12. Lee, L. J. H.; Chan, C. C.; Chung, C. W.; Ma, Y. C.; Wang, G. S.; Wang, J. D., Health Risk Assessment on Residents Exposed to Chlorinated Hydrocarbons Contaminated in Groundwater of a Hazardous Waste Site. *J Toxicol Env Heal A* **2002,** *65*, (3-4), 219-235.

13. United States Environmental Protection Agency Groundwater and Drinking Water. //www.epa.gov/safewater/dwh/t-voc/vinylchl.html

14. Keppler, F.; Borchers, R.; Pracht, J.; Rheinberger, S.; Scholer, H. F., Natural Formation of Vinyl Chloride in the Terrestrial Environment. *Environ Sci Technol* **2002,** *36*, (11), 2479-2483.

15. Kielhorn, J.; Melber, C.; Wahnschaffe, U.; Aitio, A.; Mangelsdorf, I., Vinyl chloride: Still a cause for concern. *Environ Health Persp* **2000,** *108*, (7), 579-588.

16. Vogel, T. M.; Mccarty, P. L., Biotransformation of Tetrachloroethylene to Trichloroethylene, Dichloroethylene, Vinyl-Chloride, and Carbon-Dioxide Under Methanogenic Conditions. *Appl Environ Microb* **1985,** *49*, (5), 1080-1083.

17. Parsons, F.; Wood, P. R.; Demarco, J., Transformations of Tetrachloroethene and Trichloroethene in Microcosms and Groundwater. *J Am Water Works Ass* **1984,** *76*, (2), 56-59.

18. Vogel, T. M.; Mccarty, P. L., Abiotic and Biotic Transformations of 1,1,1-Trichloroethane Under Methanogenic Conditions. *Environ Sci Technol* **1987,** *21*, (12), 1208-1213.

19. Carter, S. R.; Jewell, W. J., Biotransformation of Tetrachloroethylene by Anaerobic Attached-Films at Low-Temperatures. *Water Res* **1993,** *27*, (4), 607-615.

20. Distefano, T. D.; Gossett, J. M.; Zinder, S. H., Reductive Dechlorination of High-Concentrations of Tetrachloroethene to Ethene by an Anaerobic Enrichment Culture in the Absence of Methanogenesis. *Appl Environ Microb* **1991,** *57*, (8), 2287-2292.

21. Freedman, D. L.; Gossett, J. M., Biological Reductive Dechlorination of Tetrachloroethylene and Trichloroethylene to Ethylene Under Methanogenic Conditions. *Appl Environ Microb* **1989,** *55*, (9), 2144-2151.

22. Dieter, H. H.; Kerndorff, H., Presence and Importance of Organochlorine Solvents and Other Compounds in Germany's Groundwater and Drinking Water. *Ann Ist Super Sanita* **1993,** *29*, 14.

23. Wiedemeier, T. H.; et al. Technical Protocol for Evaluating Natural Attenuation of Chlorinated Solvents in Groundwater. EPA/600/R-98/128. http://www.epa.gov/oerrpage/superfund/resources/gwdocs/protocol.htm

24. Smith, A. M., Ethylene in Soil Biology. *Annu Rev Phytopathol* **1976,** *14*, 53-73.

25. Zeikus, J. G., Biology of Methanogenic Bacteria. *Bacteriol Rev* **1977,** *41*, (2), 514-541.

26. Alvarez-Cohen, L.; Speitel, G. E., Kinetics of Aerobic Cometabolism of Chlorinated Solvents. *Biodegradation* **2001,** *12*, (2), 105-126.

27. Broholm, K.; Ludvigsen, L.; Jensen, T. F.; Ostergaard, H., Aerobic Biodegradation of Vinyl Chloride and Cis-1,2-Dichloroethylene in Aquifer Sediments. *Chemosphere* **2005,** *60*, (11), 1555-1564.

28. Freedman, D. L.; Danko, A. S.; Verce, M. F., Substrate Interactions During Aerobic Biodegradation of Methane, Ethene, Vinyl Chloride and 1,2-Dichloroethenes. *Water Sci Technol* **2001,** *43*, (5), 333-340.

29. Madigan, M. T.; Martinko, J. M.; Dunlap, P. V.; Clark, D. P., *Brock Biology of Microorganisms*. 12 ed.; 2009.

30. Bradley, P. M.; Chapelle, F. H., Anaerobic Mineralization of Vinyl Chloride in Fe(III)-Reducing, Aquifer Sediments. *Environ Sci Technol* **1996,** *30*, (6), 2084-2086.

31. Bradley, P. M.; Chapelle, F. H., Role for Acetotrophic Methanogens in Methanogenic Biodegradation of Vinyl Chloride. *Environ Sci Technol* **1999,** *33*, (19), 3473-3476.

32. Bradley, P. M.; Chapelle, F. H., Acetogenic Microbial Degradation of Vinyl Chloride. *Environ Sci Technol* **2000,** *34*, (13), 2761-2763.

33. He, J. Z.; Ritalahti, K. M.; Aiello, M. R.; Loffler, F. E., Complete Detoxification of Vinyl Chloride by an Anaerobic Enrichment Culture and Identification of the Reductively Dechlorinating Population as a *Dehalococcoides* Species. *Appl Environ Microb* **2003,** *69*, (2), 996-1003.

34. Muller, J. A.; Rosner, B. M.; von Abendroth, G.; Meshulam-Simon, G.; McCarty, P. L.; Spormann, A. M., Molecular Identification of the Catabolic Vinyl Chloride Reductase from *Dehalococcoides* sp. strain VS and Its Environmental Distribution. *Appl Environ Microb* **2004,** *70*, (8), 4880-4888.

35. Sung, Y.; Ritalahti, K. M.; Apkarian, R. P.; Loffler, F. E., Quantitative PCR Confirms Purity of Strain GT, A Novel Trichloroethene-to-Ethene-Respiring *Dehalococcoides* Isolate. *Appl Environ Microb* **2006,** *72*, (3), 1980-1987.

36. Wisconsin Department of Natural Resources, Understanding Chlorinated Hydrocarbon Behavior in Groundwater: Investigation, Assessment and Limitations of Monitored Natural Attenuation. In Resources, W. D. o. N., Ed. 2003.

37. Gossett, J. M., Sustained Aerobic Oxidation of Vinyl Chloride at Low Oxygen Concentrations. *Environ Sci Technol* **2010,** *44*, (4), 1405-1411.

38. Bradley, P. M.; Chapelle, F. H., Microbial Mineralization of VC and DCE Under Different Terminal Electron Accepting Conditions. *Anaerobe* **1998,** *4*, (2), 81-87.

39. Bradley, P. M.; Chapelle, F. H., Effect of Contaminant Concentration on Aerobic Microbial Mineralization of DCE and VC in Stream-Bed Sediments. *Environ Sci Technol* **1998,** *32*, (5), 553-557.

40. Mattes, T. E.; Alexander, A. K.; Coleman, N. V., Aerobic Biodegradation of the Chloroethenes: Pathways, Enzymes, Ecology, and Evolution. *Fems Microbiol Rev* **2010,** *34*, (4), 445-475.

41. Arp, D. J.; Yeager, C. M.; Hyman, M. R., Molecular and Cellular Fundamentals of Aerobic Cometabolism of Trichloroethylene. *Biodegradation* **2001,** *12*, (2), 81-103.

42. Jin, Y. O.; Mattes, T. E., Adaptation of Aerobic, Ethene-Assimilating *Mycobacterium* Strains to Vinyl Chloride as a Growth Substrate. *Environ Sci Technol* **2008,** *42*, (13), 4784-4789.

43. Verce, M. F.; Ulrich, R. L.; Freedman, D. L., Transition from Cometabolic to Growth-Linked Biodegradation of Vinyl Chloride by a *Pseudomonas* sp. Isolated on Ethene. *Environ Sci Technol* **2001,** *35*, (21), 4242-4251.

44. Dedysh, S. N.; Knief, C.; Dunfield, P. F., *Methylocella* Species are Facultatively Methanotrophic. *J Bacteriol* **2005,** *187*, (13), 4665-4670.

45. Edwards, C.; Hales, B. A.; Hall, G. H.; McDonald, I. R.; Murrell, J. C.; Pickup, R.; Ritchie, D. A.; Saunders, J. R.; Simon, B. M.; Upton, M., Microbiological Processes in the Terrestrial Carbon Cycle: Methane Cycling in Peat. *Atmos Environ* **1998,** *32*, (19), 3247-3255.

46. Hanson, R. S.; Hanson, T. E., Methanotrophic Bacteria. *Microbiol Rev* **1996,** *60*, (2), 439-+.

47. Semprini, L.; Grbic-Galic, D.; McCarty, P. L.; Roberts, P. V., Methodologies for Evaluating In Situ Bioremediation of Chlorinated Solvents. In EPA/600/R-92/042, Ed. Cincinnati: US EPA Center for Environmental Research Information, 1992.

48. Semprini, L.; Hopkins, G. D.; Roberts, P. V.; Mccarty, P. L., Pilot Scale Field Studies of Insitu Bioremediation of Chlorinated Solvents. *J Hazard Mater* **1992,** *32*, (2-3), 145-162.

49. Semprini, L.; Mccarty, P. L., Comparison between Model Simulations and Field Results for Insitu Biorestoration of Chlorinated Aliphatics .2. Cometabolic Transformations. *Ground Water* **1992,** *30*, (1), 37-44.

50. Bowman, J., The Methanotrophs – The Families *Methylococcaceae* and *Methylocystaceae*. *Prokaryotes 5: 266–289, DOI: 10.1007/0-387-30745-1_15.* **2006**.

51. Dedysh, S. N.; Panikov, N. S.; Tiedje, J. M., Acidophilic Methanotrophic Communities from Sphagnum Peat Bogs. *Appl Environ Microb* **1998,** *64*, (3), 922-929.

52. McDonald, I. R.; Bodrossy, L.; Chen, Y.; Murrell, J. C., Molecular Ecology Techniques For the Study of Aerobic Methanotrophs. *Appl Environ Microb* **2008,** *74*, (5), 1305-1315.

53. Berestovskaya, Y. Y.; Vasil'eva, L. V.; Chestnykh, O. V.; Zavarzin, G. A., Methanotrophs of the Psychrophilic Microbial Community of the Russian Arctic Tundra. *Microbiology* **2002,** *71*, (4), 460-466.

54. Omelchenko, M. V.; Vasilyeva, L. V.; Zavarzin, G. A., Psychrophilic Methanotroph from Tundra Soil. *Curr Microbiol* **1993,** *27*, (5), 255-259.

55. Bodrossy, L.; Holmes, E. M.; Holmes, A. J.; Kovacs, K. L.; Murrell, J. C., Analysis of 16S rRNA and Methane Monooxygenase Gene Sequences Reveals a Novel Group of Thermotolerant and Thermophilic Methanotrophs, *Methylocaldum* gen. nov. *Arch Microbiol* **1997,** *168*, (6), 493-503.

56. Islam, T.; Jensen, S.; Reigstad, L. J.; Larsen, O.; Birkeland, N. K., Methane Oxidation at 55 Degrees Celsius and pH 2 by a Thermoacidophilic Bacterium Belonging to the *Verrucomicrobia* Phylum. *P Natl Acad Sci USA* **2008,** *105*, (1), 300-304.

57. Lin, J. L.; Radajewski, S.; Eshinimaev, B. T.; Trotsenko, Y. A.; McDonald, I. R.; Murrell, J. C., Molecular Diversity of Methanotrophs in Transbaikal Soda Lake Sediments and Identification of Potentially Active Populations by Stable Isotope Probing. *Environ Microbiol* **2004,** *6*, (10), 1049-1060.

58. Dunfield, P. F.; Khmelenina, V. N.; Suzina, N. E.; Trotsenko, Y. A.; Dedysh, S. N., *Methylocella silvestris* sp nov., A Novel Methanotroph Isolated from an Acidic Forest Cambisol. *Int J Syst Evol Micr* **2003,** *53*, 1231-1239.

59. Tsien, H. C.; Bratina, B. J.; Tsuji, K.; Hanson, R. S., Use of Oligodeoxynucleotide Signature Probes for Identification of Physiological Groups of Methylotrophic Bacteria. *Appl Environ Microb* **1990,** *56*, (9), 2858-2865.

60. Murrell, J. C.; McDonald, I. R.; Gilbert, B., Regulation of Expression of Methane Monooxygenases by Copper Ions. *Trends Microbiol* **2000,** *8*, (5), 221-225.

61. Prior, S. D.; Dalton, H., The Effect of Copper Ions on Membrane Content and Methane Monooxygenase Activity in Methanol-Grown Cells of *Methylococcus-Capsulatus* (*Bath*). *J Gen Microbiol* **1985,** *131*, (Jan), 155-163.

62. Stanley, S. H.; Prior, S. D.; Leak, D. J.; Dalton, H., Copper Stress Underlies the Fundamental Change in Intracellular Location of Methane Mono-Oxygenase in Methane-Oxidizing Organisms - Studies in Batch and Continuous Cultures. *Biotechnol Lett* **1983,** *5*, (7), 487-492.

63. Morton, J. D.; Hayes, K. F.; Semrau, J. D., Effect of Copper Speciation on Whole-Cell Soluble Methane Monooxygenase Activity in *Methylosinus Trichosporium* OB3b. *Appl Environ Microb* **2000,** *66*, (4), 1730-1733.

64. Kopp, D. A.; Lippard, S. J., Soluble Methane Monooxygenase: Activation of Dioxygen and Methane. *Curr Opin Chem Biol* **2002,** *6*, (5), 568-576.

65. Csaki, R.; Bodrossy, L.; Klem, J.; Murrell, J. C.; Kovacs, K. L., Genes Involved in the Copper-Dependent Regulation of Soluble Methane Monooxygenase of *Methylococcus capsulatus* (*Bath*): Cloning, Sequencing and Mutational Analysis. *Microbiol-Sgm* **2003,** *149*, 1785-1795.

66. Stainthorpe, A. C.; Lees, V.; Salmond, G. P. C.; Dalton, H.; Murrell, J. C., The Methane Monooxygenase Gene-Cluster of *Methylococcus-Capsulatus* (*Bath*). *Gene* **1990,** *91*, (1), 27-34.

67. Merkx, M.; Lippard, S. J., Why OrfY? Characterization of MMOD, A Long Overlooked Component of the Soluble Methane Monooxygenase from *Methylococcus capsulatus* (*Bath*). *J Biol Chem* **2002,** *277*, (8), 5858-5865.

68. Lieberman, R. L.; Rosenzweig, A. C., Crystal Structure of a Membrane-Bound Metalloenzyme That Catalyses the Biological Oxidation of Methane. *Nature* **2005,** *434*, (7030), 177-182.

69. Lieberman, R. L.; Rosenzweig, A. C., Biological Methane Oxidation: Regulation, Biochemistry, and Active Site Structure of Particulate Methane Monooxygenase. *Crit Rev Biochem Mol* **2004,** *39*, (3), 147-164.

70. Bodrossy, L.; Kovacs, K. L.; McDonald, I. R.; Murrell, J. C., A Novel Thermophilic Methane-Oxidising *Gamma-Proteobacterium*. *Fems Microbiol Lett* **1999,** *170*, (2), 335-341.

71. Bowman, J. P.; McCammon, S. A.; Skerratt, J. H., *Methylosphaera hansonii* gen. nov., sp. nov., A Psychrophilic, Group I Methanotroph from Antarctic Marine-Salinity, Meromictic Lakes. *Microbiol-Uk* **1997,** *143*, 1451-1459.

72. Heyer, J.; Berger, U.; Hardt, M.; Dunfield, P. F., *Methylohalobius crimeensis* gen. nov., sp. nov., A Moderately Halophilic, Methanotrophic Bacterium Isolated from Hypersaline Lakes of Crimea. *Int J Syst Evol Micr* **2005,** *55*, 1817-1826.

73. Kalyuzhnaya, M. G.; Stolyar, S. M.; Auman, A. J.; Lara, J. C.; Lidstrom, M. E.; Chistoserdova, L., *Methylosarcina lacus* sp. nov., A Methanotroph from Lake Washington, Seattle, USA, and Emended Description of the Genus *Methylosarcina*. *Int J Syst Evol Micr* **2005,** *55*, 2345-2350.

74. Rahalkar, M.; Bussmann, I.; Schink, B., *Methylosoma difficile* gen. nov., sp. nov., A Novel Methanotroph Enriched by Gradient Cultivation from Littoral Sediment of Lake Constance. *Int J Syst Evol Micr* **2007,** *57*, 1073-1080.

75. Wise, M. G.; McArthur, J. V.; Shimkets, L. J., *Methylosarcina fibrata* gen. nov., sp. nov. and *Methylosarcina quisquiliarum* sp. nov., Novel Type I Methanotrophs. *Int J Syst Evol Micr* **2001,** *51*, 611-621.

76. Dedysh, S. N.; Berestovskaya, Y. Y.; Vasylieva, L. V.; Belova, S. E.; Khmelenina, V. N.; Suzina, N. E.; Trotsenko, Y. A.; Liesack, W.; Zavarzin, G. A., *Methylocella tundrae* sp nov., A Novel Methanotrophic Bacterium from Acidic Tundra Peatlands. *Int J Syst Evol Micr* **2004,** *54*, 151-156.

77. Dedysh, S. N.; Khmelenina, V. N.; Suzina, N. E.; Trotsenko, Y. A.; Semrau, J. D.; Liesack, W.; Tiedje, J. M., *Methylocapsa acidiphila* gen. nov., sp nov., A Novel Methane-Oxidizing and Dinitrogen-Fixing Acidophilic Bacterium from Sphagnum Bog. *Int J Syst Evol Micr* **2002,** *52*, 251-261.

78. Dedysh, S. N.; Liesack, W.; Khmelenina, V. N.; Suzina, N. E.; Trotsenko, Y. A.; Semrau, J. D.; Bares, A. M.; Panikov, N. S.; Tiedje, J. M., *Methylocella palustris* gen. nov., sp nov., A New Methane-Oxidizing Acidophilic Bacterium from Peat Bags, Representing a Novel Subtype of Serine-Pathway Methanotrophs. *Int J Syst Evol Micr* **2000,** *50*, 955-969.

79. Dunfield, P. F.; Yuryev, A.; Senin, P.; Smirnova, A. V.; Stott, M. B.; Hou, S. B.; Ly, B.; Saw, J. H.; Zhou, Z. M.; Ren, Y.; Wang, J. M.; Mountain, B. W.; Crowe, M. A.; Weatherby, T. M.; Bodelier, P. L. E.; Liesack, W.; Feng, L.; Wang, L.; Alam, M., Methane Oxidation by an Extremely Acidophilic Bacterium of the Phylum *Verrucomicrobia*. *Nature* **2007,** *450*, (7171), 879-U18.

80. Pol, A.; Heijmans, K.; Harhangi, H. R.; Tedesco, D.; Jetten, M. S. M.; den Camp, H. J. M. O., Methanotrophy Below pH1 by a New *Verrucomicrobia* Species. *Nature* **2007,** *450*, (7171), 874-U17.

81. Dolan, M. E.; Mccarty, P. L., Small Column Microcosm for Assessing Methane-Stimulated Vinyl-Chloride Transformation in Aquifer Samples. *Environ Sci Technol* **1995,** *29*, (8), 1892-1897.

82. Wilson, J. T.; Wilson, B. H., Biotransformation of Trichloroethylene in Soil. *Appl Environ Microb* **1985,** *49*, (1), 242-243.

83. Hartmans, S.; Debont, J. A. M., Aerobic Vinyl-Chloride Metabolism in *Mycobacterium-Aurum L1*. *Appl Environ Microb* **1992,** *58*, (4), 1220-1226.

84. Coleman, N. V.; Spain, J. C., Epoxyalkane: Coenzyme M Transferase in the Ethene and Vinyl Chloride Biodegradation Pathways of *Mycobacterium* strain JS60. *J Bacteriol* **2003,** *185*, (18), 5536-5545.

85. Conrad, R., Soil Microorganisms As Controllers of Atmospheric Trace Gases (H-2, CO, CH_4, OCS, N_2O, and NO). *Microbiol Rev* **1996,** *60*, (4), 609-+.

86. Oldenhuis, R.; Vink, R. L. J. M.; Janssen, D. B.; Witholt, B., Degradation of Chlorinated Aliphatic-Hydrocarbons by Methylosinus-Trichosporium Ob3b Expressing Soluble Methane Monooxygenase. *Appl Environ Microb* **1989,** *55*, (11), 2819-2826.

87. Lee, S. W.; Keeney, D. R.; Lim, D. H.; Dispirito, A. A.; Semrau, J. D., Mixed Pollutant Degradation by *Methylosinus trichosporium* OB3b Expressing Either Soluble or Particulate Methane Monooxygenase: Can The Tortoise Beat The Hare? *Appl Environ Microb* **2006,** *72*, (12), 7503-7509.

88. Yoon, S.; Semrau, J. D., Measurement and Modeling of Multiple Substrate Oxidation by Methanotrophs at 20 Degrees Celsius. *Fems Microbiol Lett* **2008,** *287*, (2), 156-162.

89. Jin, Y. O.; Mattes, T. E., A Quantitative PCR Assay for Aerobic, Vinyl Chloride- and Ethene-Assimilating Microorganisms in Groundwater. *Environ Sci Technol* **2010,** *44*, (23), 9036-9041.

90. Regenesis Oxygen Releasing Compound, Remediation of Vinyl Chloride. www.Regenesis.com

91. Mattes, T. E.; Coleman, N. V.; Chuang, A. S.; Rogers, A. J.; Spain, J. C.; Gossett, J. M., Mechanism Controlling the Extended Lag Period Associated with Vinyl Chloride Starvation in *Nocardioides* sp. strain JS614. *Arch Microbiol* **2007,** *187*, (3), 217-226.

92. VanGuilder, H. D.; Vrana, K. E.; Freeman, W. M., Twenty-Five Years of Quantitative PCR for Gene Expression Analysis. *Biotechniques* **2008,** *44*, (5), 619-626.

93. Brownie, J.; Shawcross, S.; Theaker, J.; Whitcombe, D.; Ferrie, R.; Newton, C.; Little, S., The Elimination of Primer-Dimer Accumulation in PCR. *Nucleic Acids Res* **1997,** *25*, (16), 3235-3241.

94. Kanagawa, T., Bias and Aartifacts in Multitemplate Polymerase Chain Reactions (PCR). *J Biosci Bioeng* **2003,** *96*, (4), 317-323.

95. Griffiths, A. J. F.; Gelbart, W. M.; Lewontin, R. C.; Miller, J. H., *Modern Genetic Analysis*. W. H. Freeman & Company: 2002.

96. Ronaghi, M., Pyrosequencing Sheds Light on DNA Sequencing. *Genome Res* **2001,** *11*, (1), 3-11.

97. Russom, A.; Haasl, S.; Andersson, H.; Van De Wijngaart, W.; Stemme, G. Bead-Based Microfluidic Platform for Biochemical Applications. http://www.ee.kth.se/php/index.php?action=research&cmd=showproject&id=51

98. Alaska Department of Environmental Conservation, D. o. S. P. a. R., Site Summary Update - River Terrace Laundromat. In 1999.

99. Alaska Department of Environmental Conservation, C. S. P., River Terrace RV Park, Second 5 Year Review of the Record of Decision. In 2010.

100. United States Geological Survey, Chloroethene Biodegradation Potential in the "Lower" Contaminant Plume, River Terrace RV Park, Soldotna, Alaska. In Survey, U. S. G., Ed. 2004.

101. Bradley, P. M.; Richmond, S.; Chapelle, F. H., Chloroethene Biodegradation in Sediments at 4 Degrees C. *Appl Environ Microb* **2005,** *71*, (10), 6414-6417.

102. CH2MHill *Long-term Monitoring Report SWMUs 2B, 2C, and 2E, Naval Air Station Oceana, Virginia Beach, Virginia*; 2009.

103. CH2MHill *Treatability Study Report SWMUs 2B, 2C, and 2E, Naval Air Station, Oceana, Virginia Beach, Virginia*; 2007.

104. Cook, L. J.; Hickman, G.; Chang, A.; Landin, P.; Reisch, T. *Comparison of Aerobic and Anaerobic Biotreatments of Low-Level Vinyl Chloride*.

105. Town of Carver Open Space Committee, Town of Carver 2010-2015 Open Space & Recreation Plan. In 2010.

106. Fogel, S.; Begley, J. F.; LeBlanc, C. R. *Biodegradation of Low Concentrations of Vinyl Chloride in Groundwater by Ethene-Oxidizing Bacteria*.

107. Begley, G. S.; Fogel, S.; Begley, J. F., Microbiological Performance Monitoring for Aerobic Bioremediation of a Low Concentration Vinyl Chloride Plume. In.

108. Johnson, D. R.; Lee, P. K. H.; Holmes, V. F.; Alvarez-Cohen, L., An Internal Reference Technique For Accurately Quantifying Specific mRNAs by Real-Time PCR With an Application to the tceA Reductive Dehalogenase Gene. *Appl Environ Microb* **2005,** *71*, (7), 3866-3871.

109. Kreader, C., Relief of Amplification Inhibition in PCR with Bovine Serum Albumin or T4 Gene 32 Protein. *Appl. Environ. Microbiol.* **1996,** *62*, (3), 1102-1106.

110. V. Wintzingerode, F.; Göbel, U. B.; Stackebrandt, E., Determination of Microbial Diversity in Environmental Samples: Pitfalls of PCR-Based rRNA Analysis. *Fems Microbiol Rev* **1997,** *21*, (3), 213-229.

111. Cheng, Y. S.; Halsey, J. L.; Fode, K. A.; Remsen, C. C.; Collins, M. L. P., Detection of Methanotrophs in Groundwater by PCR. *Appl Environ Microb* **1999,** *65*, (2), 648-651.

112. Holmes, A. J.; Costello, A.; Lidstrom, M. E.; Murrell, J. C., Evidence That Particulate Methane Monooxygenase and Ammonia Monooxygenase May Be Evolutionarily Related. *Fems Microbiol Lett* **1995,** *132*, (3), 203-208.

113. Lyew, D.; Guiot, S., Effects of Aeration and Organic Loading Rates on Degradation of Trichloroethylene in a Methanogenic-Methanotrophic Coupled Reactor. *Appl Microbiol Biot* **2003,** *61*, (3), 206-213.

114. Nadkarni, M. A.; Martin, F. E.; Jacques, N. A.; Hunter, N., Determination of Bacterial Load by Real-Time PCR Using a Broad-Range (Universal) Probe and Primers Set. *Microbiology* **2002,** *148*, (Pt 1), 257-66.

115. Martineau, C.; Whyte, L. G.; Greer, C. W., Stable Isotope Probing Analysis of the Diversity and Activity of Methanotrophic Bacteria in Soils from the Canadian High Arctic. *Appl Environ Microb* **2010,** *76*, (17), 5773-5784.

116. Yergeau, E.; Hogues, H.; Whyte, L. G.; Greer, C. W., The Functional Potential of High Arctic Permafrost Revealed by Metagenomic Sequencing, qPCR and Microarray Analyses. *Isme J* **2010,** *4*, (9), 1206-1214.

117. Fuse, H.; Ohta, M.; Takimura, O.; Murakami, K.; Inoue, H.; Yamaoka, Y.; Oclarit, J. M.; Omori, T., Oxidation of Trichloroethylene and Dimethyl Sulfide by a Marine *Methylomicrobium* Strain Containing Soluble Methane Monooxygenase. *Biosci Biotech Bioch* **1998,** *62*, (10), 1925-1931.

118. Life Technologies Ten Most Common Real-Time qPT-PCR Pitfalls. http://www.ambion.com/techlib/tn/102/17.html

119. Stein, L. Y.; Bringel, F.; DiSpirito, A. A.; Han, S.; Jetten, M. S. M.; Kalyuzhnaya, M. G.; Kits, K. D.; Klotz, M. G.; den Camp, H. J. M. O.; Semrau, J. D.; Vuilleumier, S.; Bruce, D. C.; Cheng, J. F.; Davenport, K. W.; Goodwin, L.; Han, S. S.; Hauser, L.; Lajus, A.; Land, M. L.; Lapidus, A.; Lucas, S.; Medigue, C.; Pitluck, S.; Woyke, T., Genome Sequence of the Methanotrophic *Alphaproteobacterium Methylocystis* sp Strain Rockwell (ATCC 49242). *J Bacteriol* **2011,** *193*, (10), 2668-2669.